

TuQ

Progress Report No. 1

Studies of Adsorption-Desorption and Partitioning
of Dredged Material Contaminants

Dominic M. Di Toro
John D. Mahony

Environmental Engineering and Science Program
and
Chemistry Department
Manhattan College, Bronx, N.Y. 10471

October 1984

Cooperative Agreement CR810970-01-0

Acknowledgment

This progress report contains research performed for both the EPA Narragansett Environmental Research Laboratory and the NOAA Office of Marine Pollution Assessment. The topic of each project is similar - the particles being investigated are quite different (Sewage Sludge and Dredged Material). It is felt that it would be more instructive to combine the progress reports in order to highlight the similarities found for both types of materials and to present a more comprehensive discussion of the status of the sorption model.

Summary

The experimental work this year has focused on the generation and analysis of consecutive desorption isotherms using atomic absorption techniques in order to analyze the desorption behavior of the native particle bound metal as it interacts with various aqueous phases. The radionuclide isotherms were used mainly to validate the desorption model, investigate the effects of adsorption and desorption times, and perfect technique.

The desorption model described below fits the experimental data quite well and generally yields consistent results for the isotherm parameters. A nonlinear least squares fitting program estimates the isotherm parameters and the desorbable fraction of the metal. It also computes standard errors of the estimates so that comparisons can be made considering the uncertainty of the estimates.

It has been found that desorption of native metal from sewage sludge and Black Rock Harbor sediment follow the same framework as previously found applicable to radionuclides and clean particles (clay and quartz desorption). The difference is that a substantially smaller fraction of the total native metal is desorbable. Whereas with metal adsorbed to clean particles just prior to desorption, approximately one half or more of the metal will eventually desorb, the percentage for native metal is much less. For pure water desorption less than 1% desorbs. With seawater the percentage is higher, perhaps 5-20%, depending upon which metal is being considered, but the data are as yet not extensive enough for statistical precision.

With respect to organic chemicals the primary effort has been to complete an analysis of literature data in order to investigate the applicability of the same desorption model (Appendix II). Remarkably enough the reversible component partition coefficient expression derived from the metal-clean particle experiments fits the neutral hydrophobic chemical sorption data over seven orders of magnitude in partition coefficient (Appendix II, fig. 4). In addition, the isotherm parameters can be predicted from chemical (octanol/water partition coefficient, K_{ow}) and particle properties (fraction organic carbon, f_{oc} , and particle concentration, m). Thus for neutral hydrophobic chemicals and suspensions of particles, the desorption partitioning problem is essentially solved.

The particle interaction model (Appendix I and II), from which the expression for reversible partition coefficient follows suggests that for stationary particles as would be the case in sediments the partition coefficient would be the same as the low particle concentration limit of partition coefficient found in suspension experiments. This has been found to be the case for hexachlorobiphenyl. Syringe migration experiments produced the same partition coefficient as predicted from the particle interaction model applied to suspensions (Appendix II and III). We intend to examine whether this is a general finding by concentrating a significant effort on syringe migration experiments.

The examination of desorption of hydrophobic chemicals from dredged material and sewage sludge will be made using radiotagged chemicals with high specific activity (~ 10 Ci/m mole). Two have been purchased: benzo(a)pyrene ($\log K_{ow} = 6.5$) and 2-amino anthracene ($\log K_{ow} = 4.13$). These are suitable for both consecutive desorption experiments and syringe migration studies. Other chemicals are being acquired that fill in the range of K_{ow} . These are of lower specific activity ($\sim 10m$ Ci/m mole) and are only suitable for syringe experiments.

The question of complete tagging of a particle with the tracer neutral organic chemical has been addressed by work reported by Karickhoff and Morris (1984, in press). They estimate the time to complete adsorption and desorption equilibrium to be on the order of $f_{oc} K_{ow}$ (days). Hence only reversible component sorption is experimentally accessible for B(a)P regardless of whether native chemical or tracers are used. Even for 2-amino

anthracene and Black Rock Harbor sediment ($f_{oc} = 5\%$) a tagging time of 500 days is suggested. Long term tagging experiments will be attempted but it appears that no complete equilibration is possible.

Additional experiments using model particles have been performed in order to elucidate the particle concentration effect. Two micron spherical glass beads have been used to generate nickel adsorption-desorption isotherms at varying particle concentrations. These particles also exhibit the particle concentration effect (fig. 11) in accord with the proposed model (fig. 12). We regard this as strong proof that the effect is not an artifact of particle separation. Field data for nickel and PCB sorption also conform (fig. 13-14).

Publication of results is proceeding. Appendix I has been submitted to Environmental Science and Technology and the reviews (mostly favorable) have just been received. Appendix II will be submitted to Chemosphere shortly. The syringe migration paper (Appendix III) has been submitted to Environmental Science and Technology. We expect to write a paper detailing the findings of the sewage sludge and sediment results.

I. Introduction

The purpose of this research project is to continue the development and testing of a model of phase partitioning that describes the adsorption and desorption of heavy metals and organic chemicals to suspended and sedimented particles. The model is based upon separating sorbed chemical into two components: the reversible or labile fraction, r_x , which reversibly adsorbs and desorbs, and a resistant or non-labile fraction, r_o , which does not appreciably desorb in time scales of hours to days. The partitioning of the reversible component is described via a linear isotherm: $r_x = \pi_x c$ with partition coefficient, π_x . A completely developed theory would:

- 1) specify the behavior of π_x as a function of chemical, particle, and aqueous phase properties
- 2) specify, or provide a measurement method for particles such as sewage sludge or dredged sediment for which the exposure history is unknown, of the reversibly bound fraction r_x/r_T of the total particle bound chemical concentration, r_T .
- 3) be applicable to both suspended particles and stationary sediments.

Progress toward this goal has been appreciable and a usable framework is now available which appears to apply to all particle types examined so far. Some preliminary evidence suggests that for the simplest situation (neutral hydrophobic chemicals and organic carbon containing particles) the above requirements for a complete theory are being approached.

II. The Model

Consider a sample of dredged sediment or sewage sludge with a total concentration r_T ($\mu\text{g/g}$) of sorbed chemical. A portion, $r_x^{(0)}$ ($\mu\text{g/g}$) of the chemical is reversibly sorbed - the zero superscript is a convenient notation for the initial state of the particles before desorption is initiated. The remainder, $r_o = r_T - r_x^{(0)}$, is not desorbable during the short time scales being examined.

A convenient way of thinking about desorption is to analyze the results of consecutive cycles of desorption into a fixed volume of uncontaminated

aqueous phase at a fixed particle concentration, m . For the first cycle, the reversible component rapidly equilibrates to produce an aqueous concentration, $c^{(1)}$ and a new (smaller) reversible component concentration, $r_x^{(1)}$. These are related via the partition coefficient:

$$r_x^{(1)} = \pi_x c^{(1)} \quad (1)$$

If no chemical is lost to the experimental vessel then by mass balance:

$$c_T = mr_T = m(r_o + r_x^{(0)}) = m(r_o + r_x^{(1)}) + c^{(1)} \quad (2)$$

where c_T is the total chemical concentration on a volumetric basis ($\mu\text{g/L}$), and m is the particle concentration (g/L). Hence:

$$mr_x^{(0)} = mr_x^{(1)} + c^{(1)} = (m\pi_x + 1)c^{(1)} \quad (3)$$

where the second equality follows from the partitioning eq. (1). Thus:

$$c^{(1)} = \frac{m r_x^{(0)}}{1 + m\pi_x} \quad (4)$$

For the second ($i=2$) and subsequent cycles the vessel is centrifuged, a volume of aqueous phase is removed (α = volume fraction remaining), replaced with uncontaminated aqueous phase such that m is unchanged, and the vessel is re-equilibrated. Again by mass balance:

$$mr_o + mr_x^{(1)} + \alpha c^{(1)} = mr_o + mr_x^{(2)} + c^{(2)} \quad (5)$$

so that:

$$c^{(2)} = \frac{\alpha + m\pi_x}{1 + m\pi_x} c^{(1)} \quad (6)$$

where the isotherm equation $r_x^{(i)} = \pi_x c^{(i)}$ is used for $r_x^{(1)}$ and $r_x^{(2)}$. By a similar argument for subsequent cycles:

$$c^{(i)} = \left(\frac{\alpha + m\pi_x}{1 + m\pi_x} \right)^{i-1} c^{(1)} \quad (7)$$

so that the dissolved concentration in consecutive desorptions follow a decreasing geometric series and these data, $c^{(i)}$, would plot as a straight line versus i on semi-log paper. The slope would give π_x . Using eq. (4) for $c^{(1)}$ yields

$$c^{(i)} = \frac{m}{1 + m\pi_x} \left(\frac{\alpha + m\pi_x}{1 + m\pi_x} \right)^{i-1} r_x^{(0)} \quad (8)$$

so that the intercept yields $r_x^{(0)}$, the initial reversible component concentration. Finally the sorbed concentration at each cycle is:

$$r^{(i)} = r_o + r_x^{(i)} \quad (9)$$

$$= r_o + \pi_x c^{(i)} \quad (10)$$

which yields r_o , the resistant component concentration.

For each particle type (sludge, Black Rock Harbor sediment) and aqueous phase (nanopure water, seawater) a set of isotherms are generated by using different particle concentrations, m_j . Typically four particle concentrations spanning the range 100-3000 mg/L are used. Fig. 1 illustrates typical results for aqueous concentrations $c^{(i)}$ (left hand side) and $r^{(i)}$ (right hand side). The semi-logarithmic behavior of $c^{(i)}$ is apparent as is the curvature of $r^{(i)}$ reflecting the presence of a resistant component concentration.

In order to analyze each of these isotherm sets it is necessary to know how π_x varies with respect to m_j since each isotherm within a set is obtained at a differing particle concentration. Contrary to expectations, π_x can be a strong function of m . This central feature of reversible partitioning is discussed below and in Appendices I and II where a particle interaction model is proposed to establish the functional form of the relationship. That such an effect is important can be seen directly from the aqueous concentration versus desorption cycle behavior. The logarithmic

concentration behavior from eq. (7) is:

$$\ln c_j^{(i)} = (i-1) \ln \left(\frac{\alpha + m_j \pi_x}{1 + m_j \pi_x} \right) + \ln c_j^{(1)} \quad (11)$$

As solids concentration, m_j , increases the slope should progressively become less negative until it approaches $\ln(m_j \pi_x / m_j \pi_x) = \ln(1) = 0$. Note, however, in fig. 1 that at the higher solids concentrations, and in the case of the Black Rock Harbor sediment all the slopes of each isotherm, are nearly the same (the lines are parallel) indicating that $m_j \pi_x$ is constant so that π_x must be decreasing with increasing m_j . Table 1 presents the π_x derived from the slopes of $\ln c_j^{(i)}$ versus i and m_j for these isotherms. The reciprocal relationship is evident.

The vertical displacement of $c_j^{(1)}$, the cycle 1 concentration, as m_j increases is also related to this effect. As m_j increases the aqueous concentration should increase following:

$$c_j^{(1)} = \frac{m_j}{1 + m_j \pi_x} r_x^{(0)} \quad (12)$$

Again if π_x were constant than as m_j increases $c_j^{(1)}$ should approach $r_x^{(0)} / \pi_x$, a constant. But these data indicate that the displacement persists even at large particle concentrations, suggesting again that $m_j \pi_x$ is constant.

These arguments are meant only illustrate the consequences of π_x varying with m . The quantitative results are obtained by fitting the data to eq. (8) and eq. (10) using a nonlinear least squares program. The program chooses the model parameters such that they minimize the sum of the squared differences between observations \hat{c}_j , \hat{r}_j and model calculations $c_j^{(i)}$, $r_j^{(i)}$:

$$\sigma^2 = \sum_i \sum_j (\log \hat{c}_j^{(i)} - \log(c_j^{(i)}))^2 + (\log \hat{r}_j^{(i)} - \log(r_j^{(i)}))^2$$

where $c_j^{(i)}$ and $r_j^{(i)}$ are given by eq. (8) and (10). The reversible component partition coefficient is given by:

$$\pi_x = \frac{\pi_{xc}}{1 + m\pi_{xc}/v_x} \quad (13)$$

which establishes the functional dependency of π_x to particle concentration, m . Appendix I and II present the rationale and the derivation. The parameters are π_{xc} (the classical, low particle concentration limiting partition coefficient $\pi_x \rightarrow \pi_{xc}$ as $m \rightarrow 0$) and v_x , the slope of π_x versus m for large particle concentration ($\pi_x \rightarrow v_x/m$ for m large). These specify the behavior of π_x . Fig. 2 presents some early adsorption-single desorption isotherm data fit to eq. (13) using nonlinear least squares. Note the strong inverse relationship between π_x and m for large m as well as the approach to π_{xc} as m decreases. For a complete analysis of consecutive desorption isotherms the remaining parameters are $r_x^{(0)}$ and r_o , the reversible and resistant component concentrations. Thus four parameters are fit to the data. In fact since $r_x^{(0)} + r_o = r_T$, which is presumably constant, only three parameters are needed to completely characterize a set of isotherms. This is a reasonably parsimonious representation of a large quantity of data.

If a complete theory were available it would then provide the parameters π_{xc} , v_x and $r_x^{(0)}/r_T$ as a function of chemical, particle, and aqueous phase properties. It is clear at this stage of the research that the three parameter formulation is descriptive of data for many chemical and particle types and in particular for sewage sludge and dredged sediment - heavy metal sorption. In the following sections this framework is applied to consecutive desorption experiments using both radionuclides and native heavy metals.

III. Consecutive Desorption - Cd^{115} : Effect of Adsorption and Desorption Times

The original research plan was to investigate the effects of various experimental variables: adsorption time, desorption time, etc. using radionuclides. The hope was that by using sufficiently long adsorption times the resistant component sites could be radiolabeled. Fig. 3-5 present the

results for Ridgewood sludge and Black Rock Harbor sediment in seawater. Table 2 lists the isotherm parameters. Fig. 3 compares adsorption times of $t_{ads} = 1, 4$ and 9 days from the same tagging vessel. Some increase in r_o is observed but the effect is not dramatic. For $t_{ads} = 18$ and 25, Fig. 4, a dramatic change is evident. However these isotherms were obtained using a previously uncapped vessel. Progressive color changes in the first adsorption vessel (Fig. 3 results) indicated oxidation was occurring whereas the second tube maintained its color until it was sampled.

Similar results were obtained for the Black Rock Harbor sediment (Fig. 5). Small changes were observed and the somewhat erratic results are attributed to partial oxidation.

It was decided that the adsorption tagging procedure using radionuclides was not convincing since one could never be sure that the radiotag was isotopically exchanged with all sites. Hence the useful information in Table 2 is only the reversible component parameters, v_x and π_{xc} . These ranged from $v_x = 0.2 - 2.0$ and $\pi_{xc} \sim 2000 - 8000$ L/kg. Where π_{xc} is not listed in this and subsequent tables it is because the data are representable by the high particle concentration limit: $\pi_x = v_x/m$ so that π_{xc} could not be estimated.

The effect of increasing desorption time for each cycle is examined in Fig. 6 and Table 3. No significant changes were observed from $t_{des} = 1$ hr to 5-7 days.

IV. Consecutive Desorption - Native Metal Results

The major experimental effort for the latter half of this year was directed toward perfecting the techniques for directly measuring total and dissolved metal concentrations using atomic absorption flame and graphite techniques. Clean procedures and digestion techniques were established and checked. Duplicates are employed for each particle concentration. One hour desorptions are used for each cycle.

Fig. 7 and Table 4 illustrate the results for Ridgewood sludge and nanopure water as the aqueous phase. Copper, chromium and zinc were analyzed. Only a small percent of any of the total metal is in the reversible

Table 2

Effect of Adsorption Time
Cd¹¹⁵ - Ridgewood Sludge - Seawater

Isotherm #	t _{ads} (days)	v _x	π _{xc} (L/kg)	(0)		r _o (μg/g)	σ(log ₁₀)
				r _x (μg/g)	r _o (μg/g)		
186	1	11.2 ± 2.65	4570 ± 716	2.30 ± 0.10	0.214 ± 0.067	0.348	
188	4	2.24 ± 0.724	3390 ± 1370	2.76 ± 0.20	1.67 ± 0.20	0.484	
193	9	2.29 ± 0.68	5500 ± 2300	2.47 ± 0.19	1.12 ± 0.18	0.546	
196*	18	5.30 ± 16.7	832 ± 620	0.147 ± 0.02	4.79 ± 0.42	0.495	
202*	25	0.238 ± 0.11	-	0.216 ± 0.02	3.84 ± 0.363	0.53	
<u>Cd¹¹⁵ - Black Rock Harbor - Seawater</u>							
192	11	0.759 ± 0.41	8320 ± 6980	19.1 ± 2.9	3.45 ± 2.0	1.18	
197	18	0.466 ± 0.09	3550 ± 2300	15.1 ± 0.84	6.89 ± 0.49	0.401	
201*	25	0.473 ± 0.38	-	14.5 ± 4.3	1.86 ± 1.77	2.2	

* New tube used

Table 3
 Effect of Desorption Time
Cd¹¹⁵ - Ridgewood - Seawater

Isotherm #	t_{ads} (days)	v_x	π_{xc} (L/kg)	$r_x(0)$ ($\mu\text{g/g}$)	r_o ($\mu\text{g/g}$)	$\sigma(\log_{10})$
115	0.042 (1 hr)	0.562 ± 0.24	-	5.11 ± 0.74	1.32 ± 0.45	1.16
121	5	0.295 ± 0.08	-	5.40 ± 0.15	1.03 ± 0.15	0.88
114	7	0.229 ± 0.16	-	3.58 ± 1.31	0.10 ± 0.08	2.53

Table 4

AA Isotherm Parameters

Ridgewood Sludge - Nanopure Water (pH = 7.8-8.1)

Isotherm #	Sorbate	v_x	π (L/kg)	r_x ($\mu\text{g/g}$)	r ($\mu\text{g/g}$)	$\sigma(\log_{10})$
7	Cu	1.97 ± 0.88	6410 ± 8350	12.4 ± 1.14	2900 ± 194	0.546
7	Cr	3.70 ± 0.75	5150 ± 1550	2.11 ± 0.12	807 ± 26	0.260
7	Zn	2.80 ± 1.70	-	9.57 ± 3.03	3440 ± 340	0.795

Black Rock Harbor Sediment - Borate Buffer (pH = 9)

8	Cu	4.28 ± 1.71	2090 ± 829	7.21 ± 0.67	2660 ± 123	0.28
8	Cr	2.74 ± 7.16	1850 ± 5800	2.24 ± 0.66	1306 ± 211	1.06

Table 5
 AA Isotherm Parameters
 Ridgewood Sludge - Nanopure Water
 1 day desorption for each cycle

Isotherm #	Sorbate	v_x	π_{xc} (L/kg)	r_x ($\mu\text{g/g}$)	r_0 ($\mu\text{g/g}$)	$\sigma(\log_{10})$
12	Cr	6.56 ± 3.12	4680 ± 3400	24.9 ± 4.9	613 ± 440	0.435
12	Zn	31.6 ± 28	$23,990 \pm 35,000$	1350 ± 1240	558 ± 3300	0.486
<u>Ridgewood Sludge - 75% Nanopure Water, 25% Seawater</u>						
9	Cu	22.8 ± 108	2360 ± 2700	71.6 ± 29	1832 ± 168	0.508
9	Cr	0.875 ± 0.50	-	3.42 ± 0.64	937 ± 170	1.44
9	Zn	1.91 ± 0.85	-	362 ± 67	1350 ± 119	0.783

Table 7
 Isotherm Parameters for N⁶³ Sorption
 Borate Buffer - pH=9

Individual Data Sets

Sorbent	v_x	π_{xc} (L/kg)	$\sigma(\log_{10})$
2 μ glass spheres	0.550 \pm 0.344	826 \pm 647	0.300
Quartz particles	0.934 \pm 0.246	1965 \pm 618	0.217
Cellulose	0.454 \pm 0.087	16,070 \pm 4900	0.100
Montmorillonite	0.931 \pm 0.110	48,380 \pm 8510	0.080

Joint Data Set

Sorbent	π_{xc}
2 μ glass spheres	715 \pm 246
Quartz particles (Mil-U-Sil 5)	2380 \pm 938
Cellulose	11,240 \pm 3700
Montmorillonite	57,100 \pm 21,100

component: $r_x^{(0)}/r_T < 0.5\%$ although the partition coefficients are not large: $\pi_{xc} \sim 5000 - 6400$ L/kg and $v_x \sim 2-4$ is in the range of that found for the radioisotopes. The conformity of the model to the data is evident as well as the reproducibility of the data - note that the log scale for $r^{(i)}$ is one cycle.

Fig. 8 (Table 4) present the results for Black Rock Harbor sediment in borate buffer (0.1 mM) which was necessary to stabilize the pH. Again only a small percentage of the metal is in the reversible phase $r_x^{(0)}/r_T < 0.3\%$. Partitioning parameters are not dissimilar to those for Ridgewood sludge although the π_{xc} 's do appear somewhat lower. The similarity is somewhat surprising considering the difference between the two particle types.

Fig. 9 (Table 5) illustrates the effect of 1 day desorption times between cycles. Some increase in reversible component sorption is suggested but the statistical errors of estimation are too large to draw any firm conclusions.

Fig. 10 (Table 5) illustrates the effects of desorption into dilute seawater. It appears that substantially more copper ($r_x^{(0)}/r_T \sim 4\%$) and zinc ($r_x^{(0)}/r_T \sim 20\%$) is desorbable in contrast to the nanowater case of $< 0.5\%$. These seawater experiments are initial attempts. The matrix effects are being eliminated as well as problems with contamination. However it is clear even from these data that substantial fractions of the native heavy metal are not desorbable into seawater. The use of completely reversible partitioning theory would greatly overestimate the aqueous concentration and greatly underestimate the quantity of metal that remains bound to the sludge and/or sediment as it settles to the sediment.

V. Summary of Metal Isotherm Parameters

The data generated and analyzed to date are summarized in Table 6 the purpose of which is to provide an overview of the behavior of the isotherm parameters. The most striking feature is that there is relatively little

variation in v_x and π_{xc} for all the metal/sorbent/aqueous phase combinations that have been investigated: $v_x = .7 - 4.0$ and $\pi_{xc} = 2000 - 6500$ L/kg. One would have expected π_{xc} to vary more dramatically especially as the aqueous phase is changed from nano-pure water to seawater reflecting the ionic strength increase. Only small variations in v_x are not too surprising anymore (although still puzzling) since only small changes are observed for organic chemicals as well (Appendix II).

The most dramatic variation is in the fraction desorbable. For Cd which is adsorbed prior to the desorption, 30-60% is desorbable. For desorption of native metal into low ionic strength solutions, the desorbable fraction is less than 1%. The preliminary dilute seawater results suggest that this fraction may be higher for copper and zinc at least. However it is too soon to tell conclusively. More complete seawater desorption isotherms are planned to establish the validity of this trend.

Table 6
Summary of Isotherm Parameters

Sorbate	Sorbent	Aqueous Phase	v_x	π_{xc} (L/kg)	$r_x^{(0)}/r_T$ (%)
Cd ¹¹⁵	Ridgewood	Seawater	2.5	4000	60
Cd ¹¹⁵	Black Rock	Seawater	0.65	6000	30
Cu	Ridgewood	Nanowater	2.0	6500	0.4
Cr	Ridgewood	Nanowater	3.7	5200	0.25
Zn	Ridgewood	Nanowater	2.8	-	0.28
Cu	Black Rock	Borate	4.3	2000	0.27
Cr	Black Rock	Borate	2.7	1900	0.17
Cu	Ridgewood	1/4 Seawater	-	2400	3.9
Cr	Ridgewood	1/4 Seawater	0.88	-	0.36
Zn	Ridgewood	1/4 Seawater	1.9	-	21

VI. Particle Concentration Effect

The most surprising and puzzling feature of reversible component partitioning is the particle concentration effect. Attempting to establish that this effect is not an artifact has prompted a number of experimental designs (Resuspension and Dilution experiments, Appendix I).

Another approach is to use a particle that is unambiguously separated by centrifugation so that no third phase arguments apply. Toward this end we have examined 2 μm glass spheres (Duke Scientific Corp.) in the Ni^{63} -Borate system. Fig. 11 presents the adsorption data which clearly shows the particle concentration effect. It is difficult to imagine what artifact could account for these results.

In addition, as a model particle for organic coatings we examined the behavior of cellulose particles over a range of particle concentrations. These data together with montmorillonite and quartz particle data are analyzed using nonlinear least square fits to obtain v_x , π_{xc} for each particle type. They are listed in Table 7. Essentially the same v_x results for each data set. A joint fit with a common v_x is also tabulated and shown in Fig. 12 as π_x vs m and in normalized form. Note the excellent fit of the data regardless of particle type. Whereas π_{xc} ranges from ~ 700 L/kg for the glass spheres to 11,200 L/kg for cellulose to 57,000 L/kg for montmorillonite v_x is essentially constant.

The glass sphere data will be refined but it is clear that as simple a particle as can be imagined exhibits the same qualitative and quantitative behavior as more complex polydisperse particle suspensions (clay, quartz, sediment, sludge).

VII. Field Data

The sorption model employed in this project is not just descriptive of laboratory experimental data. Field data for which both total and dissolved concentrations and suspended solids measurements are available also appear ~~to display the particle concentration effect and are in conformity with the~~ particle interaction model prediction, eq. (13). An analysis of STORET heavy metal data is in process. Fig. 13 presents the results for nickel

partition or, more precisely, distribution coefficient for all appropriate STORET-stream data. The distribution coefficients are log averages over one-half log 10 cycles of suspended solids concentration intervals: 3-10, 10-30; 30-100 mg/L etc. The top left panel compares the log mean + log standard deviation to the reversible partition coefficient expression eq. (13). Note that π_{xc} is an order of magnitude larger than that found for montmorillonite but that v_x is essentially the same. The top right panel compares the same data to an equation which includes a lower bound. It fits the data marginally better but does not change the estimates for π_{xc} and v_x . The lower panels compare the behavior of the distribution coefficients to pH and alkalinity. Note that although the trends are in the direction to be expected from conventional theory - increasing sorption with increasing pH and decreasing sorption with increasing alkalinity - the effects are small when compared to the changes that are related to particle concentration effects.

Suitable organic chemical field data are more scarce. Only for PCB's has a substantial quantity of data been accumulated. Fig. 14 illustrates the results. As with the nickel data, these are log averages over one half log cycles in particle concentrations for each data set. Both the field data distribution coefficients and the lab data for hexachlorobiphenyl reversible partition coefficients follow the prediction of the particle interaction model eq. (13). In particular the data from the Black Rock Harbor field sampling after the disposal (LI Sound) is in conformity with the model predictions. Note the significant differences between the laboratory adsorption and the reversible component partition coefficients, indicating the extent of non-reversibility exhibited by short time scale adsorption-desorption.

Further efforts to collect such data sets are planned since the description of field data phase partitioning is a goal of the research. These comparisons illustrate both the utility of the approach and the importance of both laboratory derived experimental information that is used to formulate the model, and the field data analyses that can be made within that framework in order to assess its applicability.

VIII. Research Plan for '84-'85

The final year's effort will be devoted to investigating two principal questions. The first is to establish the isotherm parameters and, most important, the fraction of total heavy metal in sewage sludge and Black Rock Harbor sediment that is desorbable in seawater. Toward this end it is planned to analyze three different sludge samples, one of which is heavily contaminated, and one other sample of dredged material. The procedures we have developed will be applied and the results of the analysis will be the isotherm parameters and the fraction desorbable. Future work would then be required to establish relationships between the isotherm parameters, the desorbable fraction, and the characteristics of the particles and aqueous phases.

The second question to be addressed concerns the behavior of stationary sediments. The hexachlorobiphenyl results suggests that the low particle limit partition coefficient, π_{xc} , is the partition coefficient that applies to stationary sediments. The generality of this result is the topic for this year's investigations. Syringe migration experiments are in progress in order to examine whether in fact the low particle concentration partition coefficient applies to stationary sediments. It is planned to examine both heavy metal and organic chemical migration using this technique. Sewage sludge and Black Rock Harbor sediments will be employed as well as clean sorbents (clay and quartz particles). Seawater will be the aqueous phase and the syringes will be sterilized to prevent microbial activity.

In order to prevent microbial degradation, we will investigate autoclaving as a sterilization method. This appears to be the only feasible method that guarantees sterility. In addition it is not a violent treatment. The temperature and pressure conditions are such that they do not physically disrupt even bacterial cells (H. Pritchard EPA-ERL Gulf Breeze, personal communication). Comparisons using short term adsorption-desorption isotherms with and without autoclaving will be used to confirm that no significant changes in partitioning occurs. The purpose of these syringe experiments is to examine the universality of the particle interaction model prediction that the low particle concentration limit derived from suspension experiments applies to stationary sediments. If this is indeed the case

then the problem of phase partitioning in stationary sediments and in particle suspensions will have been shown to be essentially the same problem, and the progress that has been made in the latter problem (Appendix II) can be applied directly to the stationary sediment issue.

- Fig. 1 Examples of Consecutive Desorption Isotherms
 Nickel-Ridgewood Sludge-Seawater $m = 86,430,860,2590$ mg/L
 Cadmium-Ridgewood Sludge-Seawater $m = 114,570,1140,3400$ mg/L
 Cadmium-Black Rock Harbor Sediment-Seawater $m = 180,690,2080,3470$ mg/L
- Fig. 2 Reversible Component Partition Coefficient versus Particle Concentration
- Fig. 3 Effect of Adsorption Time. Cadmium-Ridgewood Sludge-Seawater. Adsorption time = 1 day (top), 4 day (mid), 7 day (bottom). $m = 114,570,1140,3400$ mg/L
- Fig. 4 Effect of Adsorption Time. Cadmium-Ridgewood Sludge-Seawater. Adsorption time = 18 day (top), 25 day (bottom). $m = 114,570,1140,3400$ mg/L
- Fig. 5 Effect of Adsorption Time. Cadmium-Black Rock Harbor Sediment-Seawater. Adsorption time = 11 day (top), 18 day (mid), 25 day (bottom). $m = 170,690,2080,3470$ mg/L
- Fig. 6 Effect of Desorption Time. Cadmium-Ridgewood Sludge-Seawater. Desorption time = 1 hr. (top), 5 day (mid), 7 day (bottom). $m = 85,425,850,2550$ mg/L
- Fig. 7 Native Metal Desorption. Ridgewood Sludge-Nanopure Water. Desorption time = 1 hr. Copper (top) Chromium (mid), Zinc (bottom). $m = 340,680,1370,2730$ mg/L
- Fig. 8 Native Metal Desorption. Black Rock Harbor Sediment-Borate Buffer. Desorption time = 1 hr. Copper (top) Chromium (bottom). $m = 340,680,1370,2730$ mg/L
- Fig. 9 Native Metal Desorption. Ridgewood Sludge-Nanopure Water. Desorption time = 1 day. Copper (top) Chromium (mid), Zinc (bottom). $m = 340,680,1370,2730$ mg/L
- Fig. 10 Native Metal Desorption. Ridgewood Sludge-1/4 Seawater, 3/4 Nanopure Water. Desorption time = 1 hr. Copper (top), Chromium (mid), Zinc (bottom). $m = 340,680,1370,2730$ mg/L
- Fig. 11 Adsorption Isotherms. Nickel-Borate-Glass Spheres. Particle concentrations as indicated.
- Fig. 12 Reversible Component Partitioning. π_x versus m (top). Normalized Partition Coefficient versus normalized particle concentration (bottom).

Fig. 13 Nickel Distribution Coefficient versus Particle Concentration.
STORET stream data, log mean \pm log std. deviation No. of data point
indicated.

Fig. 14 PCB Distribution Coefficient versus Particle Concentration.

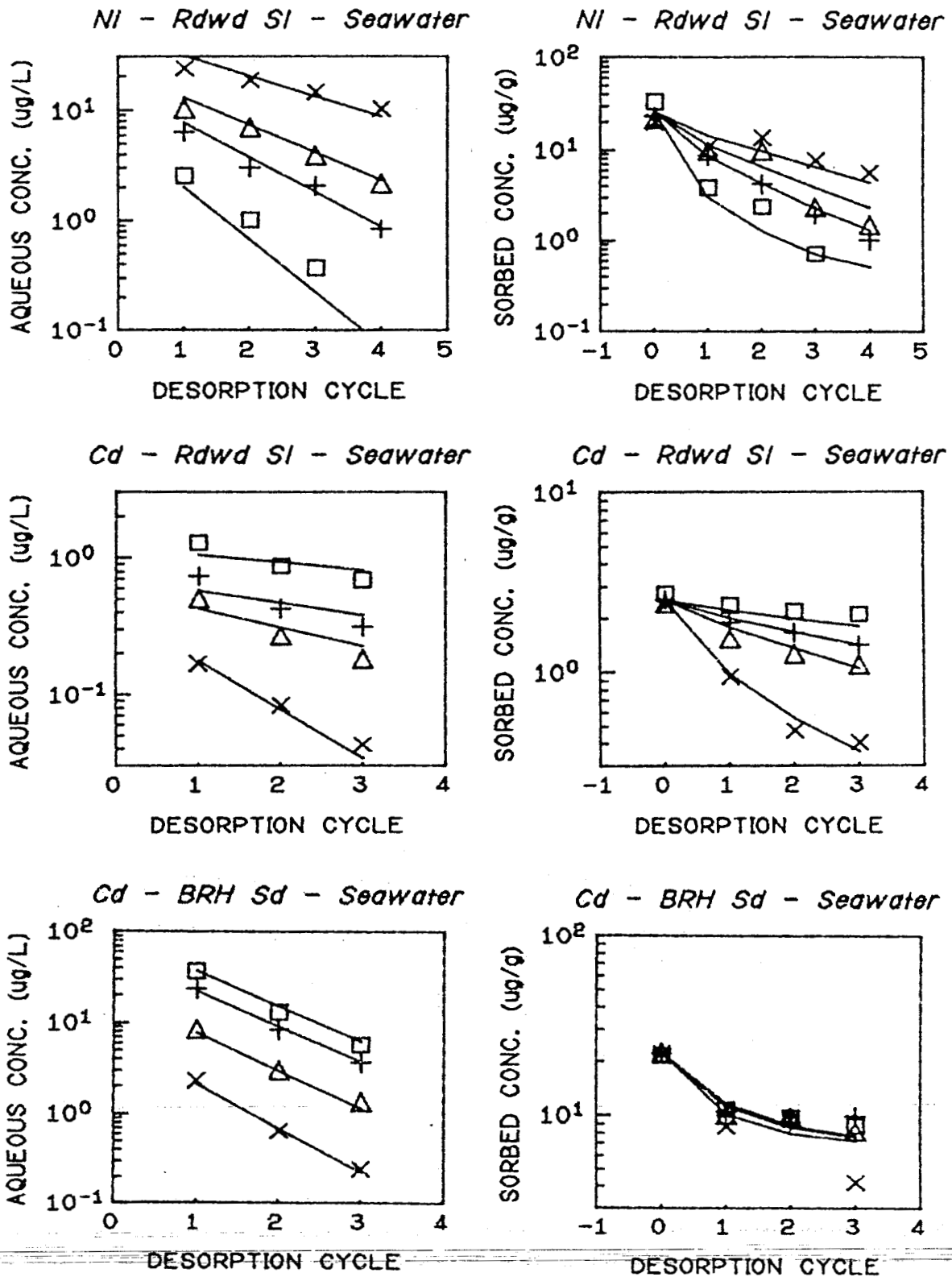
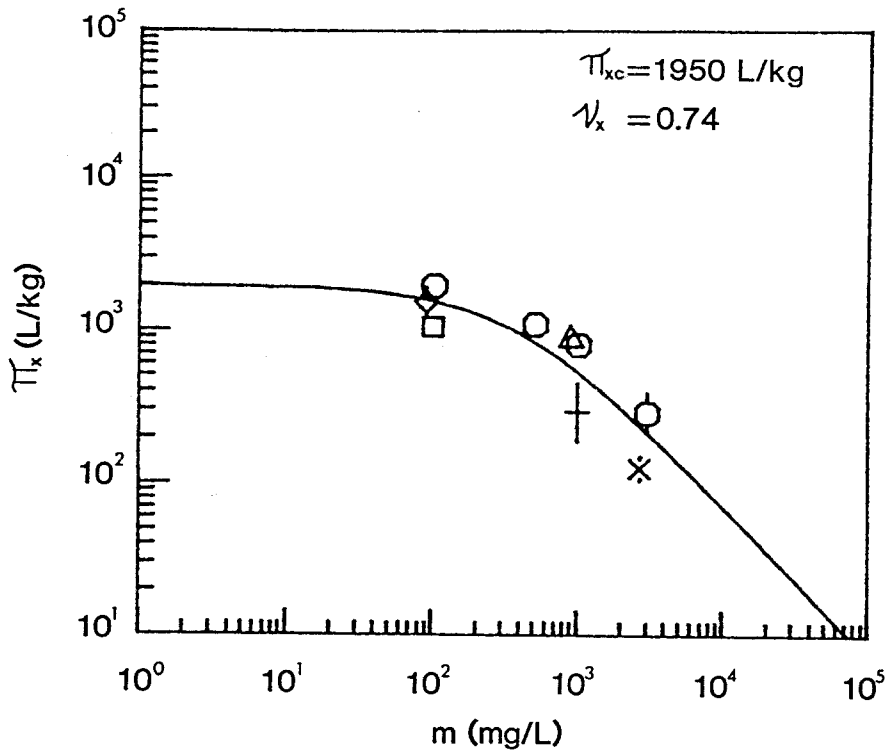


Fig. 1. Examples of Consecutive Desorption Isotherms - Nickel-Ridgewood Sludge-Seawater $m = 86,430,860,2590$ mg/L, Cadmium-Ridgewood Sludge-Seawater $m = 114,570,1140,3400$ mg/L, Cadmium-Black Rock Harbor Sediment-Seawater $m = 180,690,2080,3470$ mg/L

Ni⁶³ - SLUDGE - SEAWATER



Cd¹¹⁵ - SLUDGE - SEAWATER

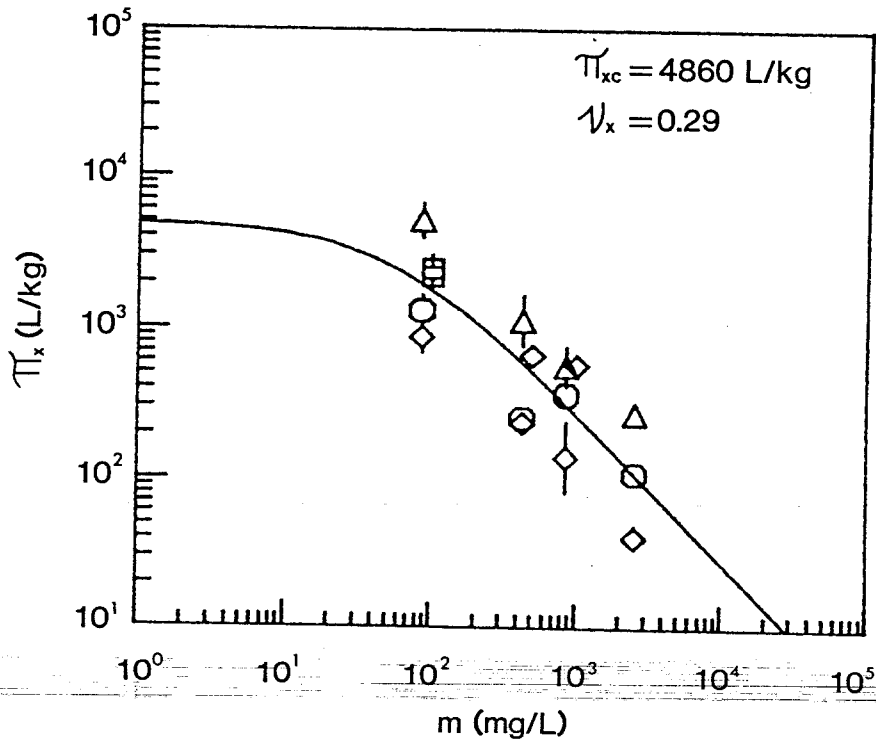


Fig. 2. Reversible Component Partition Coefficient versus Particle Concentration

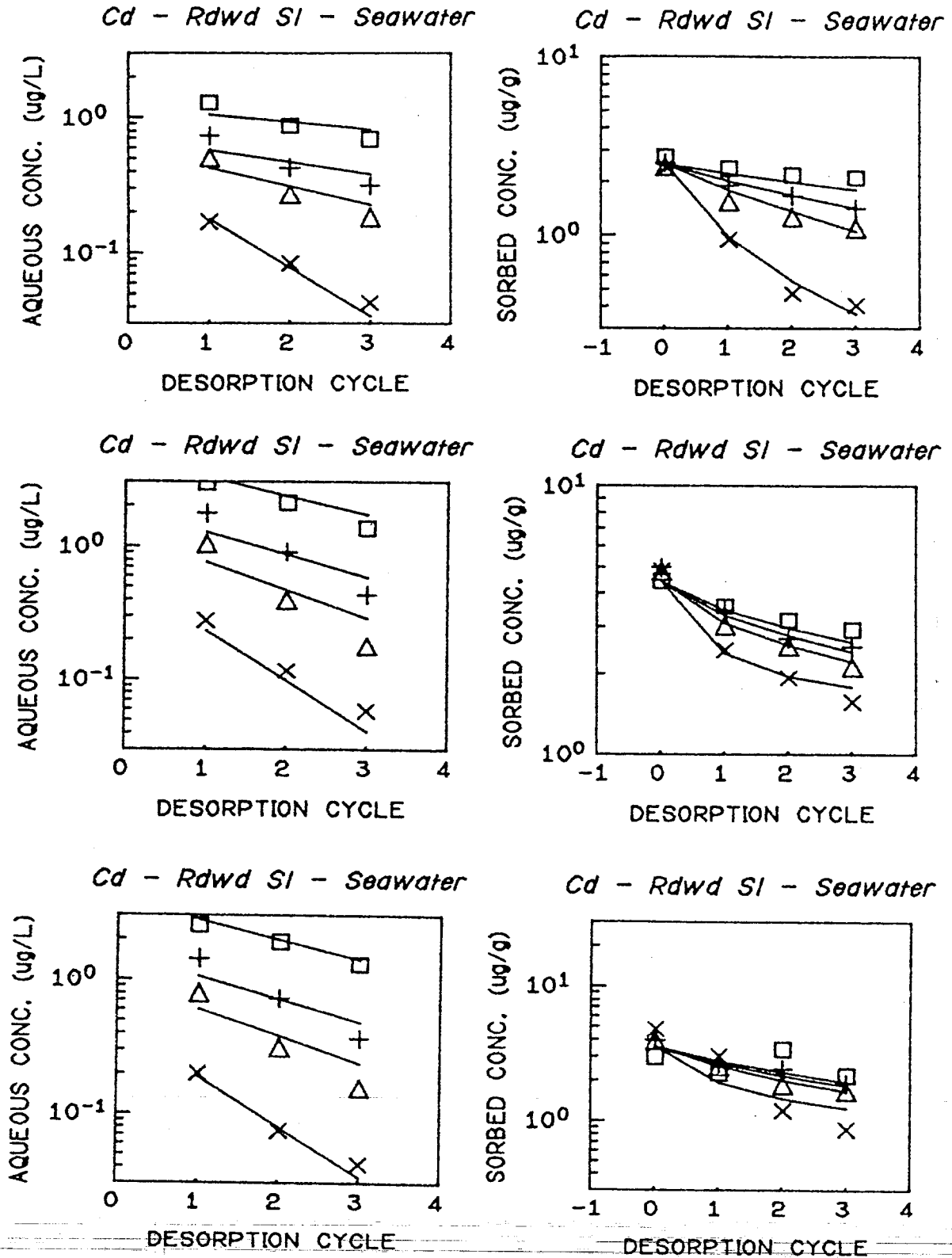


Fig. 3. Effect of Adsorption Time. Cadmium-Ridgewood Sludge-Seawater. Adsorption time - 1 day (top), 4 day (mid), 7 day (bottom). $m = 114,570,1140,3400 \text{ mg/L}$

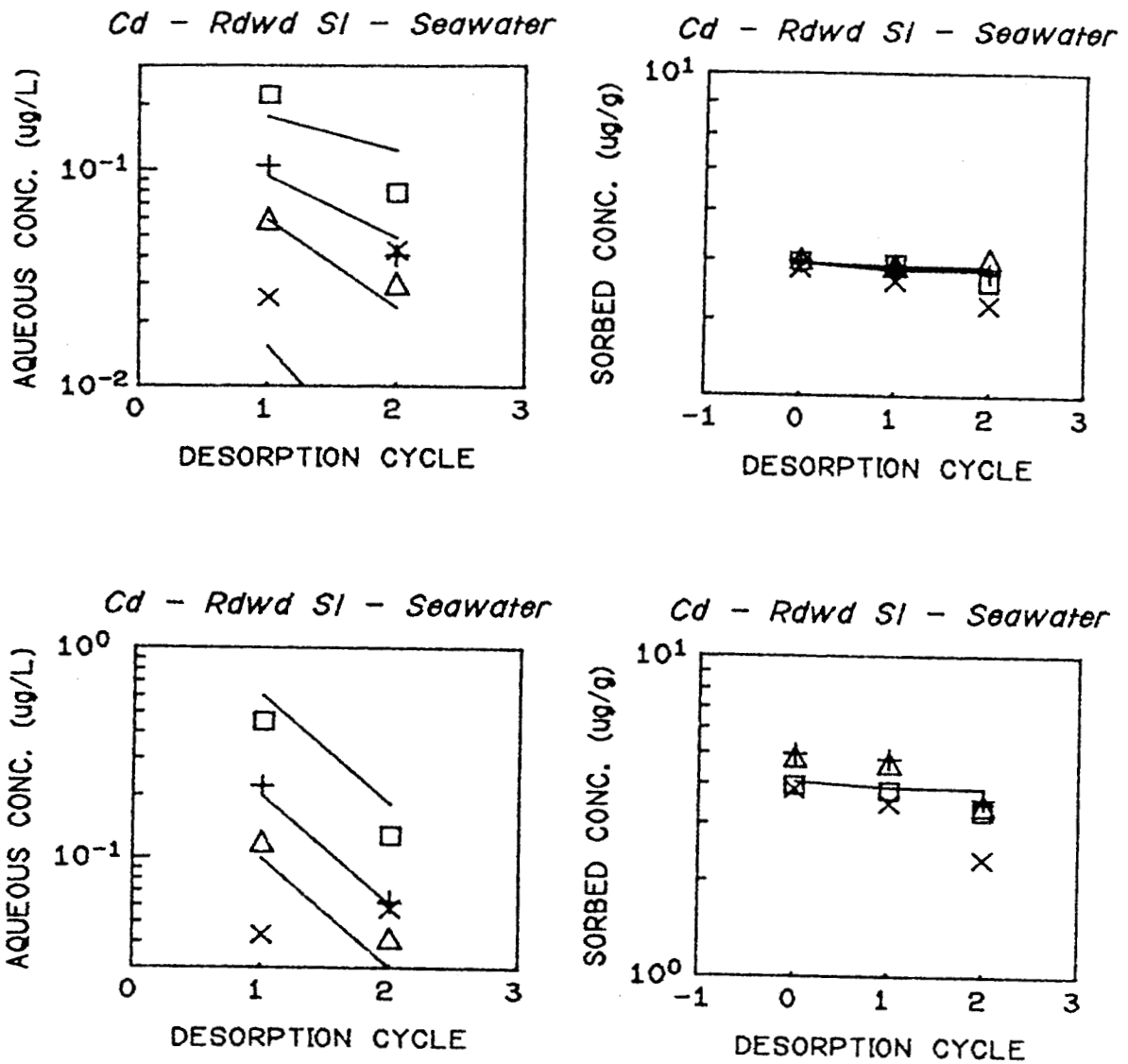


Fig. 4. Effect of Adsorption Time. Cadmium-Ridgewood Sludge-Seawater. Adsorption time = 18 day (top), 25 day (bottom), $m = 114,570, 1140,3400 \text{ mg/L}$

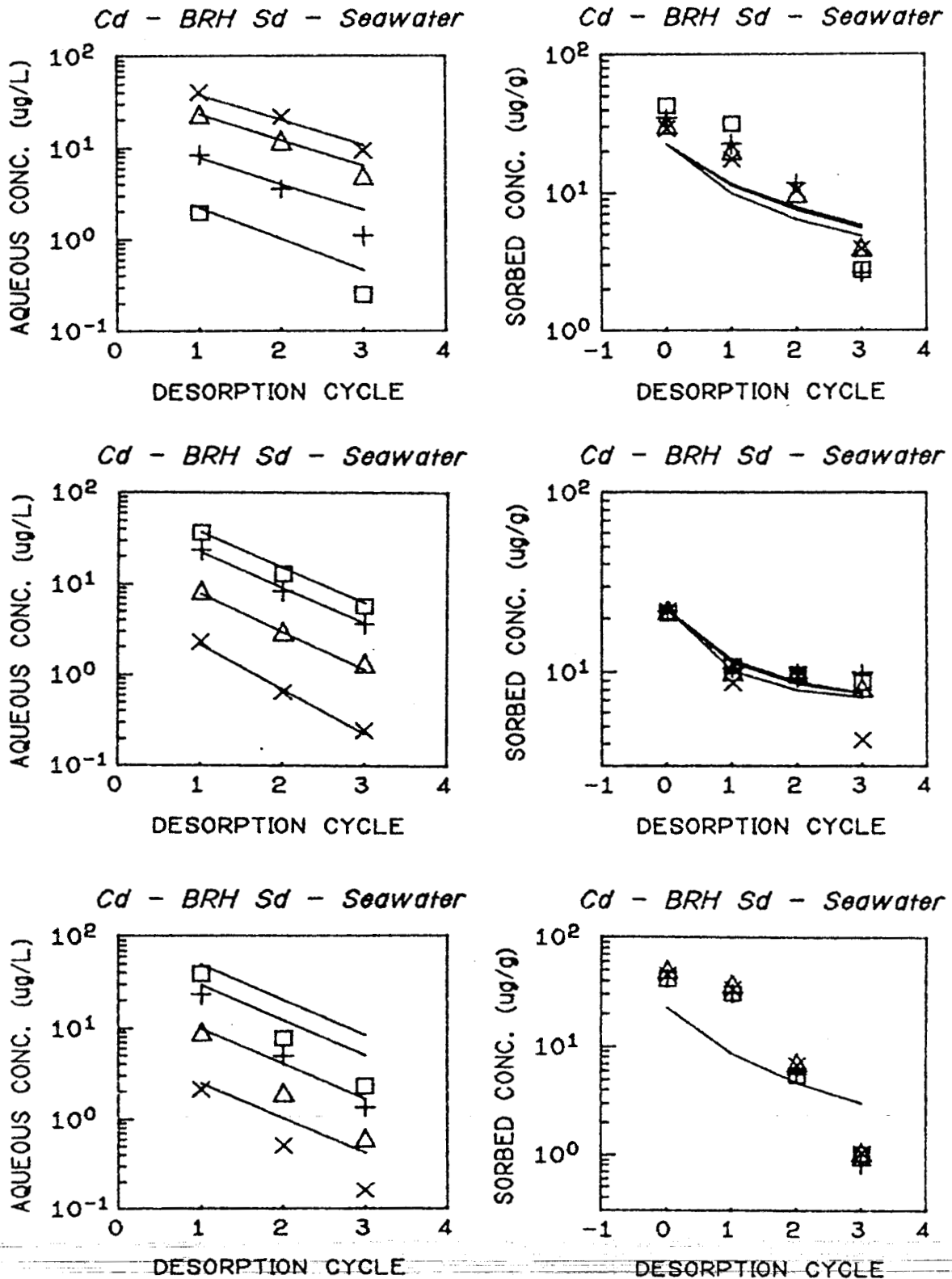


Fig. 5. Effect of Adsorption Time. Cadmium-Black Rock Harbor Sediment-Seawater. Adsorption time = 11 day (top), 18 day (mid), 25 day (bottom). $m = 170, 690, 2080, 3470$ mg/L.

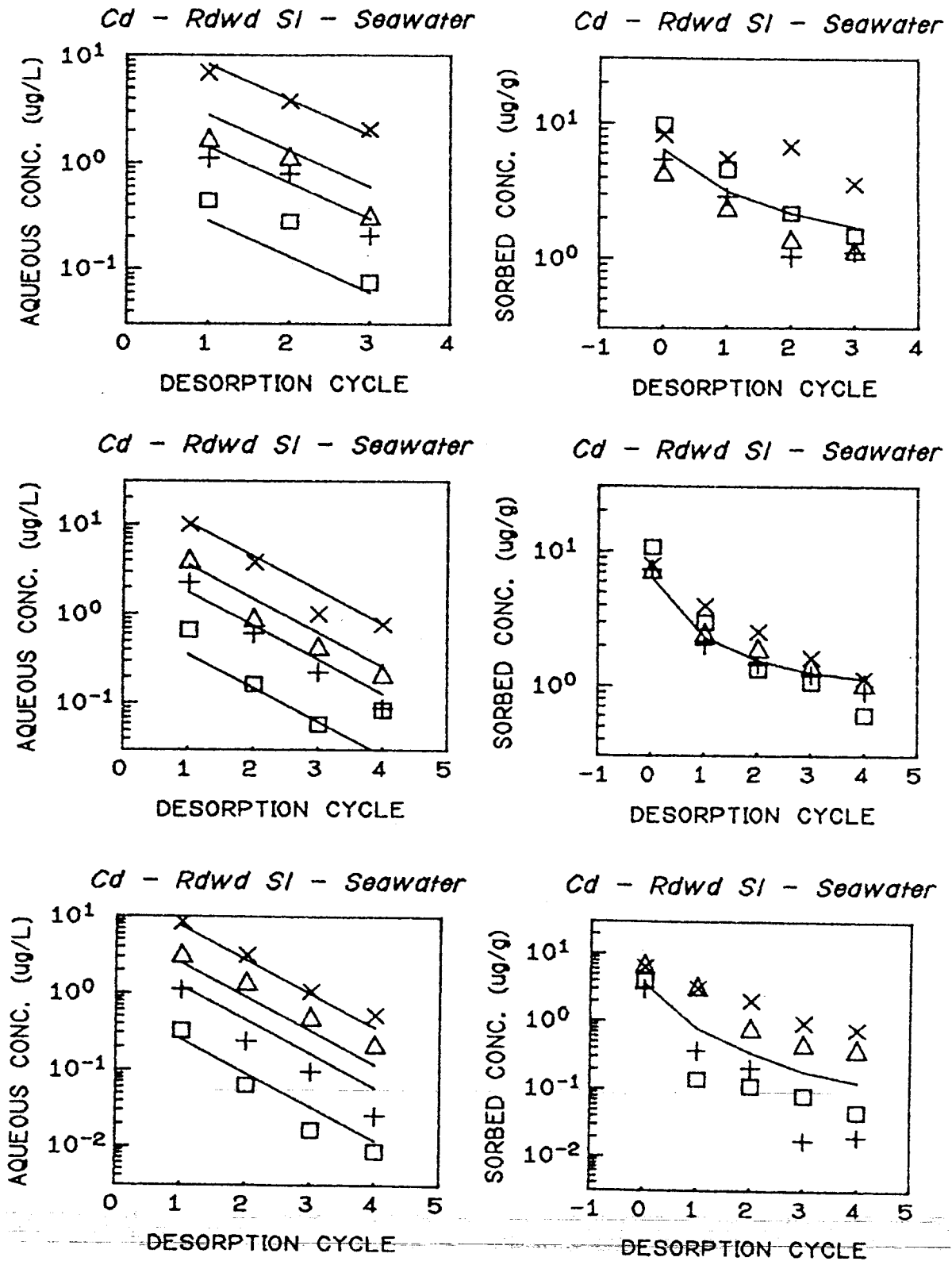


Fig. 6. Effect of Desorption Time. Cadmium-Ridgewood Sludge-Seawater. Desorption time = 1 hr. (top), 5 day (mid), 7 day (bottom). $m = 85,425,850,2550 \text{ mg/L}$.

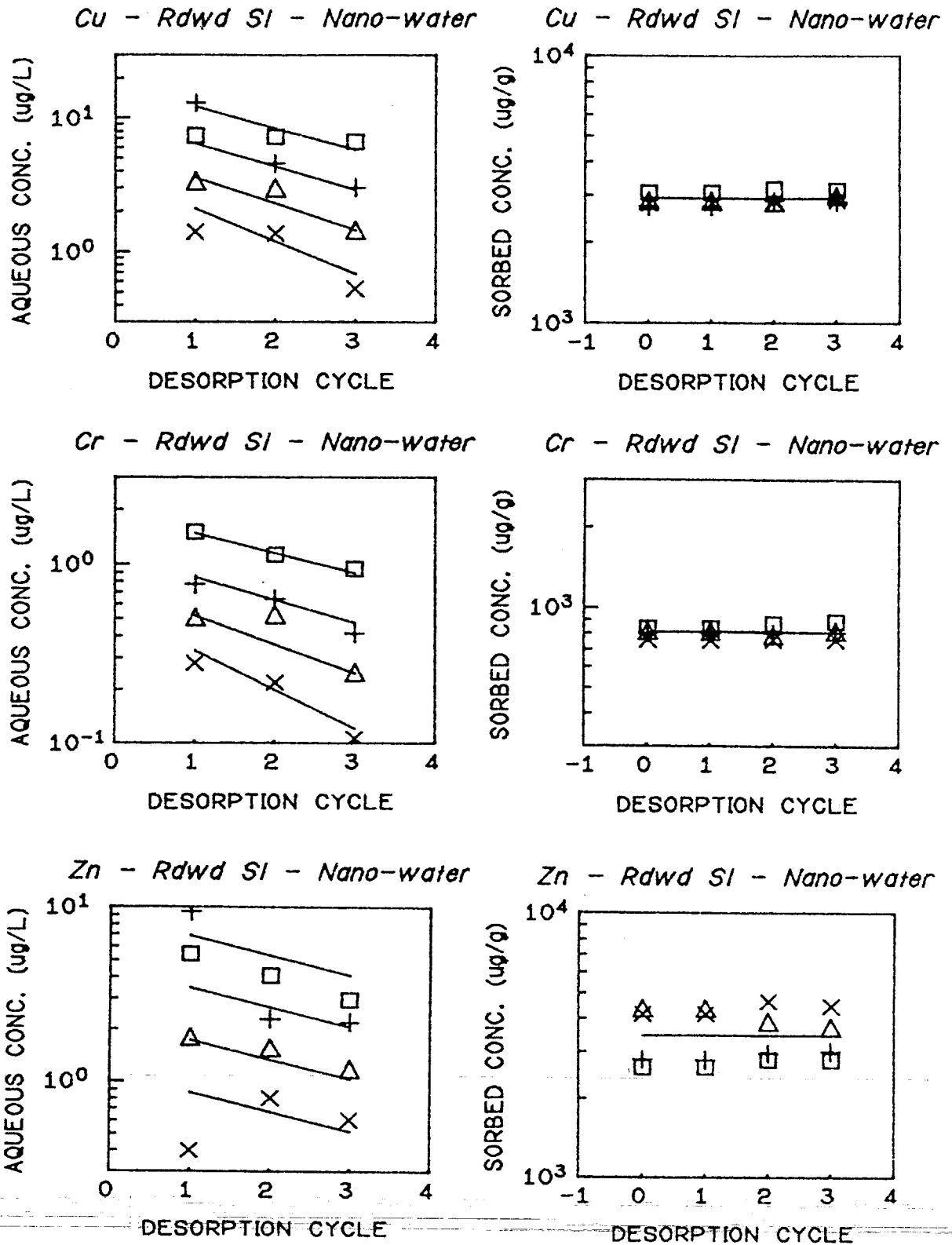


Fig. 7. Native Metal Desorption. Ridgewood Sludge-Nanopure Water. Desorption time = 1 hr. Copper (top) Chromium (mid), Zinc (bottom). $m = 340,680,1370,2730$ mg/L.

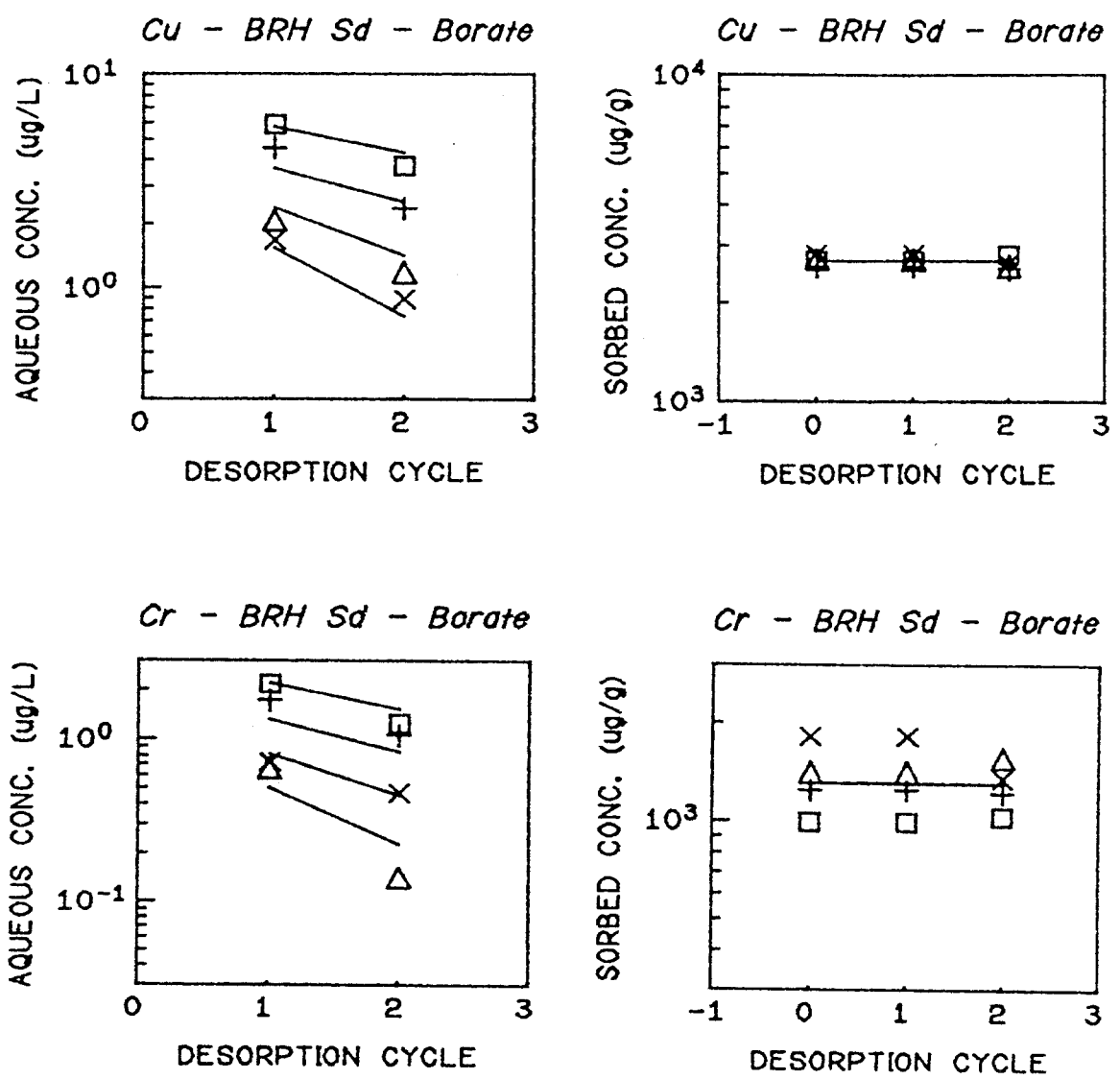


Fig. 8. Native Metal Desorption. Black Rock Harbor Sediment-Borate Buffer. Desorption time = 1 hr. Copper (top) Chromium (bottom). $m = 340, 680, 1370, 2730$ mg/L.

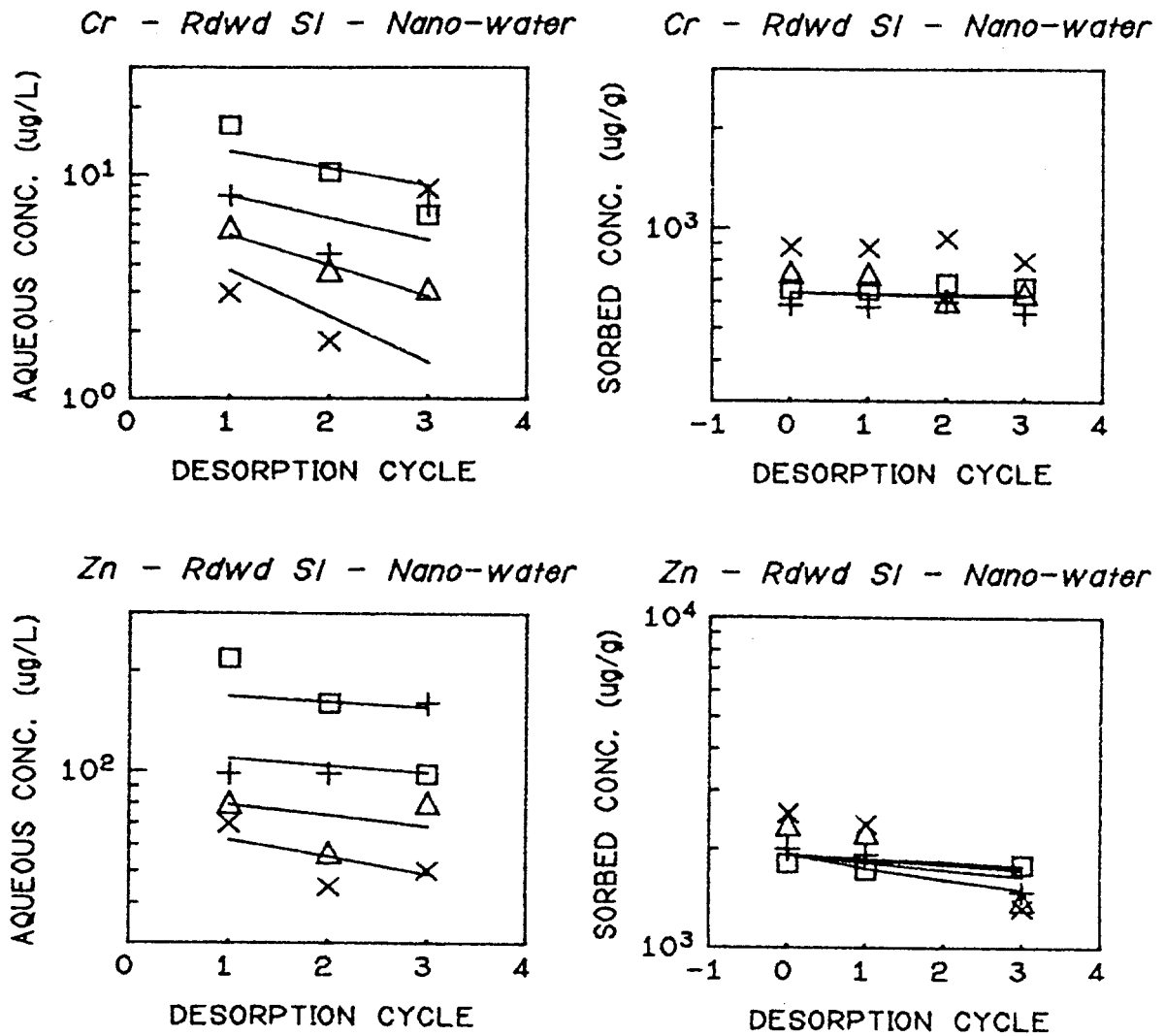


Fig. 9. Native Metal Desorption. Ridgewood Sludge-Nanopure Water. Desorption time = 1 day. Copper (top) Chromium (mid), Zinc (bottom). $m = 340,680,1370,2730$ mg/L.

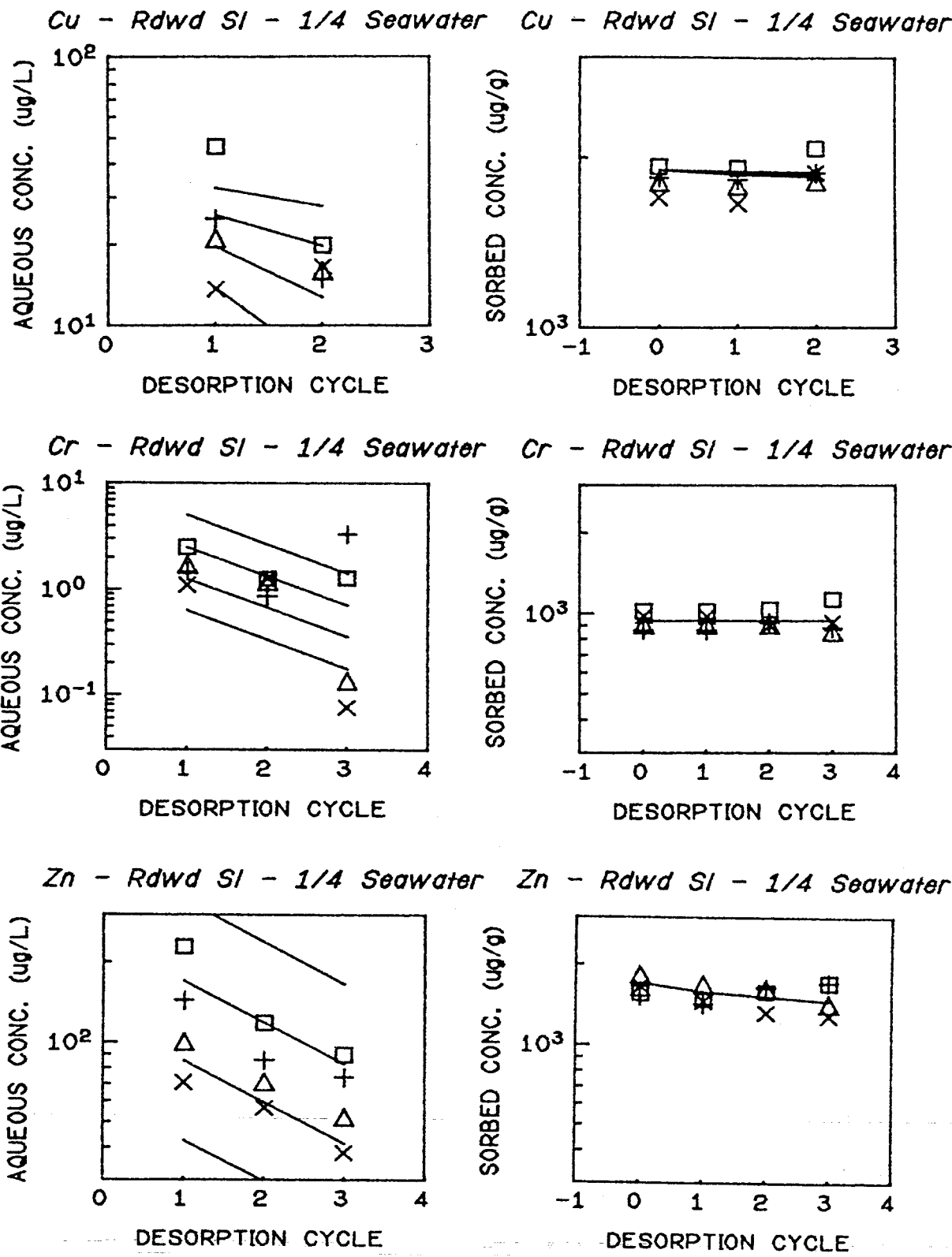
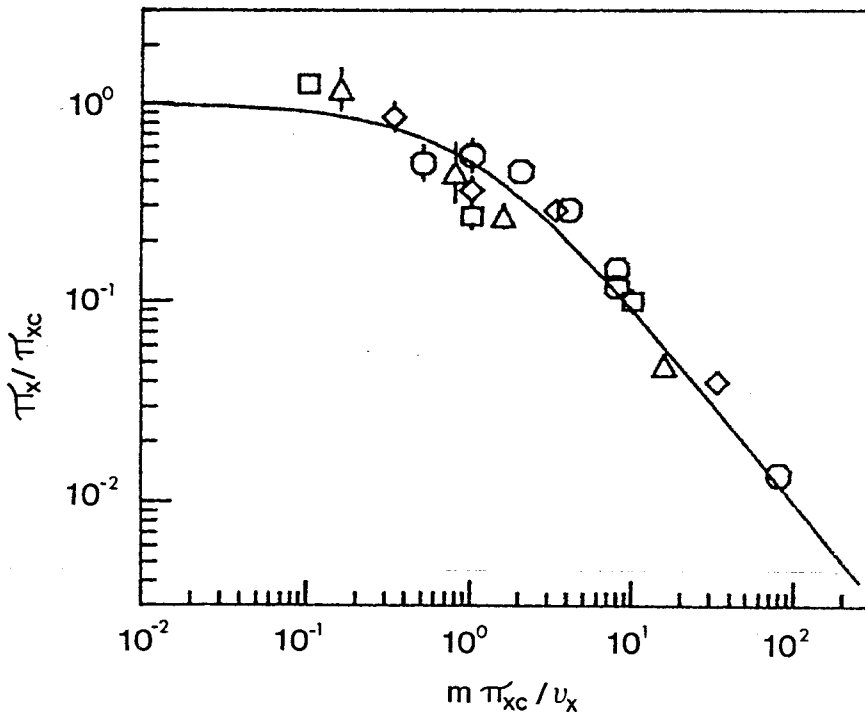
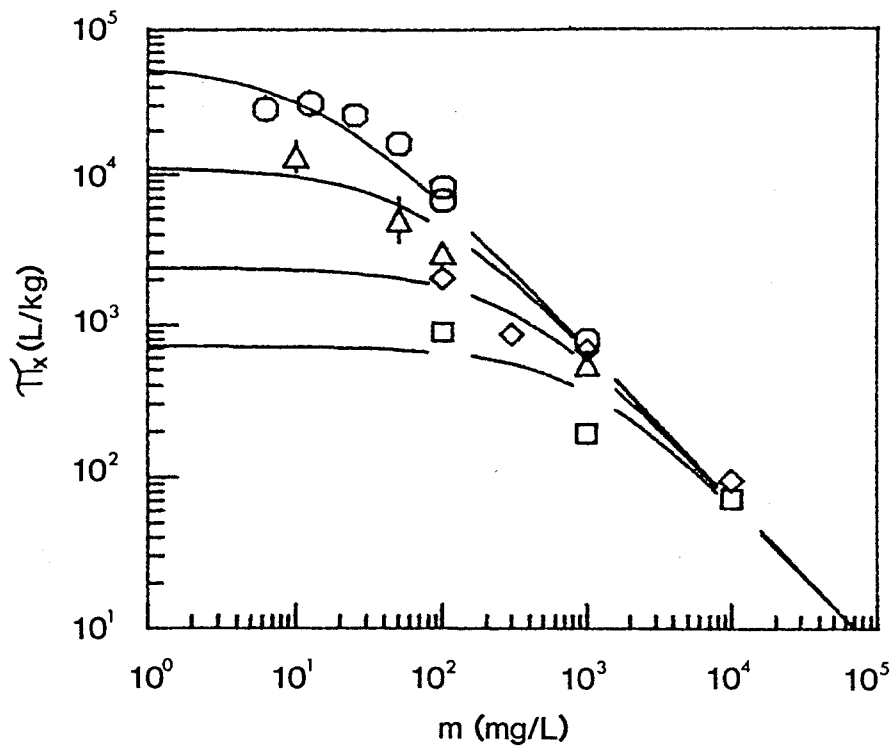


Fig. 10. Native Metal Desorption. Ridgewood Sludge-1/4 Seawater, 3/4 Nanopure Water. Desorption time = 1 hr. Copper (top), Chromium (mid), Zinc (bottom). $m = 340,680,1370,2730$ mg/L.

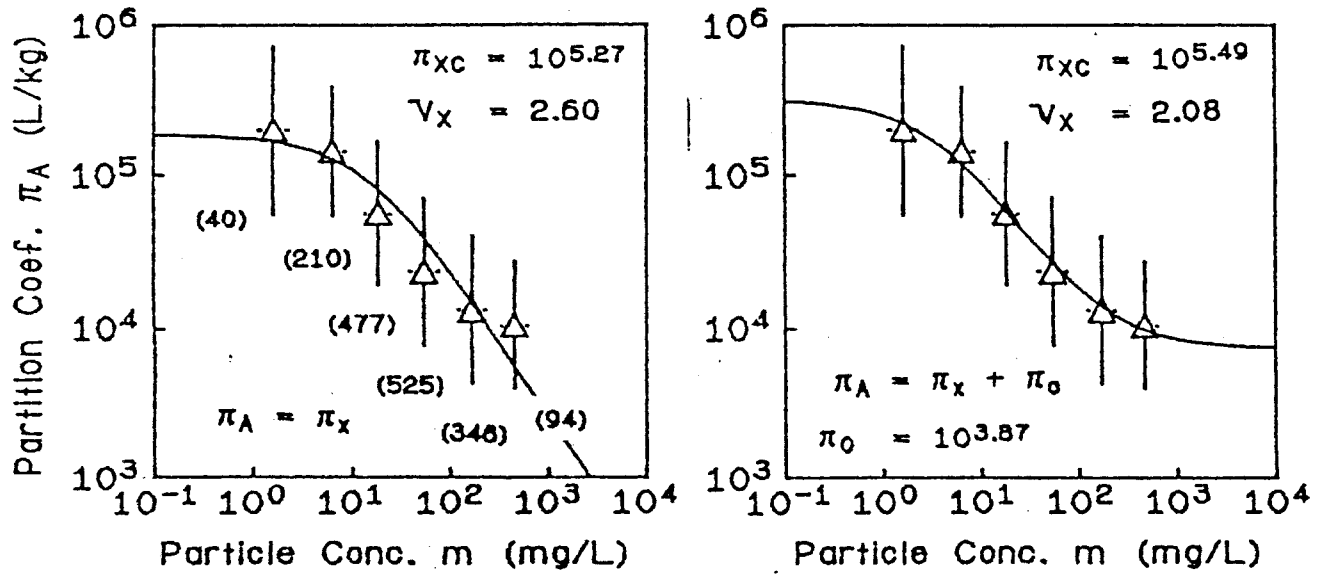


□ GLASS SPHERES △ CELLULOSE ◇ SILICA ○ CLAY

Fig. 12. Reversible Component Partitioning. π_x versus m (top). Normalized Partition Coefficient versus normalized particle concentration (bottom).

*Ni Partition Coefficient
STORET DATA - Streams*

Effect of Particle Conc.



Effect of Chemical Variables

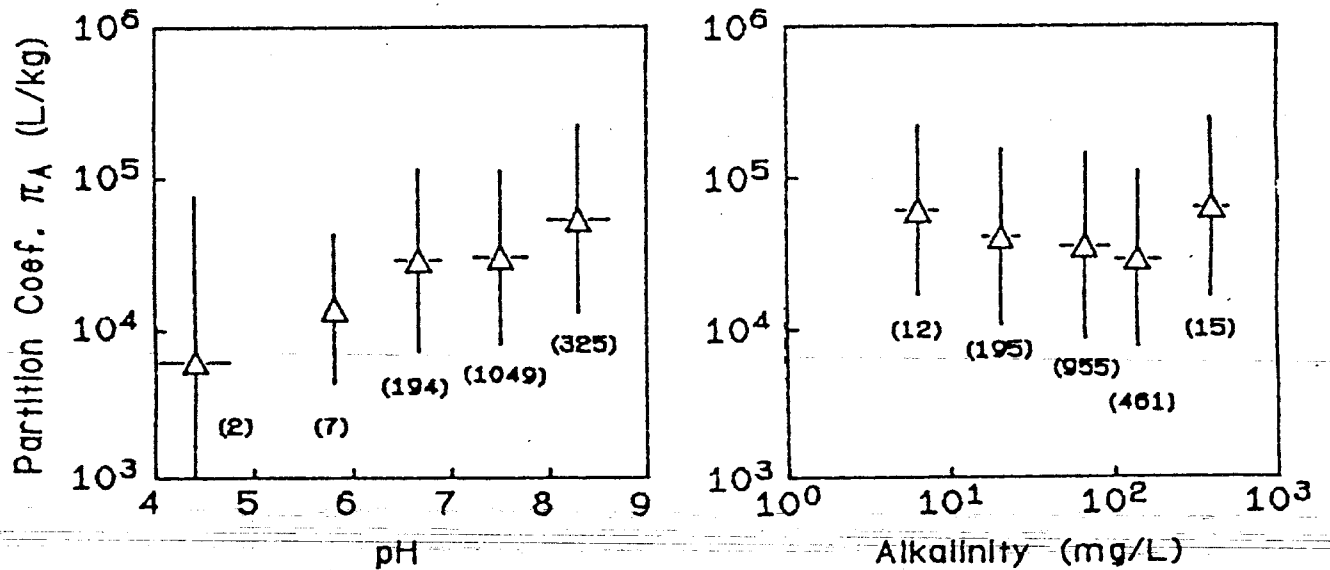


Fig. 13. Nickel Distribution Coefficient versus Particle Concentration. STORET stream data, log mean \pm log std. deviation No. of data point indicated.

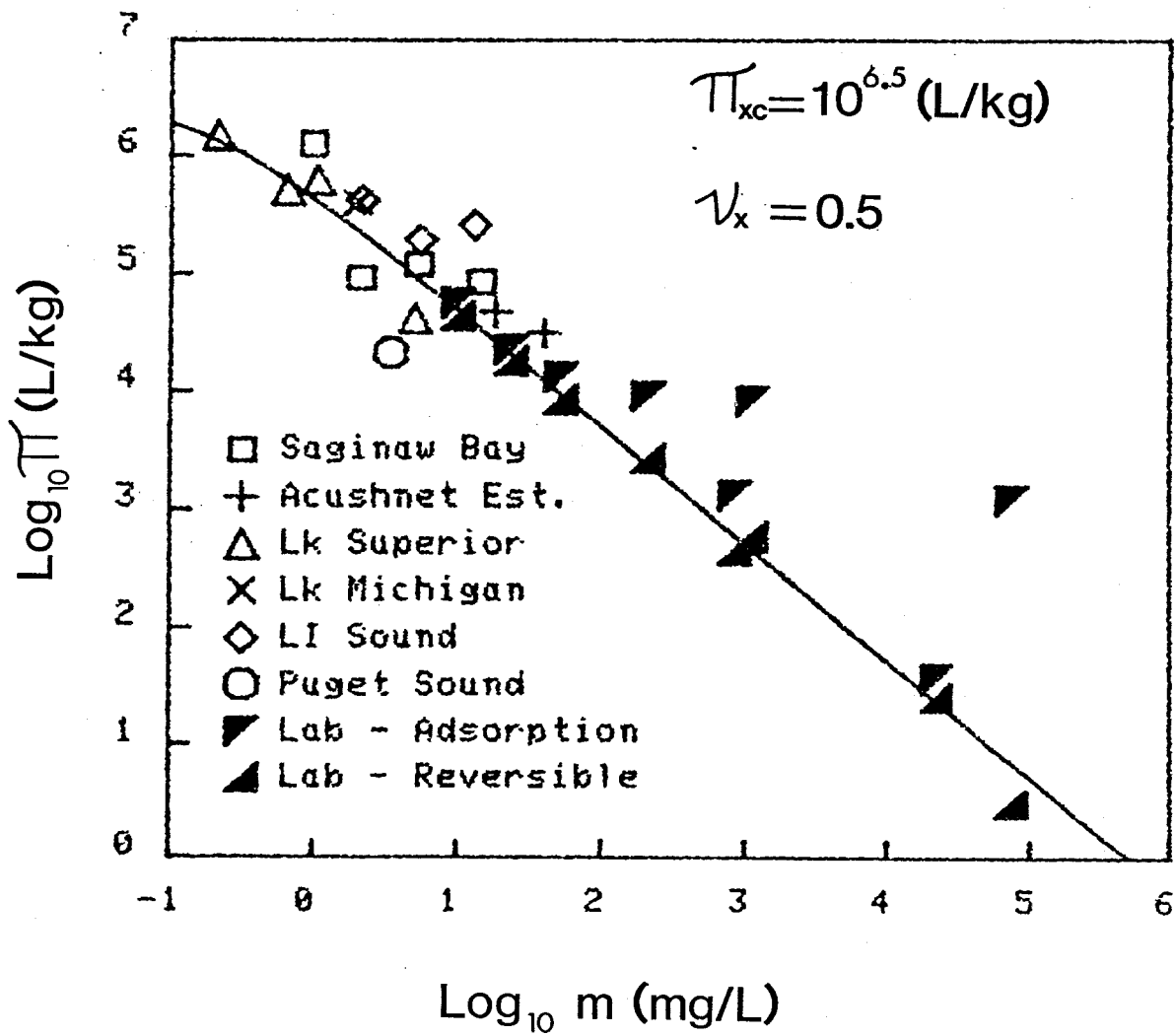


Fig. 14. PCB Distribution Coefficient versus Particle Concentration.

APPENDIX I

The Effects of Nonreversibility,
Particle Concentration, and Ionic Strength
on Heavy Metal Sorption

Dominic M. Di Toro
John D. Mahony
Paul R. Kirchgraber
Ann L. O'Byrne
Louis R. Pasquale
Dora C. Piccirilli

Environmental Engineering and Science Program
and
Chemistry Department
Manhattan College, Bronx, N.Y. 10471

June 1984

Introduction

The extent of heavy metal sorption is a critical component in the evaluation of their fate in natural water systems. Adsorption at trace concentrations is usually quantified using a linear isotherm parameterized by a distribution or partition coefficient, π , which is the slope of the isotherm. It is well established that the magnitude of the partition coefficient is a function of particle properties such as particle size (1), the nature of the oxide coating (2), organic carbon content (3), zero point of charge (4); and of chemical variables such as pH (5), ionic strength (6), and the concentration of complexing ligands (7,8). Such effects can usually be rationalized within the frameworks of solution and surface chemistry.

Less well understood is the desorption reaction. The conventional desorption tests for heavy metals are extractions using concentrated solutions of various ionic compositions (9-10) rather than adsorbate-free aqueous phase. For example after adsorption in freshwater, mixtures of freshwater and seawater are used to simulate the desorption that might occur at freshwater-estuarine transition zones (11). This is in contrast to the usual desorption tests for organic chemicals in which the same aqueous phase is used in both the adsorption and desorption steps of the experiment and which provides a direct test of reversibility.

Heavy metal desorption into various extraction solutions has been found to be incomplete, suggesting that the reaction is not completely or even moderately reversible (e.g. 12). The usual finding is that substantial quantities of the heavy metals remain associated with the particle even at extractant concentrations ($\sim 0.1M$) which should displace all the physically

adsorbed metal (see Forstner and Wittman, 13, for a review and other references). A review of the applicable desorption literature (11-22) indicates that there are almost no published heavy metal data which include adsorption and desorption isotherms using the same aqueous phase that would be suitable for testing the extent of reversibility in environmentally realistic aqueous phases.

Data for nickel and cobalt montmorillonite sorption are presented below which demonstrate that reversibility is not complete and varies as a function of chemical (pH and ionic strength) and physical (particle concentration) variables. A method for analyzing adsorption-single desorption isotherms which yields the partition coefficients of the reversible and resistant components (23) is applied in order to isolate the behavior of the reversibly sorbed heavy metal.

Perhaps the most puzzling phenomenon exhibited by heavy metal and organic chemical partitioning is the effect of the particle concentration itself. Of course the extent of sorption, that is the fraction of chemical in the sorbed state, increases with increasing particle concentration. However it has been noted that the partition coefficient tends to decrease with increasing particle concentration (24), in some cases quite dramatically. It is as if, for the analogous partitioning in gas-water systems, the Henry's constant is dependent upon the volume of the gas phase. Since such behavior has not been noted for other phase distribution coefficients a certain amount of skepticism attends these observations in particle-water systems. Although the effects of particle concentration on the partition coefficient are not infrequently noted for various heavy metal-sorbent systems in a wide variety of settings (25,26,27) they are usually explained as either experimental artifacts, or as the result of an improper chemical system descrip-

tion which ignores, for example, the presence of other important but unobserved phases such as colloidal particles or dissolved organic carbon (28).

We present below the results of simple resuspension and dilution experiments that strongly suggest the effect is due to particle interactions and not experimental artifacts or hidden variable fluctuations. An equation derived from this hypothesis describes the experimental data from a number of sorbate-sorbent systems. The model suggests that the classically conceived partition coefficient is indeed descriptive of reversible sorption at low particle concentrations but that as particle concentration is increased above a certain concentration, which is chemical and sorbent specific, the reversible partition coefficient starts to decrease and its magnitude is dependent only on particle concentration and independent of the specific sorbate-sorbent or auxiliary aqueous phase parameters such as ionic strength. It is suggested that physical rather than chemical factors are controlling in this regime.

We begin by examining the effects of the usual experimental variables, sorption time and pH, and then proceed to the particle concentration effects. Additional experiments at varying ionic strengths provide further insight into the influence of particle concentration.

Methods and Materials

Initial experiments indicated that buffered aqueous phases are necessary since pH cannot be controlled in the usual fashion by addition of acid or base to the reactors during equilibration. The reasons are that a desorption step must follow the adsorption equilibration which requires that

the vessel be a centrifuge tube making pH adjustments difficult and requiring multiple vessels for an isotherm. The inconvenience of this procedure prompted the use of buffers.

Both inorganic (borate, carbonate) and organic (sulphonic acid) buffers that were found to be noncomplexing with respect to nickel were used for the experiments. Differential Pulse Polarographic analysis was employed to measure the presence of any complexation between the metal and these buffers. No change in the half wave potential for the metal ion alone compared with that for the metal ion in the presence of the buffer was observed. It is significant to note that this method is somewhat more sensitive than those previously used for this purpose (29). In fact we have measured metal binding constants for systems previously reported to be negligible, e.g. for copper and EPPS (29), $K_f = 10^3$. Finally the similar adsorption-desorption results obtained using quite different buffers suggest that complexing is not occurring to a significant extent. This is discussed in detail below.

Adsorption-desorption isotherms were obtained by the following procedure. The aqueous phase, containing buffered distilled water and metal of known concentration tagged with ^{65}Ni or ^{60}Co , was combined with montmorillonite or quartz particles to a volume of 9 ml in a 20 ml centrifuge tube. The sorbents employed were montmorillonite (Wards Scientific) and 5 μm α -quartz particles (Min-U-Sil 5, Penn. Glass Sand Corp.). The former was chosen for its high sorptive capacity and the latter for its uniform particle size distribution and well understood surface chemistry. The initial metal concentration in the systems ranged from 200 to 3.3 $\mu\text{g/L}$; the sediment concentrations studied were 5, 10, 30, 100, 300, and 1000 mg/L for montmorillonite and 200-10,000 mg/L for quartz. The buffers were kept at the mini-

mum effective level to maintain pH during the course of the experiment (10^{-3} M). The following buffers were employed: bicarbonate (pH 7), TAPS (29) (pH 8), borate (pH 8-10), and carbonate (pH 10-11). The capped tubes were agitated until adsorption equilibrium was reached. A sample of the sediment-aqueous phase mixture is removed and the total metal concentration, c_{Ta} , was determined by liquid scintillation counting. The system was then centrifuged (6000-12,000g for 15-20 min) and the metal concentration of the aqueous phase, c_a , was similarly determined. The sorbed concentration at adsorption equilibrium is calculated by difference: $r_a = (c_{Ta} - c_a)/m$, where m is the adsorbent concentration.

For desorption steps, the contaminated aqueous phase is carefully removed leaving the sedimented solids in the tube, and uncontaminated aqueous phase is added to achieve a total volume that produces the same particle concentration as initially present at adsorption. The capped tube is agitated until desorption equilibrium is achieved. A sample of sediment-aqueous phase mixture is removed and analyzed yielding c_{Td} . After centrifugation an aqueous phase sample is removed and analyzed for c_d . The sorbed concentration is obtained by difference, $r_d = (c_{Td} - c_d)/m$.

In order to check our experimental procedures we have examined the behavior of particle-free but otherwise identically configured experiments and found no evidence of precipitation. No adsorption-desorption differences were found if preceding the adsorption step, a particle agitation, centrifugation, and resuspension are performed. Thus the particle separation is efficient in the sense that only an insignificant fraction of sorbing particles are not removed by the centrifugation.

Analysis Framework

The two component model of adsorption-desorption is designed to interpret incompletely reversible behavior illustrated in Fig. 1 as linear and logarithmic plots of isotherm data. Sorbed chemical at adsorption equilibrium, r_a , is assumed to be the sum of a reversibly sorbed component described by a linear isotherm: $r_x = \pi_x c$, and a resistant component that adsorbs following a linear adsorption isotherm: $r_o = \pi_o c_a$ but resists desorption over the time periods characteristic of experimental desorption equilibration (hours to days). Fig. 2 illustrates the model framework. From the assumption of two components it follows that for adsorption, $r_a = (\pi_x + \pi_o)c_a = \pi_a c_a$ so that the conventional adsorption partition coefficient, π_a , is the sum of the reversible and resistant component partition coefficients. During desorption, only the reversible component interacts with the solution phase following linear desorption isotherms, all with slope π_x . For each pair of adsorption, r_a, c_a and desorption, r_d, c_d concentrations it is possible to calculate the resistant component concentration by extrapolating the consecutive desorption isotherm to zero aqueous concentration:

$$r_o = (r_d - \beta r_a)/(1 - \beta) \quad (1)$$

where $\beta = c_d/c_a$ and to calculate, by difference, the reversible component concentrations $r_{xa} = r_a - r_o$ and $r_{xd} = r_d - r_o$ at adsorption and desorption equilibrium respectively. The lower panels of fig. 2 illustrate an example of the resulting component concentrations calculated in this way and their conformity to linear isotherms. The component partition coefficients can also be calculated from the adsorption, π_a , and single desorption "partition coefficient", π_d , using the relationships (23):

$$\pi_x = \frac{\pi_a}{1 + m(\pi_d - \pi_a)} \quad (2)$$

$$\pi_o = \pi_a - \pi_x \quad (3)$$

where π_a and π_d are the slopes of the linear isotherms (fig. 1). These equations require that no adsorption or desorption occurs from the vessel during desorption. The mass balance requirement is:

$$mr_a = c_d + mr_d = c_{Td} \quad (4)$$

where m is the particle concentration. Fig. 3 presents the comparison for the data to be used subsequently. The histogram of the relative error = $100\% (mr_a - c_{Td})/c_{Td}$ illustrates conformity to this assumption within $\pm 20\%$.

For each experimental condition a complete adsorption and desorption isotherm is generated, 4 to 8 duplicated concentrations over the range 3.5-200 $\mu\text{g/L}$, from which the partition coefficients are determined as the log average of the ratios: $\pi_a = r_a/c_a$, $\pi_d = r_d/c_d$. Equations (2-3) are used to compute π_x and π_o . The experimental log standard deviations are used to compute the log standard errors of π_a , π_x and π_o which are presented in the subsequent figures as error bars if they exceed the symbol size.

Kinetics

The kinetics of metal sorption are usually found to be rapid (30). For the nickel-montmorillonite-borate system both adsorption and desorption kinetics were examined by generating isotherms at varying adsorption, t_{ads} , and desorption, t_{des} , times.

The partition coefficients for varying adsorption times are shown in fig. 4. No significant change in π_a is observed for adsorption times of up

to 5 days. Some suggestion of increasing irreversibility as t_{ads} increases can be seen from the decreasing π_x and the increasing ratio $\pi_o^* = \pi_o/\pi_a$ which is the resistant component fraction: r_o/r_a , but the trend is not consistent.

A more important question is the effect of increasing desorption time, t_{des} , since incomplete reversibility may be the result of insufficient desorption time. Fig. 4 illustrates the results of increasing desorption time after a fixed $t_{ads} = 1$ hr. adsorption. The adsorption partition coefficient, π_a , variations are due to experimental fluctuations of the replicate isotherms. No significant change in π_x or π_o^* is seen to occur for up to $t_{des} = 5$ days. Hence the component concentrations seem to be in metastable equilibrium for time scales of up to 5 days. In summary no substantial kinetic effects were observed with the possible exception of an increase in the resistant component partition coefficient at longer adsorption times. At long desorption times incomplete reversibility persisted.

Effect of pH and Buffering

The strong effect of pH on metal adsorption is well known and the subject of numerous experiments and models (5,6,31,32). The usual focus is the shape of the curve of percent metal sorbed versus pH and, in particular, the pH at which adsorption begins. Since sorption is only important at a pH above this "pH edge", we concentrated at pH values above the edge and at low montmorillonite concentrations, $m = 100$ mg/l. Full adsorption-desorption isotherms were generated using different buffers in order to detect possible complexing effects. The results, shown in fig. 5, suggest a slight decrease in π_a and π_x , together with an increase in resistant component frac-

tion, π_o^* , at pH \sim 9.5 which corresponds to the pK of $\text{Ni}(\text{OH})^+$ (33). Less extensive cobalt data exhibit the reverse trend with increasing π_a and π_x between pH 8 and 9 and no significant change in resistant fraction.

In summary, no major pH effects were noted for either nickel or cobalt. Significant (20-60%) nonreversibility persisted throughout the pH range investigated with no apparent complexing effects due to the buffers.

Particle Concentration Effects: Isotherms, Resuspension and Dilution Experiments

In contrast to the effects of kinetics and pH, a significant relationship exists between partition coefficients and montmorillonite or quartz concentration. Adsorption isotherms at pH = 9 (borate) for Ni-clay at $m = 30 - 1000$ mg/L, cobalt-clay for $m = 100$ and 1000 mg/L, and Ni-quartz for $m = 600$ and $10,000$ mg/L, fig. 6, clearly show the effect of varying particle concentration.

The inverse relationship found between particle concentration and partition coefficient is certainly a most unexpected result and additional experiments were performed in order to rule out any artifacts. The most popular explanation of this phenomenon is to invoke an additional complexing agent associated with the particles which experimentally appears to be dissolved - it is not removed by the particle separation technique - but actually complexes (if it is a ligand such as dissolved organic carbon (28)) or sorbs (if it is colloidal particles (27)) some dissolved chemical. If it is assumed that the concentration of the third phase increases with the concentration of added particles then in fact an apparent reduction in partition coefficient is predicted with increasing particle concentration since the experimentally determined "dissolved" concentration is actually the sum of

the truly dissolved, and the additional sorbed or complexed chemical.

The experiments described below were designed to specifically exclude an additional complexing agent as an explanation. The design was based upon the desire to change only the particle concentration while maintaining all else constant. Two experimental designs were developed which are in a sense the inverse of each other: a resuspension procedure and a dilution procedure.

For the resuspension experiment (fig. 7), replicate controls and experimental vessels are prepared. After adsorption equilibrium is achieved, the particles and supernatant are separated by centrifugation and, only in the experimental vessels, a portion of the supernatant is removed. The volume of supernatant in the control vessels is not changed. Then the particles are resuspended into the supernatant and equilibrated, after which measurements of the total and dissolved nickel are made. In both the experimental and control vessels the particles are resuspended into the same supernatant with which they were in equilibrium. If a "dissolved" third phase is present which is not separated by centrifugation then its concentration is not changed by the partial removal of supernatant in the experimental vessels. The only modification is that the particle concentration is increased in the experimental vessels since the supernatant volume is decreased.

The results for both the controls and the experimental vessels are shown in Table 1 for montmorillonite and quartz particles. The montmorillonite controls behaved as expected: the dissolved nickel concentration at both adsorption and resuspension equilibrium are essentially equal and their ratio is unity. For the quartz experiments a slight decrease occurred in the controls presumably due to lack of complete equilibrium. The experimen-

tal vessels for all experiments clearly exhibit the particle concentration effect. The result of increasing particle concentration is apparently to decrease the partition coefficient. This causes nickel to desorb from the particles thereby increasing the dissolved nickel concentration. The average ratio of resuspension to adsorption dissolved concentrations increases in all cases whereas the average ratio for the controls is either equal to or less than one.

The dilution experiment is designed to decrease the particle concentration without any other alteration. Three parallel sets of vessels are employed: a control, an experimental vessel, and a vessel to supply additional supernatant with which to dilute the experimental vessel. After adsorption equilibrium, the supernatant from the third vessel is obtained by centrifugation and this particle-free supernatant is added to the experimental vessel. If no experimental fluctuations were present this supernatant should have the same dissolved nickel concentration as the experimental and control vessels since they are identically configured. Note that the experimental vessel is not centrifuged. The particle dilution is achieved by adding additional (identical) supernatant. The vessels are then equilibrated and the total and aqueous concentrations are measured and a comparison is made between the controls and experimental aqueous concentrations. Again if a "dissolved" third phase existed it would have the same concentration in both the experimental and control vessels. As shown in Table 2, the aqueous concentrations in the experimental vessels decrease as predicted. The particle concentration is decreased by dilution, so that the partition coefficient increases, and more nickel is removed from solution. In all the resuspension and dilution experiments, pH fluctuations were not significant ($\Delta\text{pH} < 0.3$).

Both of these experiments confirm the particle concentration dependence of the reversible partition coefficient for increasing and decreasing particle concentrations. The resuspension experiment involves centrifuging the experimental vessels but the controls for the montmorillonite experiment indicate that centrifuging and resuspension into the same supernatant volume causes no change in aqueous concentration. The only possible remaining cause is the changed particle concentration. The dilution experiment dispenses with any particle separation in the experimental vessels. The only possible experimental source of variation is that the added supernatant is at a slightly different aqueous concentration than that in the experimental vessel. A comparison of the control and supernatant aqueous concentrations do suggest that such fluctuations are present but the experimental aqueous concentrations are lower than either in all cases, thus confirming the particle concentration effect for lowered particle concentrations.

Both these experimental designs specifically exclude the possibility of a "dissolved" third phase since if it were present its concentration would be the same in both the experimental and control vessels so that its presence could not affect the difference in partitioning observed at differing particle concentrations. The hypothetical third phase could also be a competing cation. Decrease in the adsorption partitioning of lead at increasing Ca^{++} saturated montmorillonite concentrations has been explained using a competitive Langmuir isotherm with Ca^{++} as the competing cation (34). However, these experiments were conventional adsorption isotherms at various (large) clay concentrations (1-20 g/L) so that the additional clay could supply the additional cation. ~~The design of the resuspension experiment precludes this explanation.~~ In fact, any hypothesis which attempts to ex-

plain the results via an increased desorption of complexing ligands or an increased adsorption of competing cations just transfers the problem to explaining why the changes in ligand or cation concentrations occur with increasing particle concentration for an aqueous phase that is initially in equilibrium with the particles.

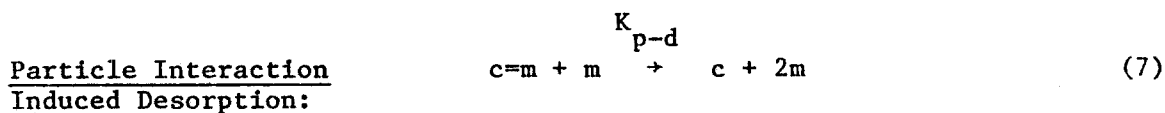
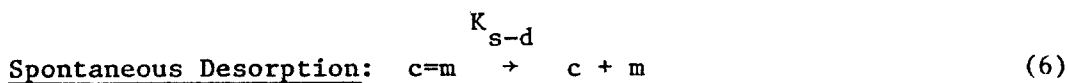
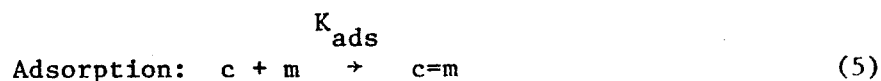
The third phase changes are specifically excluded as an explanation of the results of the resuspension and dilution experiments. Similar results have been observed for hexachlorobiphenyl - sediment and clay experiments (35) although those experiments did not include parallel controls.

Another explanation for the particle concentration effect is flocculation or at least some agglomeration of the sediment particles. This may occur initially or at some later point in the experimental procedure. The result of such a process would be to decrease the overall surface area of the adsorbent, and thus reduce the number of sites available for metal binding leading to a reduction in the value of the partition coefficient in higher sediment-concentration systems.

Extensive microscopy of representative clay and quartz suspensions including the resuspension experiments was carried out. In all cases, both the size and distribution of particles was essentially constant. These results clearly rule out particle size alteration as a means of accounting for the particle concentration effect in our experiments.

Particle Concentration Effects - A Particle Interaction Model

The resuspension and dilution experiments strongly suggest that it is the presence of particles themselves, and not a surrogate variable, that is influencing the extent of reversible partitioning. Thus it appears reasonable to expect that particle interactions somehow affect sorption. We tentatively suggest the following model for the sorption of the reversible component:



where c is the dissolved chemical concentration, $c=m$ is the reversibly sorbed chemical concentration and m is the particle concentration. The adsorption and spontaneous desorption mechanisms are the conventional representations for reversible partitioning. Particle interaction induced desorption assumes that a binary interaction between particles causes desorption to occur. The mechanism that prompts this desorption is uncertain at present.

For these three reactions at equilibrium, the reversible partition coefficient is:

$$\pi_x = \frac{[c=m]}{[c][m]} = \frac{K_{\text{ads}}}{K_{\text{s-d}} + mK_{\text{p-d}}} \quad (8)$$

A useful normalization of this expression is:

$$\pi_x = \frac{\pi_{xc}}{1 + (m \pi_{xc} / v_x)} \quad (9)$$

where $\pi_{xc} = K_{ads}/K_{s-d}$, the classical partition coefficient and $v_x = K_{ads}/K_{p-d}$, which is the slope of the π_x versus m relationship at large particle concentration:

$$\pi_x \cong \frac{v_x}{m} \quad m \gg v_x / \pi_{xc} \quad (10)$$

A convenient parameter that quantifies the particle concentration at which particle interactions become important is the ratio $K_m = v_x / \pi_{xc}$, which can be thought of as the half saturation constant for the $\pi_x - m$ relationship. That is at $m = K_m$, $\pi_x = \pi_{xc} / 2$ so that K_m is the particle concentration at which the particle interaction desorption and spontaneous desorption are of equal magnitude: $K_{s-d} = m K_{p-d}$. Fig. 8 presents Ni - montmorillonite data and the π_x relationship, eq. (9). For a tentative assignment of $\pi_o^* = 0.4$, which assumes that the resistant fraction is independent of m - the data are too scattered for a more refined hypothesis - the resulting $\pi_a = \pi_x + \pi_o$ relationship is compared to observation in fig. 8.

These π_x data and those for the Co-montmorillonite and Ni - quartz are fit to eq. (9) using a nonlinear least squares fit of $\log \pi_x$ versus $\log m$ to estimate π_{xc} and v_x . The results are given in Table 3 (Individual Data Sets). The resulting v_x are essentially equal for the three systems. A four parameter least square fit: constant v_x and an individual π_{xc} for each system yields the same result within the standard error estimates (Table 3 - Joint Data Set). The results are shown in fig. 9 for the three systems. A normalized plot of:

$$\frac{\pi_x}{\pi_{xc}} = \frac{1}{1 + m/K_m} \quad (11)$$

illustrates that these data are well represented by eq. (11) and that each system has data in both the range of m for which π_x is essentially constant: $\pi_x = \pi_{xc}$ ($m \ll K_m$) and for which π_x varies inversely with particle concentration: $\pi_x = v_x/m$ ($m \gg K_m$).

Two observations are worthy of note. For $m \ll K_m$, $\pi_x \cong \pi_{xc} = K_{ads}/K_{s-d}$, the classical reversible partition coefficient. It is a function of both the nature of the sorbate (Ni-clay: $\pi_{xc} = 45$ L/g; Co-clay: $\pi_{xc} = 5.8$ L/g) and the sorbent (compare Ni-clay to Ni-quartz: $\pi_{xc} = 1.1$ L/g) as would be expected. The surprising result is that v_x is essentially independent of both sorbate type and sorbent properties (Table 3 - Individual Data Sets). Since:

$$v_x = \frac{K_{ads}}{K_{p-d}} \quad (12)$$

is the ratio of adsorption to particle induced desorption rate, the fact that it is constant suggests that its magnitude is physically rather than chemically determined. This would be the case if, for example, both the adsorption rate and particle interaction induced desorption rate were functions of hydrodynamic factors.

Following this idea and assuming that K_{ads} is constant, the extent of reversible partitioning is determined by the magnitude of the two desorption mechanisms. The data in fig. 9 can be interpreted as follows. For small particle concentrations, the rate of spontaneous desorption exceeds the rate of particle interaction induced desorption (which is small due to the low

particle concentrations) and spontaneous desorption dominates the total desorption rate. Spontaneous desorption is expected to be a function of the strength of the chemical and electrostatic bonding and so it is chemical and surface specific. The spontaneous desorption rate is smallest for Ni-clay, yielding the highest reversible partition coefficient at small m , in decreasing order followed by Co-clay and Ni-quartz (left hand side of fig. 9). However as m increases, the rate of particle interaction induced desorption increases for all systems. Since the spontaneous desorption rate is smallest for Ni-clay, and as the particle interaction desorption rate, $m K_{d-p}$, becomes comparable to K_{s-d} for this system first, the Ni-clay reversible partition coefficient starts to decrease at relatively small particle concentrations $K_m = 18.7$ mg/L. However, the partitioning of Co-clay and Ni-quartz systems, with their larger spontaneous desorption rates, are unaffected at these particle concentrations. As m increases further, however, $m K_{p-d}$ approaches K_{s-d} for Co-clay ($K_m = 146$ mg/L) and π_x for this system starts to decrease. Not until m approaches $K_m = 786$ mg/L for the Ni-quartz system is $m K_{p-d}$ comparable to K_{s-d} for this system.

Hence π_x is a specific chemically determined constant, π_{xc} , for each system until m reaches $K_m = K_{s-d}/K_{p-d}$ for that system at which point $m K_{p-d} = K_{s-d}$ and the additional particle interaction induced desorption causes π_x to start decreasing. For large $m \gg K_m$, the spontaneous desorption rate is overwhelmed by the particle interaction induced desorption and

$$\pi_x \cong \frac{K_{ads}}{mK_{p-d}} = \frac{v_x}{m} \quad m \gg K_m \quad (13)$$

which is constant for the all sorbate-sorbent pairs. Hence all π_x curves eventually meet at high particle concentrations as shown in fig. 9. Note

that at $m = 1000$ mg/L the three systems have virtually the same π_x and the pattern continues for Ni-quartz at $m = 10,000$ mg/L. This is a consequence of the virtually constant $v_x = 0.68 - 0.91$ found experimentally.

Ionic Strength Effects

Metal-clay sorption is known to decrease significantly as ionic strength increases (36,37). We examine this effect at two particle concentrations ($m = 100$ and 1000 mg/L) using adsorption and desorption isotherms as before (pH = 9, borate buffer). The component partition coefficients are shown in fig. 10. At the low ionic strength of the buffer, the effect of particle concentration is clearly in evidence. However, as ionic strength is increased by adding NaNO_3 , the π_a values at both particle concentrations tend to become equal. The reversible component π_x 's are approaching each other, whereas the resistant component is behaving quite differently. For $m = 100$ mg/L, the system is essentially approaching complete reversibility as ionic strength increases whereas for $m = 1000$ mg/L the resistant component persists as $\sim 50\%$ of the total sorbed nickel with some decrease apparent at high ionic strength.

We offer no explanation for the resistant component behavior. However, the reversible component can be analyzed using the particle interaction desorption model. Using the observed π_x at $m = 100$ and 1000 mg/L, and eq. (8) in the form:

$$\frac{1}{\pi_x} = \frac{K_{s-d}}{K_{ads}} + \frac{K_{p-d}}{K_{ads}} m \quad (14)$$

the ratios: $\pi_{xc} = K_{ads}/K_{s-d}$ and $v_x = K_{ads}/K_{p-d}$ can be computed at each ionic strength. They are shown in fig. 11 together with the Co-clay data, and Ni-

quartz data at the ionic strength of the buffer. The results of additional Ni-quartz experiments at $I = 0.01M$, $pH = 9$, borate buffer $m = 100 - 10,000$ mg/L, fit using eq. (9) to obtain π_{xc} and v_x are also included. Once again the influence of the chemical factors: ionic strength and the specific sorbate-sorbent pair, are clearly seen for the estimated classical partition coefficient, $\pi_{xc} = K_{ads}/K_{s-d}$. If we assume that K_{ads} is constant and not chemically controlled, then the decrease in π_{xc} is due to an increase in the spontaneous desorption rate, K_{s-d} . The Ni-clay data suggest that $K_{s-d} \sim I^{1/2}$ which is the same ionic strength power law dependency for the double layer thickness (38) suggesting that the reduction in double layer thickness as I increases lowers the energy barrier and enhances spontaneous desorption. The use of more refined chemical models (31,32) to explain these relationships as well as the observed pH variations (fig. 5) is clearly possible.

The point is that the experimental data should be collected using adsorption-desorption isotherms at two particle concentrations so that π_{xc} can be estimated. The formulation of equilibrium sorption models assumes both complete reversibility and no particle interaction effects. Thus the models cannot be expected to apply to simply the adsorption partition coefficient, π_a , which is confounded by both non-reversibility: $\pi_a = \pi_x + \pi_o$, and by π_x itself varying with particle concentration (fig. 10). It is only π_{xc} , the classical low particle concentration limiting partition coefficient, that satisfies the implicit model assumptions of reversibility and no particle interaction effects.

On the other hand, for large particle concentrations ($m \gg K_m$), $\pi_x = v_x/m$ and the estimates of v_x are essentially constant and independent of ionic strength and the identity of the sorbate-sorbent pair. This is

= 0.3 (39), suggests that this finding is not just a laboratory curiosity but has wider applicability.

If in fact v_x is essentially constant and of order one, then the half saturation constant for the particle concentration effect becomes:

$$K_m = \frac{v_x}{\pi_{xc}} \sim \frac{1}{\pi_{xc}}$$

which suggests that highly sorbed chemicals (large π_{xc} say 10^6 L/kg) will exhibit particle concentration effects at low particle concentrations ($m = 1.0$ mg/L) whereas less highly sorbed chemicals ($\pi_{xc} = 10^3$ L/kg) are less likely to exhibit the effect until larger particle concentrations ($m = 1000$ mg/L) are encountered.

Acknowledgements

The authors are pleased to acknowledge the support of Thomas P. O'Connor of the Office of Marine Pollution Assessment, NOAA and Victor J. Bierman and John F. Paul of the EPA Research Laboratory, Narragansett, R.I. This investigation is the theoretical portion of more practically directed projects currently underway. The support of our group at Manhattan College: Sue Blakeney, Elizabeth Comerford, Elaine Dwyer, John Sowa, Mark Tallman, and of our colleagues: John Connolly, James Mueller, Donald O'Connor, John Jeris, Robert Thomann, and Richard Winfield is also appreciated, as is Herbert Allen's (IIT, Chicago) suggestion that we use "good" buffers.

Table 1

Resuspension Experiment
 Borate Buffer, pH = 9
 Aqueous Ni Concentrations ($\mu\text{g}/\ell$)

Montmorillonite

Control Vessels			Experimental Vessels		
Adsorption $m = 100 \text{ mg}/\ell$	Resuspension $m = 100 \text{ mg}/\ell$	Ratio	Adsorption $m = 100 \text{ mg}/\ell$	Resuspension $m = 243 \text{ mg}/\ell$	Ratio
c_a	c_{rs}	c_{rs}/c_a	c_a	c_{rs}	c_{rs}/c_a
72.6	72.2	1.00	74.7	97.3	1.30
38.9	37.8	0.97	36.8	40.4	1.10
15.9	17.0	1.07	19.1	23.4	1.23
6.18	6.33	1.02	5.32	5.87	1.10
Average ratio = 1.017			Average ratio = 1.182		

Quartz

$m = 1000 \text{ mg}/\text{L}$			$m = 1000 \text{ mg}/\text{L}$		
c_a	c_{rs}	c_{rs}/c_a	c_a	c_{rs}	c_{rs}/c_a
102.	91.9	0.901	87.3	96.0	1.10
46.8	41.6	0.889	38.3	43.7	1.41
20.1	19.0	0.945	19.7	20.4	1.04
10.1	9.32	0.923	9.80	11.9	1.21
Average ratio = 0.914			Average ratio = 1.123		

Quartz

$m = 1000 \text{ mg}/\text{L}$			$m = 1000 \text{ mg}/\text{L}$		
c_a	c_{rs}	c_{rs}/c_a	c_a	c_{rs}	c_{rs}/c_a
72.3	61.2	0.846	74.9	87.5	1.17
36.0	32.6	0.906	30.3	36.2	1.195
16.1	13.9	0.863	17.5	24.5	1.40
9.10	8.16	0.897	8.29	12.0	1.45
Average ratio = 0.878			Average ratio = 1.303		

TABLE 2
Dilution Experiment Ni-Montmorillonite (pH = 9 Borate Buffer)

Total Ni Concentrations ($\mu\text{g}/\ell$)			
Control Vessels	Supernatant Vessels	Experimental Vessels	
m = 500 mg/ ℓ	m = 500 mg/ ℓ	m = 188 mg/ ℓ	
249	261	263	
266	270	264	
269	275	266	
Dissolved Ni Concentrations ($\mu\text{g}/\ell$)			Experimental to Control Vessel Ratio
115	105	103	0.898
118	98.0	89.3	0.756
98.1	98.7	83.4	0.850
			Average Ratio = 0.835

TABLE 3

Least Square Parameter Estimates* of π_{xc} , ν_x and K_m (pH = 9, Borate Buffer)
 Joint Data Set: $\nu_x = 0.85(0.077)$

System	Individual Data Sets					
	No. of Points	π_{xc} (L/g)	ν_x	K_m (mg/L)	π_{xc} (L/g)	K_m (mg/L)
Ni-Clay	10	42.5(7.3)	0.907(0.078)	21.3(4.9)	45.5(9.9)	18.7(5.0)
Co-Clay	2	6.44	0.773	120	5.83(2.2)	146(59)
Ni-Quartz	5	1.22(0.36)	0.677(0.20)	555(280)	1.08(0.18)	786(161)

* Estimated value (standard error of estimate)

REFERENCES

1. Duursma, E.K., Gross, M.G., in Radioactivity in the Marine Environment, Nat. Acad. Sci., 1971, 147.
2. Oakley, S.M., Nelson, P.O., Williamson, K.J. Environ. Sci. Technol. 1982 15, 474.
3. Salim, R. Water Res. 1983, 17, 423.
4. James, R.O., Healy, T.W. J. Colloid Interfacial Sci. 1972, 40, 65.
5. Hohl, H., Stumm, W. J. Colloid Interfacial Sci. 1976, 55, 281.
6. Mattigod, S.V., Gibali, A.S., Page, A.L. Clay and Clay minerals 1979, 27, 411.
7. Benjamin, M.M., Leckie, J.O. Environ. Sci. Technol. 1982, 16, 162.
8. Garcia-Miragaya, J., Page, A.L. Soil Sci. Soc. Am. J. 1976, 40, 658.
9. Farrah, H., Pickering, W.F. Water, Air, and Soil Pollut., 1978 (9), 491.
10. Engler, R.M., Brannon, J.M., Rose, J., Bigham, G. in Chemistry of Marine Sediments, ed. T.F. Yen, Ann Arbor Science, 1977, p. 163.
11. van der Weijden, C.H., Arnoldus, M.J.H.L., Meurs, C.J. Neth. J. Sea. Res., 1977, Vol. 11(2), p. 130.
12. Pickering, W.F. in Zinc in the Environment, Part I, ed. J.O. Nriagu. Wiley-Interscience, 1980, p. 72.
13. Forstner, U., Wittmann, G.T.W. Metal Pollution in the Aquatic Environment. Springer-Verlag, Berlin, New York, 1979.
14. Murray, C.N., Murray, L. in Radioactive Contamination of the Marine Environment. Int. Atomic Energy Agency, Vienna, 1973, p. 105.
15. Kharkar, D.P., Turekian, K.K., Bertine, K.K. Geochim. Cosmochim. Acta., 1968, 32, 285.
16. Evans, D.W., Cutshall, N.H. in Radioactive Contamination of the Marine Environment. Int. Atomic Energy Agency, Vienna, 1973, p. 125.
17. Rozell, T.C., Andelman, J.B. ACS Series 106 Am. Chem. Soc., 1971, p. 280.
18. Bothner, M.H., Carpenter, R. in Radioactive Contamination of the Marine Environment, Inter. Atomic Energy Agency, Vienna, 1973, p. 73.

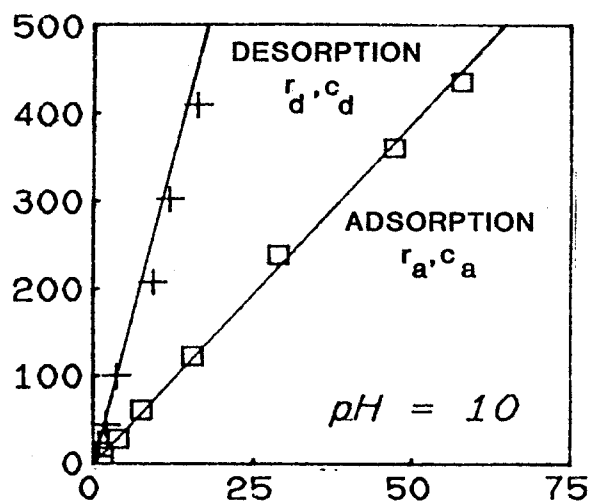
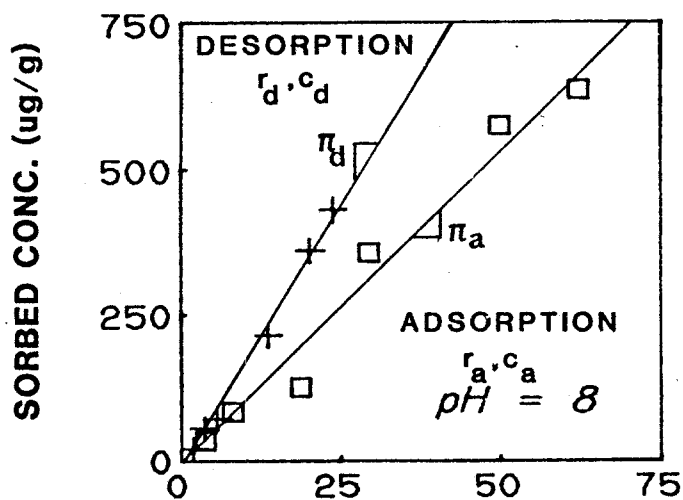
19. Duursma, E.K. in Estuarine Chemistry, ed. J.D. Burton, P.S. Liss. Academic Press, N.Y., 1976, p. 159.
20. Karimian, N., Cox, F.R. Soil Sci. Soc. Am. J., 1978, 42, 757.
21. Patel, B., Patel, S., Pawar, S., Est. & Coastal Mar. Sci., 1978, 7, 49.
22. Singh, Shah, S. Can. J. Soil. Sci., 1979, 59, 119.
23. Di Toro, D.M., Horzempa, L. Environ. Sci. Technol., 1982, 16, 594.
24. O'Connor, D.J., Connolly, J.P. Wat. Res., 1980, 14, 1517.
25. Aston, S.R., Duursma, E.K. Neth. J. Sea Res., 1973, 6, 225.
26. Schell, W.R., Sibley, T.H., Sanchez, A.L., Clayton, J.R., 1980, NUREG/CR-0803, NTIS, Springfield, Virginia.
27. Benes, P., Majer, V. Trace Chemistry of Aqueous Solutions. 1980, Elsevier, N.Y.
28. Voice, T.C., Rice, C.P., Weber, W.J. Jr. Environ. Sci. Technol., 1983, 17, 513.
29. Good, N.E., Winget, G.D., Winter, W., Connolly, T.N., Izawa, S., Singh, R.M.M. Biochemistry, 1966, 5, 467.
30. Zasoski, R.J., Burau, R.G., Soil Sci. Soc. Am. J., 1978, 42, 372.
31. Davis, J.A., Leckie, J.O. J. Colloid Interface Sci., 1978, 67, 90.
32. Bowden, J.W., Posner, A.M., Quirk, J.P. Aust. J. Soil Res., 1977, 15, 121.
33. Baes, C.F. Jr., Mesmer, R.E. The Hydrolysis of Cations, 1976. J. Wiley & Sons, N.Y.
34. Griffin, R.A., Au, A.K. Soil Sci. Soc. Am. J., 1977, 41, 880.
35. Di Toro, D.M., Horzempa, L. in Physical Behavior of PCB's in the Great Lakes, ed. D. Mackay et al., Ann Arbor Science, 1982, 89.
36. McBride, M.B., Clay and Clay Minerals, 1978, 26, 101.
37. Egozy, Y. Clay and Clay Minerals, 1980, 28, 311.
38. Stumm, W., Morgan, J.J. Aquatic Chemistry 2nd ed., 1981, 681.
39. ~~Di Toro, D.M., Horzempa, L.M., Casey, M.M., Richardson, W.L. J. Great Lakes Res., 1982, 8, 336.~~

ADSORPTION-DESORPTION ISOTHERMS

Ni-Montmorillonite-Borate

Linear Plots

$m=100$ mg/L



Logarithmic Plots

$m=100$ mg/L

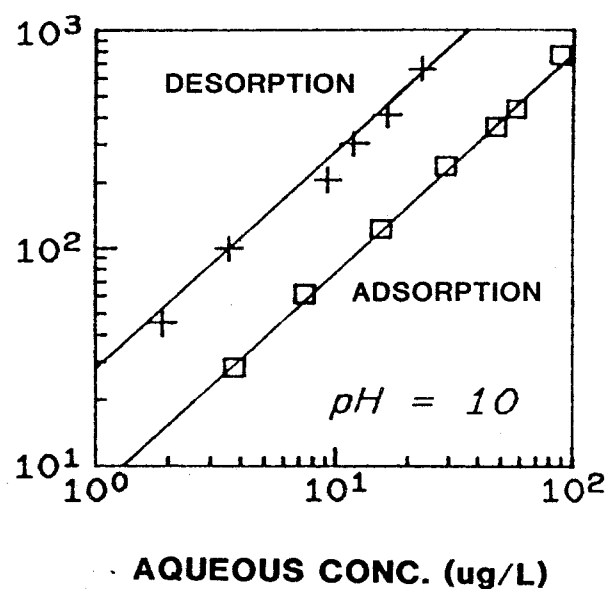
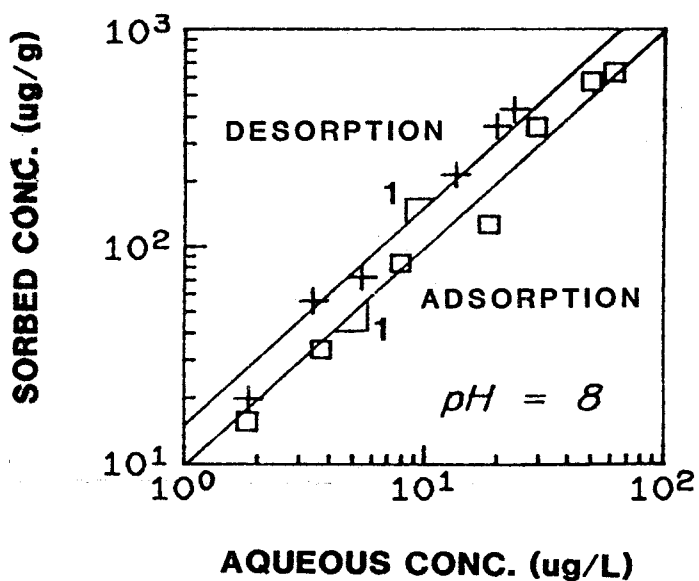
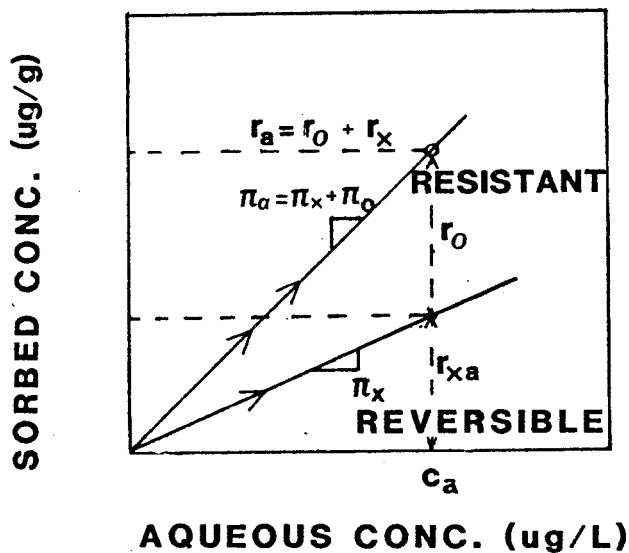
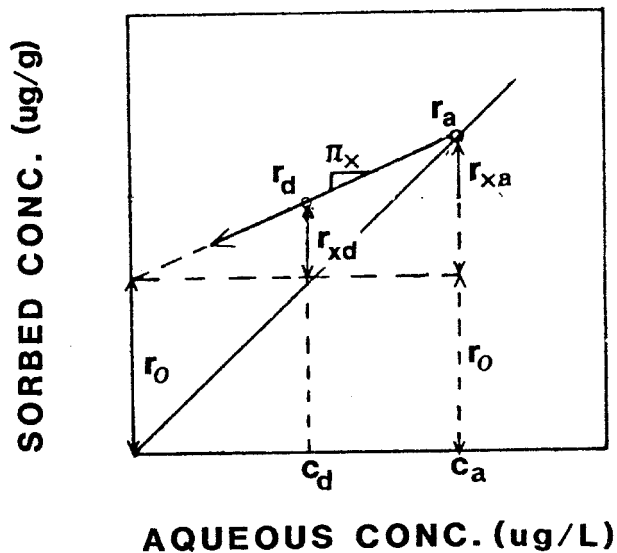


FIGURE 1

ADSORPTION



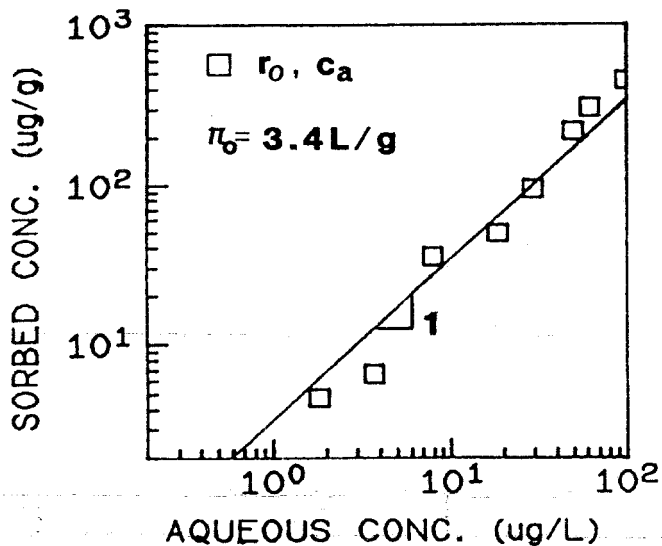
DESORPTION



Ni-Montmorillonite

pH=8, Borate Buffer, m=100mg/L

RESISTANT COMPONENT



REVERSIBLE COMPONENT

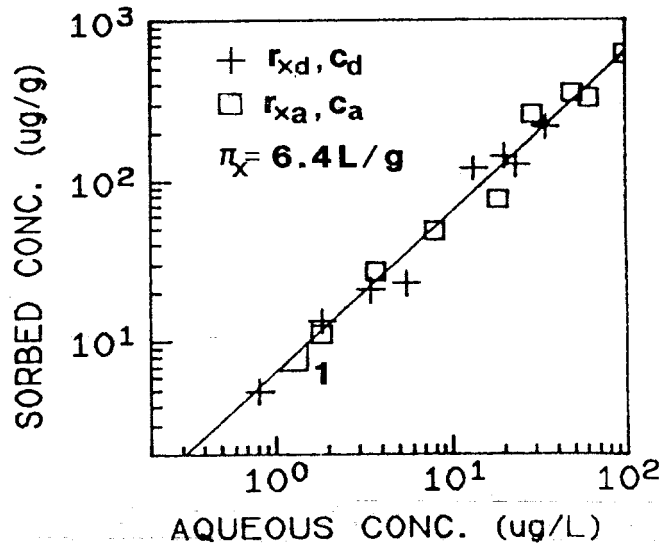


FIGURE 2

VESSEL ADSORPTION-DESORPTION

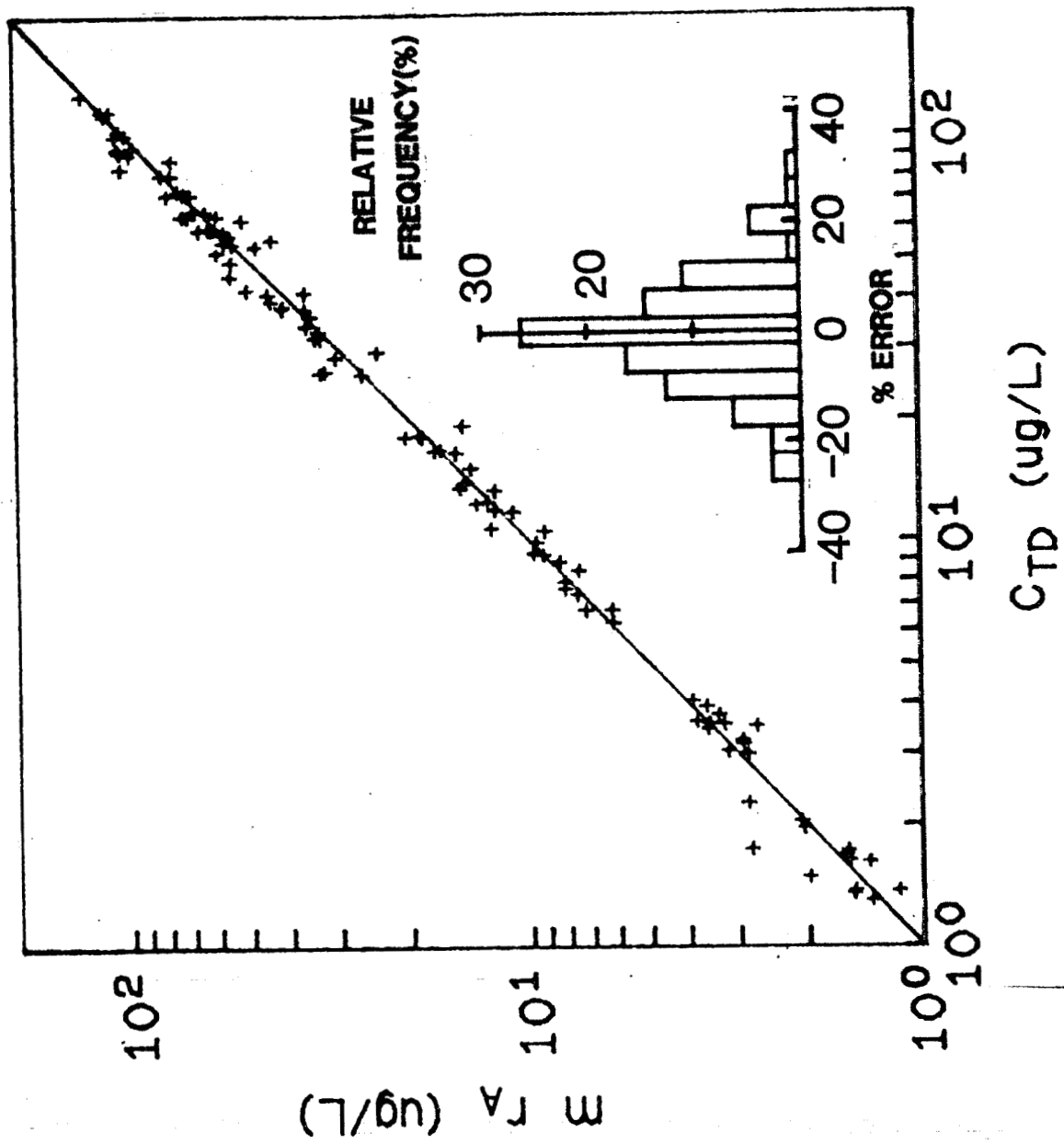


FIGURE 3

ADSORPTION KINETICS

DESORPTION KINETICS

Ni-Monmorillonite-Borate

pH=9 m=100 mg/L

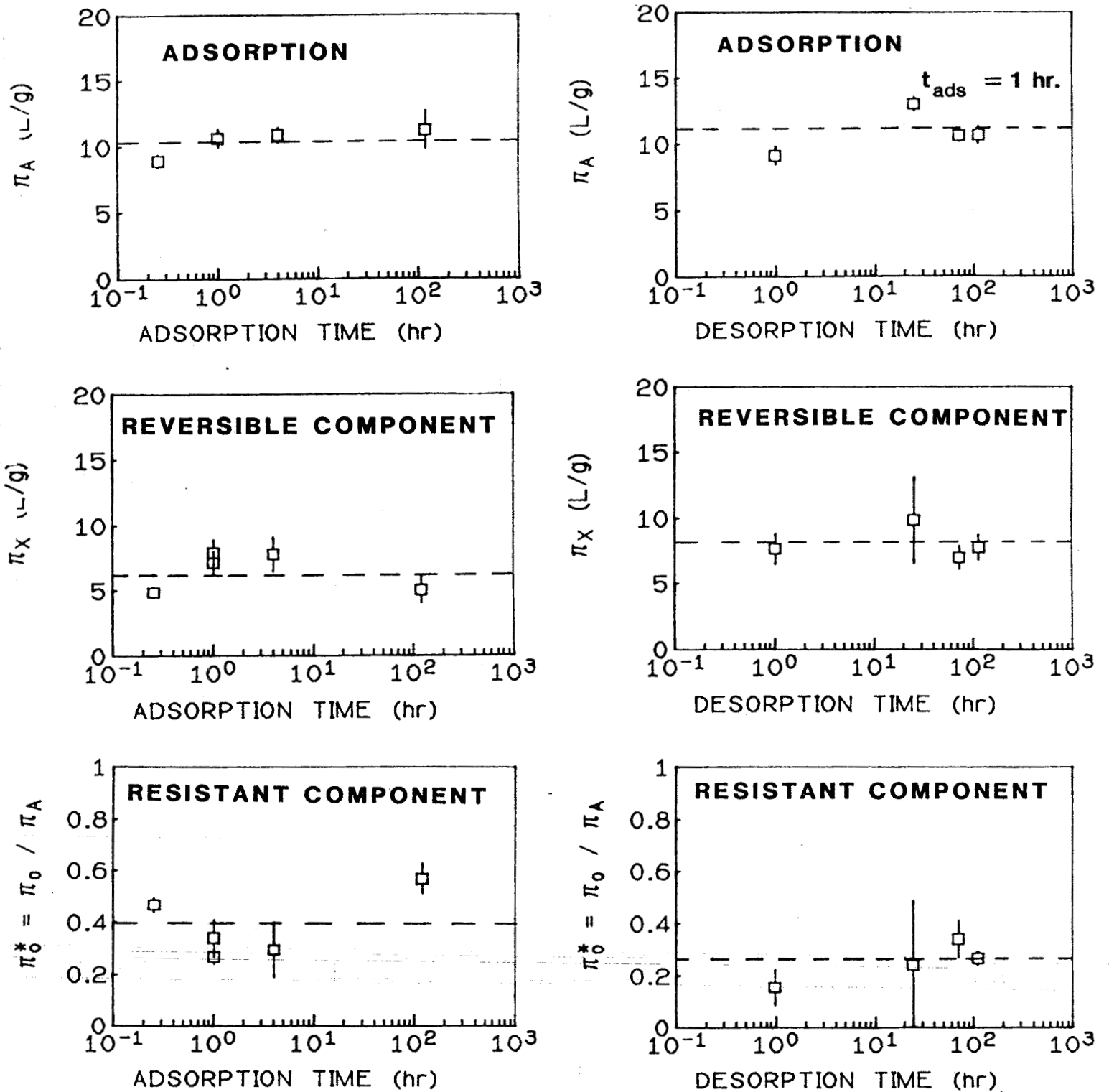


FIGURE 4

EFFECT OF pH

Montmorillonite $m=100\text{mg/L}$
ADSORPTION

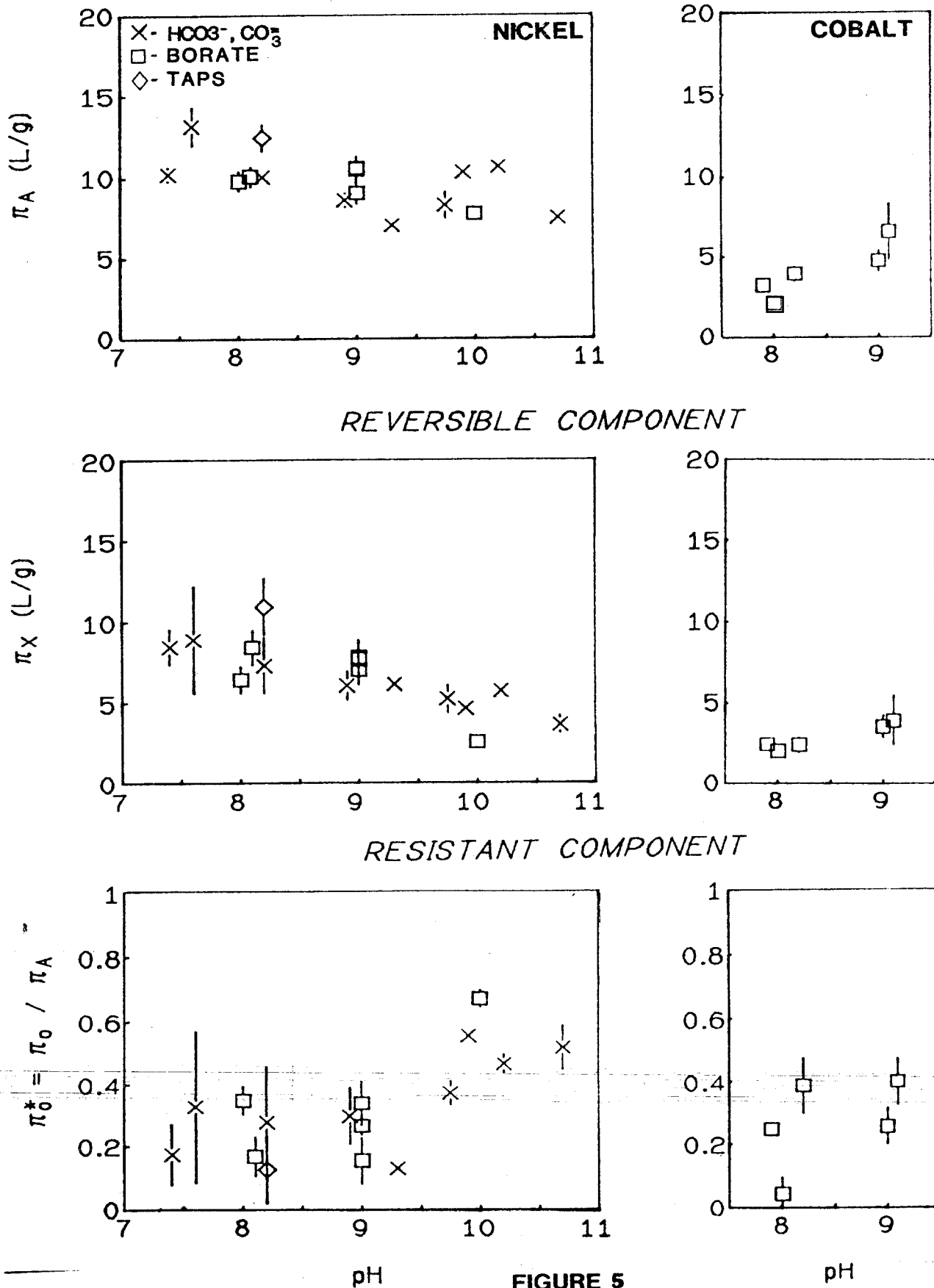


FIGURE 5

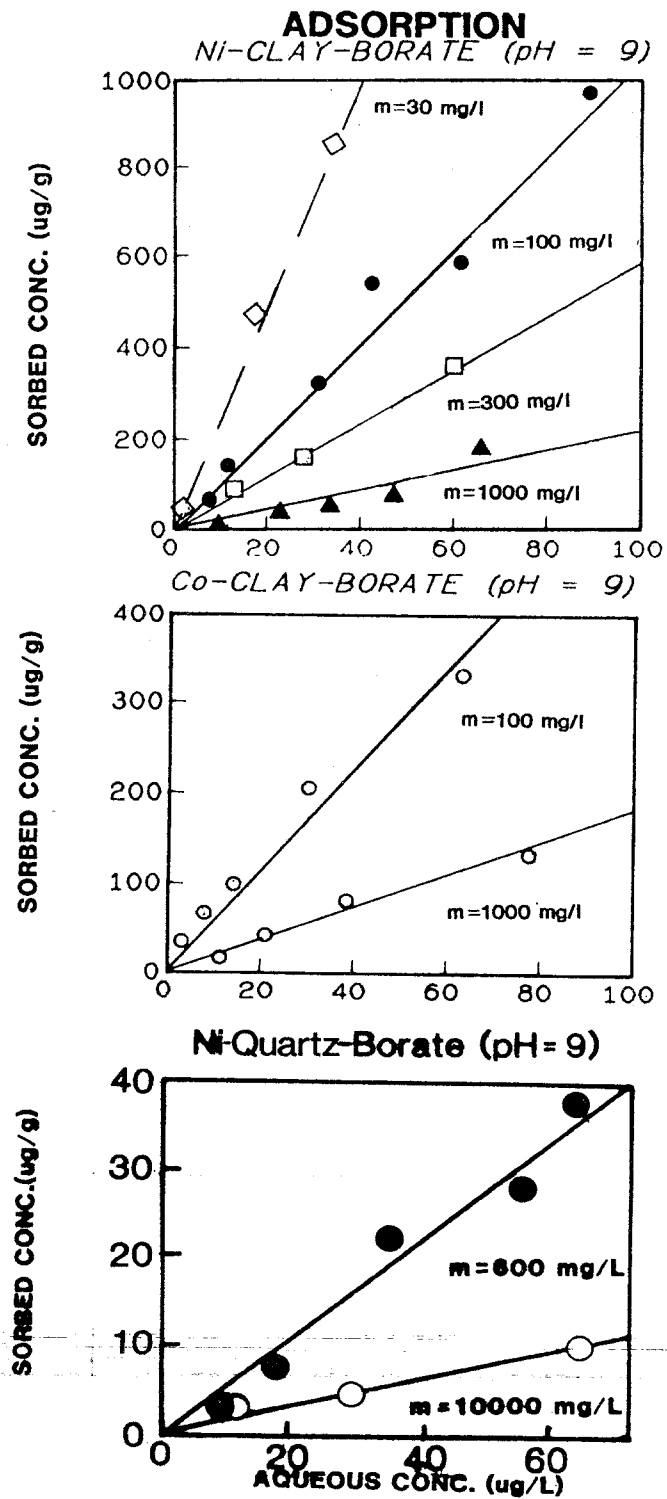
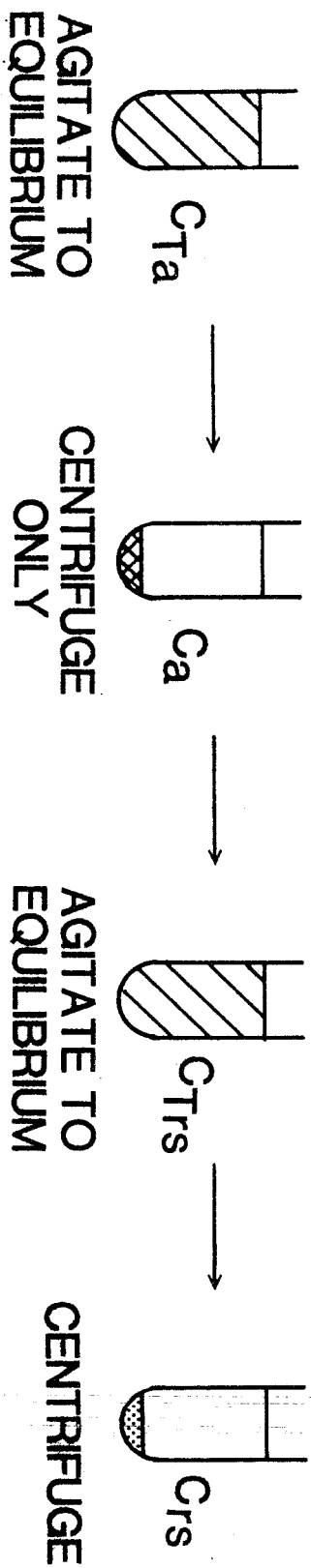


FIGURE 6

RESUSPENSION EXPERIMENT

CONTROL VESSELS



EXPERIMENTAL VESSELS

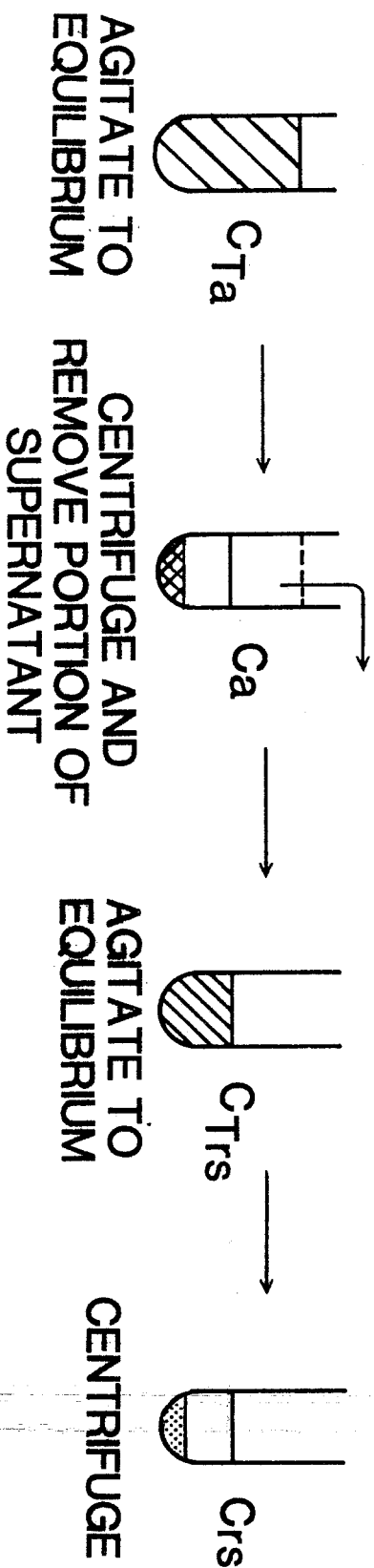


FIGURE 7

PARTICLE CONCENTRATION EFFECT

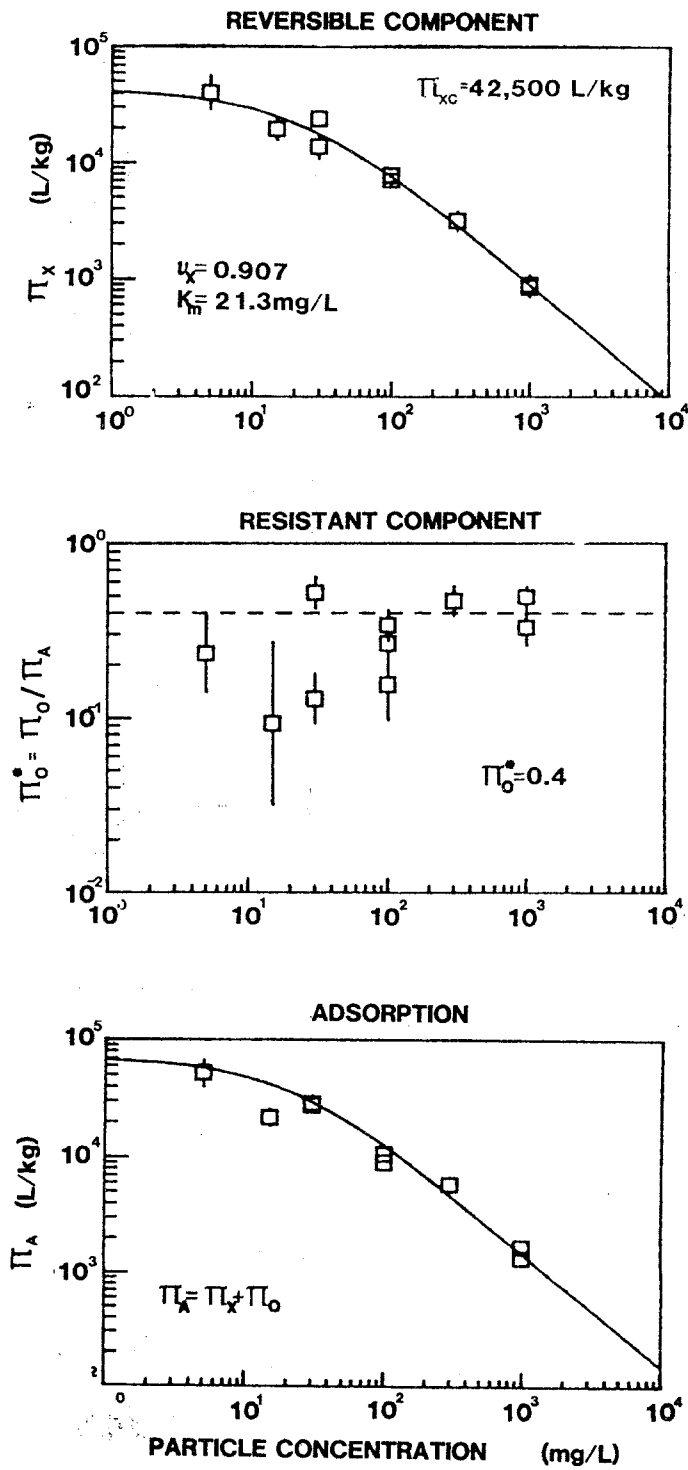


FIGURE 8

PARTICLE CONCENTRATION EFFECT REVERSIBLE COMPONENT

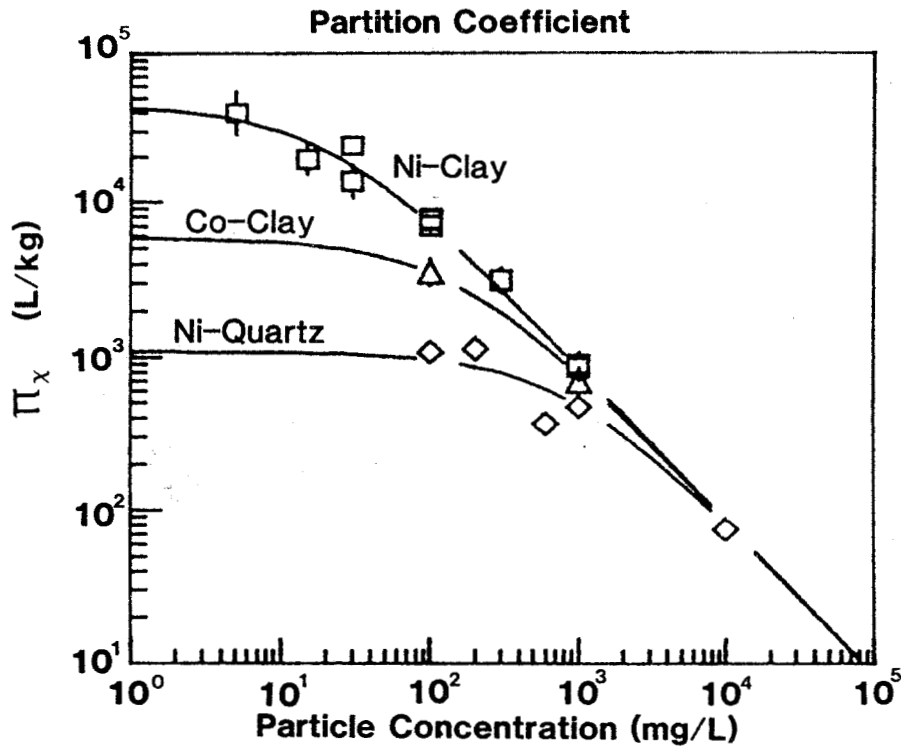
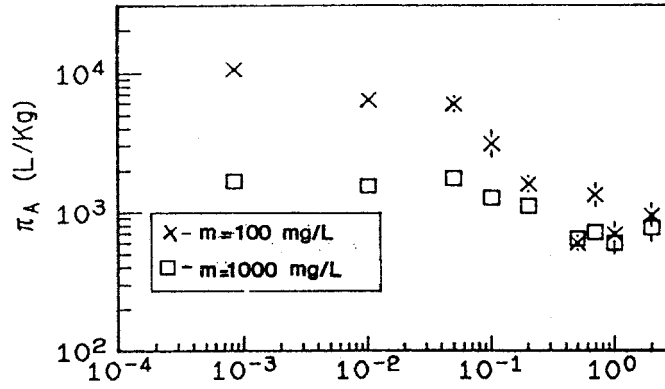


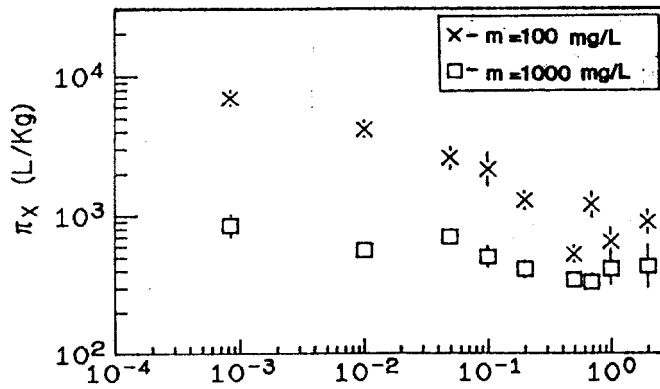
FIGURE 9

IONIC STRENGTH EFFECTS

ADSORPTION



REVERSIBLE COMPONENT



RESISTANT COMPONENT

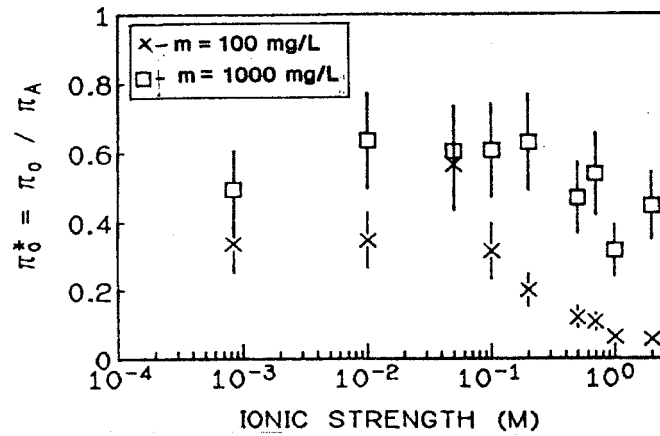
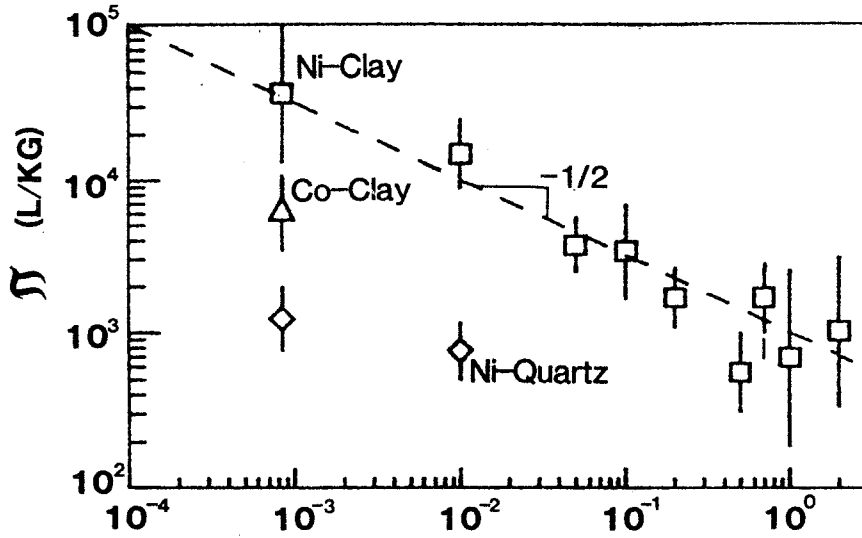
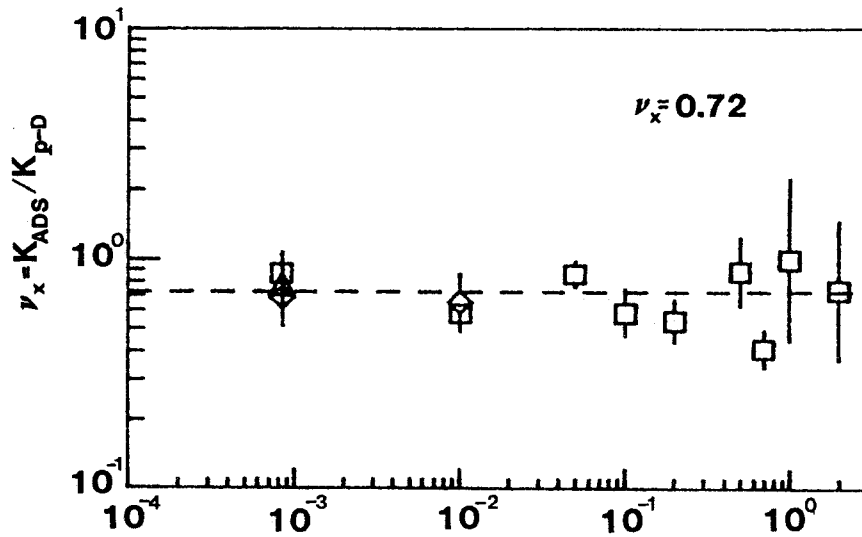


FIGURE 10

REVERSIBLE COMPONENT
CLASSICAL PARTITION COEFFICIENT



ADSORPTION/PARTICAL INTERACTION DESORPTION



HALF SATURATION CONSTANT

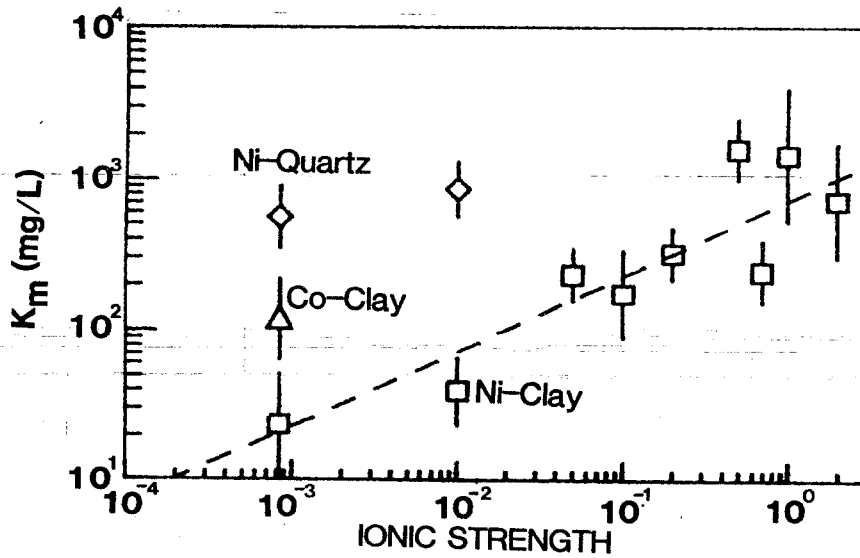


FIGURE 11

APPENDIX II

A PARTICLE INTERACTION MODEL OF REVERSIBLE ORGANIC CHEMICAL
SORPTION

Dominic M. Di Toro
Environmental Engineering and Science Program
Manhattan College, Bronx, N.Y. 10471

August 1984

INTRODUCTION

The sorption of hydrophobic organic chemicals onto soils, suspended, and sediment particles is the reaction which distinguishes the environmental fate of these chemicals from more conventional pollutants. The usual parameterization of this reaction involves the use of a partition or distribution coefficient that determines the fraction of total chemical concentration that is in the particulate and dissolved phases. The typical assumption is that the reaction is completely reversible.

Unfortunately there is a large body of experimental adsorption-desorption data (1-54) which, in almost all cases, illustrates that complete reversibility is not commonly observed. Rather it is found that, for the usual time scales of these experiments (hours-days) an apparent desorption steady state occurs that is not in conformity with the particulate and dissolved concentration distribution predicted from the adsorption steady state partition coefficient. We employ an empirical model to quantify the partition coefficient of the reversibly sorbed component and attempt to relate it to chemical and particle properties.

The most surprising and controversial of these is the particle concentration itself, whose effect on the adsorption partition coefficient has been recently stressed by O'Connor and Connolly (55). We attempt to reconcile this effect for reversible component partitioning by proposing a particle interaction model that posits an additional desorption reaction. This model is shown below to be in conformity with observations for a large set of adsorption-desorption data (1-54). However the mechanism responsible for this desorption reaction is still uncertain. This is discussed below in more detail.

METHODS

The reversible and resistant component model of sorption (38) assumes that adsorbed chemical concentration, r_a , is composed of two components; a resistant component, r_o , that does not appreciably desorb under the conditions of the experiment, and a reversible component, r_x . The key assumption is that reversible component adsorption and desorption are both governed by the same linear isotherm:

$$r_x = \pi_x c \quad (1)$$

where c is the aqueous phase concentration at either adsorption or desorption steady state.

Consider an adsorption experiment which yields an adsorbed concentration r_a at aqueous concentration c_a . Then since $r_a = r_o + r_x$:

$$r_a = r_o + \pi_x c_a \quad (2)$$

If, for a desorption into uncontaminated aqueous phase, the resulting sorbed concentration is r_d at aqueous concentration, c_d , then

$$r_d = r_o + \pi_x c_d \quad (3)$$

since only the reversible component is affected. Thus the reversible component partition coefficient can be estimated by subtracting eq. (3) from eq. (2) yielding:

$$\pi_x = \frac{r_a - r_d}{c_a - c_d} \quad (4)$$

Consider, now an adsorption isotherm comprised of $i=1, \dots, N_a$ concentrations $r(i,0)$, $c(i,0)$, the zero denoting the adsorption cycle. If, for each adsorption vessel a sequence of desorption cycles, $j=1, \dots, N_d$ are performed, yielding $r(i,j)$, $c(i,j)$, then the component model predicts that the slopes of the consecutive desorption isotherms:

$$\pi_x(i,j) = \frac{r(i,j) - r(i,j+1)}{c(i,j) - c(i,j+1)} \quad \begin{array}{l} i=1, \dots, N_a \\ j=1, \dots, N_d \end{array} \quad (5)$$

are all constant, independent of the isotherm index, i , or the desorption cycle index, j . Measurement errors and the idealized model assumptions will yield variations in each estimate. The geometric mean ignoring any negative values of $\pi_x(i,j)$, is used as the best estimate of π_x for each isotherm analyzed. Resistant component concentrations, $r_o(i)$, are estimated by subtraction:

$$r_o(i,j) = r(i,j) - \pi_x c(i,j) \quad (6)$$

and for each isotherm the geometric mean is used as the best estimate of $r_o(i)$. The component model equation for the complete isotherm is:

$$r(i,j) = r_o(i) + \pi_x c(i,j) \quad (7)$$

with π_x and $r_o(i)$ as the fitted constants.

Two examples are presented in fig. 1. The top panels illustrate the isotherm data and the conformity to the model eq. (7) using the indicated value of π_x . The middle panels compare the calculated resistant component data $r_o(i,j)$ (symbols) from eq. (6) together with the estimates of the presumed constant resistant component concentration, $r_o(i)$ (horizontal lines). The bottom panel illustrates, in these cases at least, that the adsorption of the resistant component follows a linear (unity log-log slope) isotherm

$$r_o(i) = \pi_o c_a \quad (8)$$

For parathion, the model provides an excellent fit to the data. For atrazine some deviations are present - the resistant component estimates are not exactly constant - but the fit to the experimental data (top panel) is reasonable and parsimonious since only two parameters are necessary: π_x and π_o . Fig. 2 presents other adsorption-consecutive desorption isotherms and the reversible-resistant component model isotherms (eq. 7), fit to the data as described above. These examples are chosen to illustrate that the model is applicable to isotherms from a wide range of organic and inorganic sorbates and sorbents: soils, lake sediments, and inorganic particles.

The division of sorbed chemical into two components - reversible and resistant - can be viewed as a convenient operational method that distinguishes between the rapidly sorbed, labile component, which also rapidly desorbs; and a nonlabile slowly desorbing component. In fact a kinetic description of the sorption process is more fundamentally correct. The gas purge experiments of Karickhoff (56) are a direct examination of these phenomena. He finds both a labile (rapidly adsorbing

and desorbing) component and a nonlabile component with slower desorption rates. The separation we propose essentially isolates the labile component partitioning behavior within the context of available consecutive desorption experimental data.

A substantial portion of the reversible component partition coefficients analyzed below are computed from reported adsorption and consecutive desorption data using the average slope method (Table 1). Unfortunately not all reported desorption experiments include the actual data. For these cases estimates of π_x are made in various ways, depending on the reported results. The estimation equations are based upon the definition of π_x , eq. (4), and a mass balance requirement:

$$mr_a + \alpha c_a = mr_d + c_d \quad (9)$$

where m is the particle concentration and α is the volume fraction of aqueous phase not removed before uncontaminated aqueous phase is added to initiate desorption. This equation requires that the chemical remaining in the vessel both on the particles, mr_a , and in the remaining aqueous phase, αc_a , be accounted for after desorption as either on the particles, mr_d , or in the aqueous phase c_d . This is equivalent to assuming that no significant vessel adsorption or desorption occurs during desorption equilibration. Only experiments for which essentially the same particle concentration was maintained throughout are considered. Where possible the standard deviation of the estimated π_x is also computed. The result is over 200 estimates of π_x from these reported experiments for a wide variety of sorbates and sorbents.

REVERSIBLE PARTITION COEFFICIENTS: NEUTRAL ORGANIC CHEMICALS

The adsorption partitioning of neutral organic chemicals to soils and sediment particles has been shown to be a function of the weight fraction of sediment organic carbon, f_{oc} , and the octanol-water partition coefficient, K_{ow} , of the chemical (see Ref. 57 for an excellent review). The basic relationship is that the organic carbon normalized adsorption partition coefficient $K_{oc} = \pi_a / f_{oc}$ is sediment independent so long as the swelling clay weight fraction of that sediment is not

large and that a relationship exists between K_{oc} and K_{ow} of the form:

$$\log K_{oc} = a_0 + a_1 \log K_{ow} \quad (10)$$

Fig. 3 examines this relationship for the reversible component partition coefficients, π_x , sequentially plotted using various symbols with standard deviations indicated if they exceed the symbol size. The conventional organic carbon normalization applied to the reversible partition coefficient π_x/f_{oc} is plotted directly above the symbol as a plus. Directly below the symbol the quantity $m\pi_x$ is displayed as a cross if $m < 1$ kg/L. For $m = 1$ kg/L, $m\pi_x = \pi_x$ numerically and the cross is omitted for clarity of presentation. For each chemical-reference set, the data are ordered by increasing m and, for each m , by increasing f_{oc} of the sorbent. The horizontal dotted lines are the K_{ow} for each chemical.

It is apparent that for low K_{ow} chemicals $\pi_x/f_{oc} \sim K_{ow}$ but that as $\log K_{ow} > 3$ this equality breaks down and in some cases π_x/f_{oc} is significantly less than K_{ow} . A careful examination of fig. 3 indicates that the deviation from $\pi_x/f_{oc} \sim K_{ow}$ is correlated to the extent that $m\pi_x$ approaches 1 and in particular that $m\pi_x$ appears to be bounded in the region of $m\pi_x \sim 1$. Note especially the lower panel of fig. 3 where π_x/f_{oc} is markedly lower than K_{ow} and the crosses are all of order one. This suggests that $m\pi_x \sim 1$ sets an upper limit to the extent of reversible sorption and in particular that the particle concentration itself influences the extent of sorption.

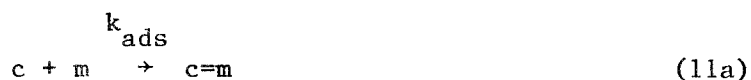
The observation that particle concentration affects the adsorption partition coefficient has been suggested previously by O'Connor and Connolly (55) who noted that certain chemicals strongly exhibited the effect whereas other chemicals were less affected. Significant particle concentration effects have been observed for hexachlorobiphenyl (HCBP) sorption (39). In particular it has been observed that π_x is inversely related to m via $\pi_x = v_x/m$ and that the values of v_x observed for various particle types, to within a factor of four (0.3-1.2), are independent of sediment particle properties such as f_{oc} and particle identity (clay, silica etc). The experimental range of particle concentration was $m = 10-22,000$ mg/L.

This puzzling finding prompted the present analysis of available adsorption-desorption data for other chemicals in order to assess the generality of the finding.

PARTICLE INTERACTION MODEL

One immediate problem is that the relationship $\pi_x = v_x/m$ cannot persist indefinitely as $m \rightarrow 0$ since one is left with the absurd prediction that, in the limit, a single particle can reversibly sorb the same quantity of HCBP as can collectively be sorbed by many particles.

We have recently suggested a model for reversible component sorption (58) which relies upon the hypothesis that, in addition to the usual adsorption and desorption reactions:



where c is dissolved chemical, m is the particle concentration, and $c=m$ is sorbed chemical concentration, there exists an additional desorption reaction for the reversible component:



which occurs as particles interact, possibly via close encounters or collisions. At steady state these reactions imply that

$$\pi_x = \frac{[c=m]}{[c][m]} = \frac{k_{\text{ads}}}{k_{\text{s-d}} + mk_{\text{p-d}}} = \frac{\pi_{\text{xc}}}{1 + m\pi_{\text{xc}}/v_x} \quad (13)$$

where $\pi_{\text{xc}} = k_{\text{ads}}/k_{\text{s-d}}$, the classical reversible partition coefficient, and $v_x = k_{\text{ads}}/k_{\text{p-d}}$, the ratio of adsorption to particle interaction induced desorption rate. Note that at low particle concentrations $\pi_x \rightarrow \pi_{\text{xc}}$ which predicts that at sufficiently low particle concentration, there should be no effect on the extent of reversible sorption but that at large particle concentrations, $\pi_x \rightarrow v_x/m$ so that $m\pi_x \sim v_x$. This

suggests that the reason π_x/f_{oc} is systematically less than K_{ow} for certain chemicals (fig. 3) is that additional particle induced desorption is lowering π_x .

This model provides a framework within which to analyze the π_x data presented in fig. 3. Following conventional adsorption theory we expect that $\pi_{xc} = f_{oc} K_{oc}^x$ so that K_{oc}^x is the proper organic carbon normalization for the reversible partition coefficient at the low particle concentration limit; and that the octanol-water partition coefficient parameterizes the extent of chemical sorption to particle organic carbon. The result is that π_x is a function of m , f_{oc} , and K_{ow} via:

$$\pi_x = \frac{f_{oc} K_{oc}^x}{1 + mf_{oc} K_{oc}^x / v_x} \quad (14)$$

and

$$\log_{10} K_{oc}^x = a_0 + a_1 \log_{10} K_{ow} \quad (15)$$

The superscript x is used to emphasize that K_{oc}^x applies to reversible component partitioning. The idea is that $\pi_x \rightarrow \pi_{xc}$ at low particle concentrations and in this limit the classical reversible partition coefficient, π_{xc} , is given by the usual organic carbon, octanol-water relationships: $\pi_{xc} = f_{oc} K_{oc}^x$ with K_{oc}^x given by eq. (15). However at larger particle concentrations, $mf_{oc} K_{oc}^x \gg v_x$, only the particle concentration is important so that $\pi_x \rightarrow v_x/m$. In this region particle induced desorption is overwhelming spontaneous desorption and only the particle concentration, m , and the ratio $v_x = k_{ads}/k_{p-d}$ controls the extent of reversible partitioning.

A nonlinear least squares fit (59) of eqs. (14, 15) to the neutral organic chemical data using the K_{ow} given in Table 2, and for which $f_{oc} > 0$ ($N = 129$ points) yields the parameter values (v_x , a_0 , a_1) shown in Table 3. The observed versus calculated π_x 's for each data point and a normalized plot of the entire data set as log averages over ranges of the x-axis are shown in fig. 4. The fit to eqs. (14, 15) is remarkable considering the range of chemicals, particle types, and the number of independent experiments and experimentalists. Figs. 5 and 6 present the

individual chemical data in normalized form. It is interesting to note that even for moderate $\log K_{oc}^x$ chemicals ($\sim 2.5 - 3.0$, fig. 5) the particle concentration effect is observed at higher mf_{oc} values. Conversely high K_{oc}^x chemicals (e.g. Kepone, pp' DDT, fig. 6) can be examined at low enough mf_{oc} so that $\pi_x \cong f_{oc} K_{oc}^x$ as expected from hydrophobic partitioning theory. At large mf_{oc} values these and other high K_{oc}^x chemicals exhibit a 3-4 order of magnitude suppression of π_x relative to the low mf_{oc} limit.

For certain chemicals enough data are available to fit eq. (14), individually. The results of the nonlinear least squares fit (v_x, K_{oc}^x) are listed in Table 3 and displayed in fig. 7 versus the chemical's K_{ow} . The log linear relationship of K_{oc}^x to K_{ow} is apparent. What is curious is the tendency of v_x to be larger, $v_x \sim 2-4$, for the lower K_{ow} chemicals and to drop abruptly with Terbufos and remain at $v_x \sim 0.5-1.0$ for the remaining chemicals. Whether this is an artifact of the data sets analyzed or a real indication that, in fact, v_x is not universally a constant is not clear. Certainly a variable $v_x = k_{ads}/k_{p-d}$ is closer to one's intuitive expectations than is a constant v_x . More experiments in the transition region are clearly warranted. From the above data analysis it appears that v_x is of order one plus or minus roughly one half an order of magnitude.

EFFECTS OF CHEMICAL AND PARTICLE PROPERTIES AND CONCENTRATION

The proposed reversible component partitioning model has two distinct regions in which particle concentration either does or does not have an effect on π_x . For $mf_{oc} K_{oc}^x \ll v_x$, $\pi_x \cong f_{oc} K_{oc}^x$ which is a linear function of f_{oc} and K_{oc}^x . Fig. 8 presents the data for $mf_{oc} K_{oc}^x < 1$. The expected relationships: π_x/f_{oc} versus K_{oc}^x with the line corresponding to eq. (15), and π_x/K_{oc}^x versus f_{oc} with the line corresponding to the expected linear relationship are shown. There are no apparent systematic deviations.

Conversely for $mf_{oc} K_{oc}^x \gg v_x$ only particle concentrations determine the magnitude of π_x . Fig. 9 presents the data for $mf_{oc} K_{oc}^x > 3$. Again no systematic deviations are apparent. It is interesting to note that even for chemicals with fairly low K_{ow} 's - the chemicals in the upper

panel range from $\log_{10} K_{ow} = 2.81$ to 3.81 - the particle concentration can dominate π_x if it and f_{oc} are large enough. In addition chemicals with large K_{ow} 's can exhibit extremely low reversible partitioning at high particle concentrations (e.g. HCBP, DDT, and Aroclor 1254).

We illustrate these effects on reversible partitioning using actual adsorption-desorption data in fig. 10 which are plots of adsorption - and single or consecutive desorption isotherms. Only one of the isotherms (there are typically 4 or 5) are plotted for each sorbent for clarity. For Diuron ($\log_{10} K_{ow} = 2.81$) we expect $K_{oc}^x = 595$ and for $m = 0.2$ kg/L the breakpoint in f_{oc} above which f_{oc} should not influence π_x is $f_{oc} = v_x / (mK_{oc}^x)$ (Table 3) i.e. $f_{oc} = 5.5\%$. Note that the slope of the consecutive desorption isotherms, π_x , is increasing from $f_{oc} = 1.9$ to 2.3% but that it slows its increase at $f_{oc} = 6.2\%$ and is essentially constant as f_{oc} increases to 9.3% . For Terbufos at the same particle concentration, since K_{ow} is almost an order of magnitude larger than for Diuron, the breakpoint in f_{oc} is correspondingly less: $f_{oc} = 0.24\%$ (Table 3). And, in fact, as shown in fig. 10 the slopes for $f_{oc} = 0.51$ - 18.4% are all essentially equal as predicted.

Conversely for large K_{ow} chemicals, varying the particle concentration for the same particle type strongly affects the slope. For both Kepone and HCBP at $f_{oc} \cong 5\%$, the particle concentration breakpoint $m = v_x / (f_{oc} K_{oc}^x)$ is $m = 84$ mg/L and $m = 5$ mg/L respectively (Table 3) and as m increases beyond these values indeed the slope of the desorption isotherms decrease.

The predicted relationships: both the absence of π_x increases as f_{oc} increases at constant m (Terbufos), as well as the particle concentration effect (Kepone and HCBP) can be directly seen in these examples. Thus they are not artifacts of the data reduction techniques used to generate π_x but are real features of reversible component partitioning.

REVERSIBLE PARTITIONING - ORGANIC ACIDS, BASES AND INORGANIC SORBENTS

The particle interaction model can only be directly tested if, for each chemical of interest, the data span a large enough range in mf_{oc} so that π_{xc} and v_x can both be estimated. Alternately an independent

method of estimating π_{xc} can be utilized such as that employed in the previous section for neutral organic chemicals and organic carbon containing particles where $\pi_{xc} = f_{oc} K_{oc}^x$ and K_{oc}^x is estimated from K_{ow} . For ionizable organic chemicals or for sorption onto inorganic particles no analogous methods are available. Thus no direct test is possible.

However the model does make one prediction that is not dependent upon the magnitude of π_{xc} :

$$\pi_x = \frac{\pi_{xc}}{1 + m\pi_{xc}/v_x} = \frac{v_x/m}{1 + \frac{v_x}{m\pi_{xc}}} < \frac{v_x}{m} \quad (16)$$

namely that π_x should be less than v_x/m regardless of the magnitude of π_{xc} . Hence plots of π_x versus m should either exhibit values below v_x/m corresponding to insignificant particle interaction induced desorption, or along the line $\pi_x = v_x/m$ corresponding to desorption being dominated by the particle interaction desorption mechanism.

Fig. 11 presents the observations for neutral organic chemicals and inorganic sorbents (nearly all clays). With rare exceptions the points are either below or on the line corresponding to $v_x \cong 1$. Fig. 12 presents similar results for organic acids and bases and the few available inorganic chemical data. Without an independent or at least generally applicable method of estimating π_{xc} , no further test is possible. However the substantial number of observed π_x that are near v_x/m suggests that the particle concentration effect on reversible partitioning is not limited to just neutral organic chemicals and organic carbon containing particles, but is a ubiquitous feature of reversible component partitioning.

A large set of metal sorption data: Ni, Co as sorbates with montmorillonite and quartz as sorbents that has the requisite range in particle concentration are also in conformity with the same reversible component partitioning model (58) employed above, eq. (14), thus supporting this view.

ALTERNATE POSSIBILITIES - A THIRD PHASE

The most popular explanation (60-62) for the particle concentration effect is that in addition to the aqueous and particle phases there exists a sorbing (third) phase which is not removed from the supernate by the particle separation technique (usually centrifugation) employed to operationally measure the "dissolved" concentration. This third phase is identified as being either dissolved organic matter or colloidal particles. To apply this hypothesis to reversible component partitioning we assume that the "dissolved" concentrations at adsorption and desorption steady state, c_a and c_d , are the sum of the truly dissolved concentrations, c'_a and c'_d , and that sorbed (or complexed) to the nonseparated third phase, $m'_a r'_a$ and $m'_d r'_d$, where m'_a and m'_d are the nonseparated third phase aqueous concentrations (kg/L) and r'_a and r'_d are the sorbed chemical concentrations (mg/kg-third phase) at adsorption (a) and desorption (d) steady states. Thus

$$c_a = c'_a + m'_a r'_a \quad (17)$$

$$c_d = c'_d + m'_d r'_d \quad (18)$$

and π_x (eq. 3) becomes:

$$\pi_x = \frac{r_a - r_d}{(c'_a + m'_a r'_a) - (c'_d + m'_d r'_d)} \quad (19)$$

or

$$\pi_x = \frac{r_a - r_d}{c'_a(1 + m'_a \pi'_a) - c'_d(1 + m'_d \pi'_d)} \quad (20)$$

where π'_a and π'_d are the adsorption and single desorption partition coefficients for the nonseparated phase. To convert this expression to that found to be descriptive of the data, eq. (14), a number of assumptions are required: (1) that the concentration of nonseparated third phase at adsorption and desorption steady states (for each consecutive desorption step) are equal: $m'_a = m'_d = m'$ and (2) that the partitioning to this phase is reversible: $\pi'_a = \pi'_d = \pi'$ in which case eq. (20) becomes:

$$\pi_x = \frac{r_a - r_d}{(c'_a - c'_d)(1 + m'\pi')} \quad (21)$$

Defining:

$$\pi_{xc} = \frac{r_a - r_d}{c'_a - c'_d} \quad (22)$$

as the "true" partition coefficient the result is:

$$\pi_x = \frac{\pi_{xc}}{1 + m'\pi'} \quad (23)$$

In order to convert this equation to eq. (14), which describes the data, multiply $m'\pi'$ by $m\pi_{xc}/m\pi_{xc} = 1$ so that:

$$\pi_x = \frac{\pi_{xc}}{1 + m\pi_{xc} \left(\frac{m'\pi'}{m\pi_{xc}} \right)} \quad (24)$$

from which v_x in eq. (14) is:

$$v_x = \frac{m\pi_{xc}}{m'\pi'} \quad (25)$$

The empirical finding that $v_x \cong 1$ requires that

$$m'\pi' \cong m\pi_{xc} \quad (26)$$

For neutral organic chemical and organic carbon containing particles: $\pi_{xc} = f_{oc} K_{oc}^x$ and if we assume (3) that the same normalization applies to the nonseparated phase: $\pi' = f'_{oc} K_{oc}^x$, then eq. (26) requires that

$$m'f'_{oc} \cong mf_{oc} \quad (27)$$

that is, that the quantity of organic carbon associated with the nonseparated phase is approximately equal to that contained in the separated particles. Alternately if specific surface area, σ (m^2/kg), is a proper normalization for inorganic particles then $\pi_{xc} = \sigma K_{\sigma}$ and $\pi' = \sigma' K_{\sigma}$ so

that $v_x \approx 1$ requires that

$$m'\sigma' \approx m\sigma \quad (28)$$

i.e. that the surface area/unit aqueous phase volume (m^2/L) for the nonseparated and separated phase, which presumably are particles in the case of inorganic sorbents, be equal.

There are a number of difficulties with this explanation. If we assume that the third phase are colloidal particles, it requires that nonseparable particles be in the same concentrations at adsorption, m'_a , and desorption, m'_d . If they are not separated at the adsorption step - they remain in the aqueous phase after the first centrifugation - they are then discarded when the supernatant is removed and uncontaminated aqueous phase is added. Thus during the desorption agitation they must be regenerated to the same concentration as they were present during adsorption. Further the requirement that follows from $v_x \approx 1$, eqs. (27-28) demands that they be quantitatively of equal sorptive capacity as the separated particles. That these specialized requirements obtain for all experiments, particles, etc. analyzed above appears to be highly unlikely. In fact for one HCBP experiment (Ref. 39, Sta. #69) the particles were wet sieved and only the greater than 75 μm particles were employed. This π_x is in conformity with the rest of the HCBP data (fig. 6).

If, on the other hand, the third phase is assumed to be dissolved organic carbon that desorbs from the particles, then the requirement (eq. 27) that $m'f'_{oc} \approx mf_{oc}$ forces the conclusion that there is as much dissolved organic carbon in the aqueous phase as there is particulate organic carbon in the particulate phase, per unit aqueous phase volume, at both adsorption and at each desorption. In fact $m'f'_{oc} = mf_{oc}$ requires that desorbable particle organic carbon has a partition coefficient of ~ 1 L/kg-organic carbon which is extremely small. Even liquid octanol which has an aqueous solubility of $\sim 10^{-3}$ M and therefore a partition coefficient of $\sim 10^3$ L/mole-octanol = 10.4 L/kg-organic carbon is ten-fold larger than that required for desorbable organic carbon.

Another difficulty with such a low partition coefficient is that substantial organic carbon would be removed at each desorption cycle. Hence at adsorption equilibrium, one-half of the original particulate organic carbon mass must desorb and be in solution. Since this is discarded before desorption is initiated, it is difficult to see how $m'_a = m'_d$. Rather $m'_d = m'_a/2^j$ where j is the desorption cycle index. It would further suggest that simply washing particles in water should remove substantial quantities of particle-bound organic carbon. Finally it is difficult to see how dissolved organic carbon could be implicated with inorganic sorbents.

Perhaps the most convincing experiments which appear to preclude nonseparable third phase as an explanation are resuspension experiments (58,63) in which, instead of desorption into new uncontaminated aqueous phase, the particles are resuspended into a reduced volume of the aqueous phase remaining after adsorption and centrifugation. For this experimental design the concentration of the nonseparated third phase in the supernatant must be the same at both adsorption and resuspension equilibration. Only the concentration of the separated particles is increased by resuspension into a reduced aqueous phase volume. For these experiments the partition coefficient is observed to decrease as particle concentration increases from the adsorption to the resuspension equilibrations. If a desorbing third phase (dissolved organic carbon) is involved then the problem of explaining the decreased partitioning is just transferred to explaining why there is increased desorption of the third phase into the original supernatant when only particle concentration is increased at the resuspension equilibration.

Dilution experiments (58,63) dispense with centrifugation of the experimental vessel completely and decreases particle concentration by adding either uncontaminated aqueous phase (63) or equivalently contaminated aqueous phase from a parallel vessel (58). These experiments yield increasing partition coefficient with decreasing particle concentration.

Thus nonseparable third phase models require that the nonseparable phase has properties that are both ubiquitous, very specialized and, for desorbing organic carbon, not chemically realistic. Further they appear

to be precluded by resuspension and dilution experiments designed expressly to strongly discriminate against such models.

Desorption Kinetics and Particle Aggregation

An examination of desorption kinetics using an air stripping technique to remove dissolved chemical from the sorbent suspension (56) precludes the need for consecutive particle separations by centrifugation that characterizes the desorption data analyzed above. The results of a series of these experiments, presented by Karickhoff and Morris (64), indicates that there exists a labile component that desorbs rapidly (< 1 hr) and a nonlabile or resistant component whose desorption rate they correlate to the equilibrium partition coefficient: $K_p = f_{oc} K_{oc}$. This result and square root of time dependence of desorption of the nonlabile fraction strongly suggest intraparticle diffusion as the kinetic mechanism controlling nonlabile component desorption.

For the labile component, Karickhoff and Morris (64) found that the labile fraction of total sorbed chemical, X_l , decreased as mK_p increased, where m is the particle concentration. Their data analysis suggested:

$$X_l \approx \frac{1}{2.5 + mK_p/10} \quad (29)$$

If we identify $X_l = r_x/r_a$, consistent with the component model, eq. (1-2) then $X_l = \pi_x/\pi_a$ and if at sorption equilibrium $\pi_a = K_p = f_{oc} K_{oc}$, then:

$$X_l = \frac{\pi_x}{f_{oc} K_{oc}} \quad (30)$$

Using eq. (14) for π_x and assuming $K_{oc} = K_{oc}^x$ yields:

$$X_l = \frac{\pi_x}{f_{oc} K_{oc}^x} = \frac{1}{1 + mf_{oc} K_{oc}^x / v_x} \quad (31)$$

which is the same functional form as that suggested by Karickhoff and Morris, eq. (29). The results of a fit of their data to eq. (16), is

shown in Table 4. A significantly larger $v_x = 11.6(\pm 7.22)$ is found as well as the expected log linearity between K_{oc}^x and K_{ow} . The implication to be drawn from the larger v_x is unclear at present - in particular is it related in some way to the completely different experimental design - but the remarkable result is that the same functional form, eq. (31), also describes their data. Since third phase models clearly do not apply to their experiment we take this to be further evidence that third phase explanations are inappropriate.

Karickhoff and Morris (64) suggest that particle aggregation may be the cause of the particle concentration effect they observed. Although this may be possible we have microscopically examined inorganic particle suspensions at various concentrations that exhibit the effect (58) and find no evidence of larger aggregations at higher particle concentrations. Also, if particle aggregation were the sole cause of the decreasing labile component sorption one would expect that the functional dependency would be solely in terms of m , rather than $mf_{oc} K_{oc}^x$. The latter expression includes the chemical property K_{oc}^x and the organic carbon fraction, f_{oc} , as well as the particle concentration. It is difficult to imagine a particle aggregation model that yields this functional dependence.

Discussion

It should also be stressed that the particle interaction model which is based upon the hypothesis that an additional desorption reaction exists, eq. (12), is no more successful in explaining why a constant $v_x = k_{ads}/k_{p-d}$ appears to be characteristic of reversible component sorption, although fig. 7 suggests that it might vary systematically and the gas purge experiments suggest it may not be constant but rather a function of experiment design. One can speculate that both the adsorption and particle interaction induced desorption rate are physically rather than chemically determined by, for example, the level of turbulence induced by the agitation. While the turbulence level may be quite different among the experiments analyzed in this paper, it is only the ratio, k_{ads}/k_{p-d} , that needs to be constant and the absolute magnitude of the turbulence may cancel out of the ratio.

One piece of evidence that supports the particle interaction model is that, in the absence of agitation, the prediction $\pi_x = f_{oc} K_{oc}^x$ is verified for HCBP sorption. In a series of dual tag diffusion experiments using syringes (65) with a layer of uncontaminated sediment overlying a layer of tagged (H^3 -HCBP and C^{14} -graphite particles) sediment the K_{oc} for HCBP is estimated to be $10^{6.61 \pm 0.13}$ whereas from conventional agitated adsorption-desorption experiments (Table 3, fig. 6) K_{oc}^x is estimated to be $10^{6.50 \pm 0.31}$. This concurrence can be explained by observing that in the syringe experiments the particles are stationary and, therefore, particle interaction induced desorption which is associated with particle motion is not occurring. Hence the syringe partition coefficients should correspond to the low particle concentration limit inferred from the agitated experiments. The fact that this is the case suggests that it is particle motion and, therefore, particle interactions that enhance desorption if particle concentrations are large enough and, as a consequence, particle interactions are frequent enough for this reaction to be significant.

Finally we observe that partition coefficients (actually distribution coefficients) inferred from field measurements of dissolved and particulate chemical concentrations also display an inverse relationship to particle concentration (39,66) so that the effect is an important factor in determining the partitioning of chemicals between particulate and dissolved phases in natural waters. Preliminary analysis of collections of these data sets appear to conform to eq. (14). A detailed analysis is forthcoming.

The most significant shortcoming of the model presented above is the lack of a mechanistic explanation for the particle interaction induced desorption reaction, eq. (12). One would surely like to know what, exactly, is the physics and chemistry of this reaction. Or, more critically, if the reaction itself is the correct explanation for what appears to be the correct result, eq. (14). The success of eq. (14) in correlating large amounts of adsorption-desorption data is undeniable, fig. 4-6, but its derivation via the reaction scheme, eq. (11-12) must be regarded as speculative.

From a practical point of view, the correlative power of the model for neutral organic chemicals and organic carbon containing particles is

quite useful since a knowledge of the chemical's K_{ow} , the particle's f_{oc} and its concentration, m , suffices to determine π_x , the reversible component partition coefficient. For inorganic sorbents and ionizable or inorganic chemicals an upper bound to the expected partition coefficient, $\pi_x < v_x/m$, is available.

From a theoretical point of view, the most surprising and intuitively disturbing result is the observation that v_x is of order one (\pm one half an order of magnitude) for all chemicals and particle types examined. This generality suggests either that there exists a universal feature of reversible sorption which has heretofore been unsuspected or that the entire analysis itself is flawed in some subtle way. The author prefers to believe that the former is the case and that its explanation is via a particle interaction induced desorption reaction.

Acknowledgements

The participation of our research associates and assistants at Manhattan College: Joanne Guerriero, Michael Labiak, Salil Kharkar in the laborous task of assembling and reducing the data employed in this paper is gratefully acknowledged. Alan Felsot kindly provided the data from his useful experiments, as did John Connolly and Samuel Karickhoff. Conversations with the members of our research group: Donald O'Connor, Robert Thomann, John Connolly, John Jeris, John Mahony, and Richard Winfield were, as always, helpful and stimulating. Other colleagues have also endured discourses on this subject, and their patience and insights are appreciated. The continuing support of the EPA Large Lakes Research Station, CR807853 and CR810799 and particularly Nelson Thomas (EPA-Duluth) and William Richardson (EPA-Grosse Ile) is greatly appreciated.

TABLE 1. METHODS FOR CALCULATING π_x

Reported Data	Formula Employed (a)	References
Adsorption and Consecutive Desorption Isotherm data	Geometric Average of $\pi_x = \frac{r(i,j) - r(i,j+1)}{c(i,j) - c(i,j+1)}$	1,2,4,5,6,7,9,10,11,12 * 14, 15, 17, 33, 49, 50, 53
Adsorption and Single Desorption Isotherm data	"	3, 13, 16*, 21, 41*
Single Point Adsorption, Single or Consecutive Desorption data	"	18, 26, 28, 37, 51, 54
Adsorption and Single Desorption Partition Coefficients	$\pi_x = \frac{\pi_a - \alpha\pi_d}{1 - \alpha + m(\pi_d - \pi_a)}$	20, 23, 27, 28, 30, 35 38, 39, 40, 43, 44
Single Point Adsorption and Desorption: Sorbed data only	$\pi_x = \frac{\Delta r}{(1-\alpha)(c_T - m r)} - m \Delta r$	22, 24, 32, 34
Adsorption Isotherm Partition Coefficient	$\pi_x = \frac{\delta\pi_a}{1 - \alpha - m\delta\pi_a}$	19, 25, 29, 31
Single Point Adsorption and Desorption: Aqueous concentrations	$\pi_x = \frac{c_d - \alpha c_a}{m(c_a - c_d)}$	28
Single Point Consecutive Desorptions: Data reported as sorbed fraction remaining at cycle j	Least Square fit of: $\frac{r(1,j)}{r_T} = \frac{r_o}{r_T} + \frac{1}{1 + m\pi_x} \left(\frac{r_o}{r_T} \right)^{j-1} (1 - \frac{r_o}{r_T})^{\alpha + m\pi_x}$	45, 46, 48

(a) See Notation list for definitions

* Data reconstructed from reported Freundlich constants and mass balance equation (9)

TABLE 2. OCTANOL-WATER PARTITION COEFFICIENTS

Chemical	$\log_{10} K_{ow}$	Ref.	Chemical	$\log_{10} K_{ow}$	Ref.
Aldicarb	0.70	[67]	Beta-HCH	3.80	[69]
Carbofuran	1.60	[68]	Alpha-HCH	3.81	[69]
Monuron	2.12	[67]	Methyl Parathion	3.87	[74]
Linuron	2.19	[68]	Chlorpyrifos	4.99	[68]
Fluometron	2.20	[71]	Pyrene	5.18	[44]
Diuron	2.81	[67]	Endrin	5.34	[68]
Carbaryl	2.81	[67]	Kepone	5.50	[43]
Permethrin	2.888	[67]	DDT	5.57	[67]
Phorate	2.92	[67]	Benz(a)Anthracene	5.91	[74]
Diazinon	3.02	[67]	Aroclor 1254	6.03	[73]
Napropamide	3.10	[70]	pp' DDT	6.19	[67]
Parathion	3.40	[67]	Leptophos	6.31	[67]
Terbufos	3.68	[3]	Benz(a)Pyrene	6.50	[72]
Dieldrin	3.69	[67]	Mirex	6.89	[74]
Gamma-HCH	3.72	[69]	HCBP	7.75	[72]

TABLE 3. NONLINEAR LEAST SQUARES FIT* OF $\log_{10} \pi_x$

$$\pi_x = \frac{f_{oc} K_{oc}^x}{1 + m f_{oc} K_{oc}^x / v_x}$$

Entire data set (N = 129)

$$\log_{10} K_{oc}^x = a_0 + a_1 \log_{10} K_{ow}$$

$$v_x = 1.4(0.18); \quad a_0 = 0.178(0.16); \quad a_1 = 0.924(0.053)$$

$$\sigma(\log_{10} \pi_x) = 0.408$$

Individual Chemicals

<u>Chemical</u>	<u>No. of Data Points</u>	<u>$\log_{10} K_{oc}^x$ (L/kg)</u>	<u>v_x</u>	<u>$\sigma(\log_{10} \pi_x)$</u>
Aldicarb	5	1.01(0.16)	-	-
Diuron	18	2.60(0.10)	4.39 (2.7)	0.312
Phorate	5	2.58(0.05)	3.02 (0.46)	0.057
Parathion	17	3.45(0.12)	4.73 (1.4)	0.246
Terbufos	5	3.29(0.71)	0.952(0.31)	0.200
Lindane	7	4.04(0.42)	0.619(0.32)	0.470
Kepone	10	5.28(0.32)	0.865(0.27)	0.328
pp' DDT	6	7.16(2.4)	1.60 (0.73)	0.343
HCBP	12	6.50(0.31)	0.694(0.06)	0.109

* Parameter Estimate (Standard Error of Estimate)

TABLE 4. Least Square Fit* of $\pi_x = X_x K_x^{v_x}$ ** to Equation 14

Chemical	$\log_{10} K_{oc}^x$	$\log_{10} K_{ow}^x$	Ref. for K_{ow}
Trifluralin	3.94(0.18)	3.06, 5.34	[67], [68]
Pyrene	4.64(0.22)	4.88, 5.18	[77], [68]
Pentachlorobenzene	4.97(0.37)	4.94, 5.19	[76], [68]
Hexachlorobenzene	5.50(0.39)	5.23, 5.50	[68], [75]

* Parameter (Standard error of estimate)
 $\sigma(\log_{10} \pi_x) = 0.302$

** Karickhoff and Morris (64)

NOTATION

- $r(i,j)$ = sorbed concentration (mg/kg); i^{th} isotherm, j^{th} desorption cycle
 $c(i,j)$ = aqueous concentration (mg/L); i^{th} isotherm, j^{th} desorption cycle
 $r_a(r_d)$ = adsorption (single desorption) sorbed concentration (mg/kg)
 $c_a(c_d)$ = adsorption (single desorption) aqueous concentration (mg/L)
 $\pi_a(\pi_d)$ = adsorption (single desorption) partition coefficient (L/kg)
 π_x = reversible component partition coefficient (L/kg), eq. 3
 m = particle concentration (kg/L)
 c_T = $m r_a + c_a$ = initial total chemical concentration (mg/L)
 r_T = initial sorbed chemical concentration (mg/kg)
 Δr = $r_a - r_d$, desorbed chemical concentration (mg/kg)
 δ = $\Delta r / r_a$, fraction chemical desorbed
 α = volume fraction of aqueous phase not removed before desorption
 r_o = resistant component sorbed chemical concentration (mg/kg)
 K_{oc} = π_a / f_{oc} , organic carbon normalized adsorption partition coefficient (L/kg-organic carbon)
 K_{ow} = octanol-water partition coefficient (L/L)

REFERENCES

1. Bowman, B.T. and W.W. Sans, "Adsorption of Parathion, Fenitrothion, Methyl Parathion, Aminoparathion and Paraoxon by Na^+ , Ca^{2+} , and Fe^{3+} Montmorillonite Suspensions", Soil Sci. Am. J., Vol. 41, p. 514, 1977.
2. Wahid, P.A. and N. Sethunathan, "Sorption-Desorption of Parathion in Soils," J. Agric. Food Chem., Vol. 26, No. 1, 1978.
3. Felsot, A. and P.A. Dahm, "Sorption of Organophosphorus and Carbamate Insecticides by Soil," Agricultural and Food Chemistry, Vol. 27, No. 3, p. 557, May/June 1979.
4. de Bussetti, S.G., E.A. Ferreiro and A.K. Helmy, "Adsorption of 1,10-Phenanthroline by Some Clays and Oxides," Clays and Clay Minerals, Vol. 28, No. 2, pp. 149-154, 1980.
5. Wahid, P.A. and N. Sethunathan, "Sorption-Desorption of α , β , and γ Isomers of Hexachlorocyclohexane in Soils," Agricultural and Food Chemistry, Vol. 27, No. 5, p. 1050, Sept./Oct. 1979.
6. Swanson, R.A. and G.R. Dutt, "Chemical and Physical Processes that Affect Atrazine and Distribution in Soil Systems," Soil Science Society of America Proceedings, Vol. 37, No. 6, Nov./Dec. 1973.
7. van Genuchten, M.Th., J.M. Davidson and P.J. Wierenga, "An Evaluation of Kinetic and Equilibrium Equations for the Prediction of Pesticide Movement Through Porous Media," Soil Sci. Soc. of America Proc., Vol. 38, 1974.
8. Koskinen, W.C., G.A. O'Connor and H.H. Cheng, "Characterization of Hysteresis in the Desorption of 2,4,5-T from Soils," Soil Science Am. J., Vol. 43, 1979.
9. Davidson, J.M., G.H. Brusewitz, D.R. Backer, and A.L. Wood, "Use of Soil Parameters for Describing Pesticide Movement Through Soils," Environmental Protection Technology Series EPA-660/2-75-009, May 1975.
10. Elrashidi, M.A. and G.A. O'Connor, "Boron Sorption and Desorption in Soils," Soil Sci. Am. J., Vol. 46, p. 27, 1982.
11. Gayraud, J.P., "Etude, A L'Aide du Tritium de L'iode 131 et du Strontium 90, de la Dispersion et des Echanges Physico-Chimiques en Milieu Poreux Sature," Academie de Montpellier, Universite des Sciences et Techniques du Languedoc., 1973.

12. Fluhler, H., J. Polomski, and P. Blaser, "Retention and Movement of Fluoride in Soils," J. Environ. Qual., Vol. 11, No. 3, 1982.
13. Mukhtar, M., "Desorption of Adsorbed Ametryn and Diuron from Soils and Soil Components in Relation to Rates, Mechanisms, and Energy of Adsorption Reactions," Ph.D. Thesis, University of Hawaii, 1976.
14. Wu, C-H., N. Buehring, J.M. Davidson and P.W. Santelmann, "Napropamide Adsorption, Desorption, and Movement in Soils," Weed Science, Vol. 23, No. 6, Nov. 1975.
15. Murray, D.S., P.W. Santelmann, and J.M. Davidson, "Comparative Adsorption, Desorption, and Mobility of Dipropetryn and Prometryn in Soil," J. Agric. Food Chem., Vol. 23, No. 3, 1975.
16. Jamet, P. and M-A. Piedallu, "Mouvement du Carbofuran dans Différents Types de Soils," Phytiatrie-Phytopharmacie, 24, 279-296, 1975.
17. Peck, D.E., D.L. Corwin, and W.J. Farmer, "Adsorption-Desorption of Diuron by Freshwater Sediments," J. of Environmental Quality, Vol. 9, No. 1, p. 101, Jan.-Mar. 1980.
18. Bowman, B.T., "Method of Repeated Additions for Generating Pesticide Adsorption-Desorption Isotherm Data," Can. J. Soil Sci., 59, 435-437, Nov. 1979.
19. Wahid, P.A. and N. Sethunathan, "Sorption-Desorption of Lindane by Anaerobic and Aerobic Soils," Agric. and Food Chemistry, 28, 623, 1980.
20. Moyer, J.R., R.B. McKercher, and R.J. Hance, "Desorption of Some Herbicides from Montmorillonite and Peat," Can. J. Soil Sci., 52:439-447, Oct. 1972.
21. Miller, R.W. and S.D. Faust, "Sorption from Aqueous Solutions by Organic Clays: I. 2,4-dD By Bentone 24," in Fate of Organic Pesticides in the Aquatic Environment, ed. S.D. Faust, Adv. Chem. Series 111, Am. Chem. Soc., p. 121, 1972.
22. Weber, J.B., "Ionization and Adsorption-Desorption of Tricyclazole by Soil Organic Matter, Montmorillonite Clay, and Cape Fear Sandy Loam Soil," J. Agric. Food Chem., 30, 584-588, 1982.
23. Pierce, R.H., Jr., CE. Olney and G.T. Felbeck, Jr., "pp'-DDT adsorption to suspended particulate matter in sea water," Geochimica et Cosmochimica Acta, Vol. 38, pp. 1061-1073, 1974.
24. Mustafa, M.A. and Y. Gamar, "Adsorption and Desorption of Diuron as a Function of Soil Properties," Soil Sci. Soc. of Amer. Proc., Vol. 36, p. 561, 1972.

25. Sharom, M.S. and K.R. Solomon, "Adsorption-Desorption, Degradation, and Distribution of Permethrin in Aqueous Systems," J. Agric. Food Chem., 29, 1122-1125, 1981.
26. Huang, J-C. and C.S. Liao, "Adsorption of Pesticides by Clay Minerals," J. Sanitary Engineering Division, Proceedings of the American Society of Civil Engineers, p. 1057, Oct. 1970.
27. Wildish, D.J., C.D. Metcalfe, H.M. Akagi, and D.W. McLeese, "Flux of Aroclor 1254 Between Estuarine Sediments and Water," Bull. Environm. Contam. Toxicol. 24, 20-26, 1980.
28. Smith, J.H., W.R. Mabey, N. Bohonos, B.R. Holt, S.S. Lee, T.-W. Chou, D.C. Bomberger, and T. Mill, "Environmental Pathways of Selected Chemicals in Freshwater Systems, Part II: Laboratory Studies," EPA-600/7-78-074, May 1978.
29. Dalal, R.C., Effect of Associated Anions on Ammonium Adsorption by and Desorption from Soils, J. Agric. Food Chem. 23, 4, p. 684, 1975.
30. Saleh, F.Y., K.L. Dickson and J.H. Rodgers, Jr., "Fate of Lindane in the Aquatic Environment: Rate Constants of Physical and Chemical Processes." Institute of Applied Sciences. North Texas State Univ. Denton, Texas, 1981.
31. Picer, N., M. Picer and P. Strohal, "The Interaction of DDT with Suspended Particles in Sea Water," Water, Air, and Soil Pollut., 8(1977), p. 429.
32. Carringer, R.D., J.B. Weber, and T.J. Monaco, "Absorption-Desorption of Selected Pesticides by Organic Matter and Montmorillonite," Agric. and Food Chemistry, Vol. 23, No. 3, p. 568, May/June 1975.
33. Savage, K.E. and R.D. Wauchope, "Fluometuron Adsorption-Desorption Equilibria in Soil," Weed Science, Vol. 22, No. 2, pp. 106-110, March 1974.
34. Appelt, H., N.T. Coleman, and P.F. Pratt, "Interactions Between Organic Compounds, Minerals, and Ions in Volcanic-ash-derived Soils: I. Adsorption of Benzoate, p-OH Benzoate, Salicylate, and Phthalate Ions, Soil Sci. Soc. of Amer. Proc., Vol. 39, p. 623, 1975.
35. Fusi, P., S. Cecconi, M. Franci et C. Vazzana, "Adsorption et desorption de la pyrazone par quelques colloides organiques et minreaux," Weed Research, Vol. 16, pp. 101-109, 1976.
36. Bowman, B.T. and W.W. Sans, "Influence of Methods of Pesticide Application on Subsequent Desorption from Soils," J. Agric. Food Chem. 30, p. 147, 1982.

37. Saltzman, S., L. Kliger, and B. Yaron, "Adsorption-Desorption of Parathion as Affected by Soil Organic Matter," J. Agr. Food Chem., Vol. 20, No. 6, p. 1224, Nov./Dec. 1972.
38. Di Toro, D. M. and L.M. Horzempa. 1982. Reversible and Resistant Components of Hexachlorobiphenyl Adsorption-Desorption: Isotherms. Environ. Sci. Technol. 16, p. 594-602.
39. Di Toro, D. M. and L.M. Horzempa. 1982. Reversible and Resistant Components of PCB Adsorption and Desorption: Adsorbent Concentration Effects. J. Great Lakes Res. 8(2):336-349.
40. Di Toro, D. M., L.M. Horzempa and M.C. Casey. 1982. Adsorption and Desorption of Hexachlorobiphenyl. A. Experimental Results and Discussions B. Analysis of Exchangeable and Nonexchangeable Components. EPA-600/53-83-088.
41. Farmer, W.J., Aochi, Y. 1974. Picloram Sorption by Soils. Soil Sci. Soc. Amer. Proc. 38, p. 418-423.
42. Adams, R.S., Jr., Li, P. 1971. Soil Properties Influencing Sorption and Desorption of Lindane. Soil Sci. Soc. Amer. Proc. 35, p. 78-81.
43. Connolly, J.P. 1980. The Effect of Sediment Suspension on Adsorption and Fate of Kepone. Ph.D. Thesis. University of Texas, Austin.
44. Karickhoff, S.W., D.S. Brown, and T.A. Scott. 1979. Sorption of Hydrophobic Pollutants on Natural Sediments. Wat. Res. Res 13, p. 241-248.
45. Talbert, R.E. 1963. Studies of the Behavior of Some Triazine Herbicides in Soils. Ph.D. Thesis, University of Missouri.
46. Talbert, R.E. and O.H. Fltechall. The Adsorption of Some S-Triazines in Soils Weeds.
47. Graham-Bryce, I.J. 1967. Adsorption of Disulfoton by Soil. J. Sci. Ed. Agric. 18, p. 72-77.
48. Sharom, M.S., J.R.W. Miles, C.R. Harris and F.L. McEwen. 1980. Behaviour of 12 Insecticides in Soil and Aqueous Suspensions of Soil and Sediment. Water Research, Vol. 14(1095-1100).
49. Koskinen, W.C. 1980. Evaluation of the Batch Equilibration Method for Characterization of Adsorption-Desorption of 2,4,5-Trichlorophenoxyacetic Acid in Soils. Ph.D. Thesis, Washington St. Univ.

50. van Genuchten, M. Th., P.J. Wierenga and G.A. O'Connor. 1977. Mass Transfer Studies in Sorbing Porous Media: III. Experimental Evaluation with 2,4,5-T. Soil Science Society of America Journal. Vol. 41, No. 2, March-April 1977.
51. Couchat, Ph., F. Brissaud and J.P. Gayraud. 1980. A Study of Strontium-90 Movement in a Sandy Soil. Soil Sci. Soc. Am. J., Vol. 44.
52. Miles, J.R.W., B.T. Bowman, and E.R. Harris. 1981. Adsorption, Desorption, Soil Mobility and Aqueous Persistence of Fensulfotion and Its Sulfide and Sulfone Metabolites. J. Environ. Sci. Health, B16(3), p. 309-324.
53. Davidson, J.M. and J.R. McDougal. 1973. Experimental and Predicted Movement of three Herbicides in a Water Saturated Soil. J. Environ. Quality 2(4), p. 428-433.
54. Harris, C.I. and G.F. Warren. 1964. Adsorption and Desorption of Herbicides by Soil. Weeds, p. 120-126.
55. O'Connor, D.J. and J.P. Connolly. 1980. The Effect of Concentration of Adsorbing Solids on the Partition Coefficient. Water Res. 14, pp. 1517-1523.
56. Karickhoff, S.W. 1980. Sorption Kinetics of Hydrophobic Pollutants in Natural Sediments. Contaminants and Sediments, Vol. 2, (ed. R.A. Baker) Ann Arbor Sci. Publ. Ann Arbor, Mich., pp. 193-205.
57. Karickhoff, S.W. 1984. Organic Pollutant Sorption in Aquatic Systems. J. Hydra. Div. ASCE, Vol. 110, No. 6, pp. 707-735.
58. Di Toro, D.M., J. D. Mahony, P.R. Kirchgraber, A.L. O'Byrne, L.R. Pasquale, D.C. Piccirilli, 1984. The Effects of Nonreversibility, Particle Concentration, and Ionic Strength on Heavy Metal Sorption. Submitted for Publication Environ. Sci. Technol.
59. Marquardt, D.W. 1936. An algorithm for Least-Squares Estimation of Non-Linear Parameters. J. Soc. Indust. Appl. Math. 11(2), p. 431-441.
60. Duursma, E.K. 1976. Radioactive Tracers in Estuarine Chemical Studies, in Estuarine Chemistry, ed. J.D. Burton, P.S. Liss. Academic Press, N.Y. p. 159.
61. Voice, T.C., C.P. Rice, W.J. Weber, Jr. 1983. Effect of Solids Concentration on the Sorptive Partitioning of Hydrophobic Pollutants in Aquatic Systems. Environ. Sci. Technol. 17, p. 513-518.
62. Benes, P., V. Majer. 1980. Trace Chemistry of Aqueous Solutions, Elsevier Sci. Publ. Co., N.Y., p. 203.

63. Di Toro, D.M., L. Horzempa. 1983. Reversible and Resistant Component Model of Hexachlorobiphenyl Adsorption-Desorption: Resuspension and Dilution, in Physical Behavior of PCB's in the Great Lakes, ed. D. Mackay et al., Ann Arbor Science, p. 89.
64. Karickhoff, S.W. and K.R. Morris. 1984. Sorption Dynamics of Hydrophobic Pollutants in Sediment Suspensions. US EPA Env. Res. Lab., Athens, Ga.
65. Di Toro, D.M., J.S. Jeris, D. Ciarcia. 1984. Diffusion and Partitioning of Hexachlorobiphenyl in Sediments. Submitted for Publication Environ. Sci. Technol.
66. Eisenreich, S.J., P.D. Capel, B.B. Looney. PCB Dynamics in Lake Superior Water, in Physical Behavior of PCB's in the Great Lakes, ed. D. Mackay et al., Ann Arbor Science, p. 181.
67. Rao, P.S.C. and J.M. Davidson. Retention and Transformation of Selected Pesticides and Phosphorus in Soil-Water Systems: A Critical Review. EPA 600/3-82-060, p. 23-25.
68. Kenaga, E.E. and C.A.I. Goring. Relationship between Water Solubility, Soil Sorption, Octanol-Water Partitioning and Concentration of Chemicals in Biota in Aquatic Toxicology, ASTM Tech. Publ. # 707, Phil., Pa. p. 78.
69. Karickhoff, S.W. 1981. Semi-Empirical Estimation of Sorption of Hydrophobic Pollutants on Natural Sediments and Soils. Chemosphere 10(8), p. 833.
70. Mingelgrin, U., Z. Gerstle. 1983. Reevaluation of Partitioning as a Mechanism of Nonionic Chemicals Adsorption to Soils. J. Env. Quality 12(1).
71. Veith, G. 1983. Personal Communication, EPA Duluth Res. Lab.
72. Rapaport, R.A. and S.J. Eisenreich. 1984. Chromatographic Determination of Octanol-Water Partition Coefficients (Kow's) for 58 Polychlorinated Biphenyl Congeners. Environ. Sci. Technol. 18, 3, p. 163.
73. Water Related Environmental Fate of 129 Priority Pollutants, EPA. 1979.
74. MacKay, D., A. Bobra and W.Y. Shiu. 1980. Relationships between Aqueous Solubility and Octanol-Water Partition Coefficients. Chemosphere 9, p. 701-711.
75. Chiou, C.T. and D.W. Schmedding. 1982. Partitioning of Organic Compounds in Octanol-Water Systems, Environ. Sci. Technol., 16, p. 4-10.

76. Banerjee, S., S.H. Yalkowsky, S.C. Valvani. 1980. Water Solubility and Octanol/Water Partition Coefficients of Organics. Limitations of the Solubility-Partition Coefficient correlation. Environ. Sci. Technol. 14, p. 1227-1229.
77. Mackay, D. 1982. Correlation of Bioconcentration Factors. Environ. Sci. Technol. 16, p. 274-278.

FIGURE CAPTIONS

- Fig. 1. Components model fit to consecutive desorption data for Parathion [2] and Atrazine [6].
- Fig. 2. Components model fit to consecutive desorption data for Picloran [7], Diuron - Lake Sediment [17] SR-90 [11], Diuron - Montmorillonite [13], Fluometron [9], and Phenanthroline [4].
- Fig. 3. Sequential plot of π_x (various symbols); π_x/f_{oc} (+), $m\pi_x$ (x), ordered by increasing m and increasing f_{oc} . Vertical dotted lines separate chemicals, horizontal dotted lines are the chemical's K_{ow} .
- Fig. 4. Comparison of eq. (14-15) to data: observed versus calculated π_x (top) and in normalized form (bottom).
- Fig. 5. Normalized plots of individual chemical data.
- Fig. 6. Normalized plots of individual chemical data.
- Fig. 7. Parameters obtained from individual fits of eq. (14) to chemical data versus octanol/water partition coefficient.
- Fig. 8. Low particle concentration limit relationships: Log linearity of K_{oc} to K_{ow} (top) and linearity of normalized π_x to f_{oc} (middle and bottom). The latter two lines have slope one.
- Fig. 9. The high particle concentration limit. π_x as a function of m only.
- Fig. 10. Consecutive desorption data for varying f_{oc} (top) and particle concentration (bottom).

Fig. 11. Comparison of data to the prediction that $\pi_x < v_x/m$ for sorption to inorganic sorbents.

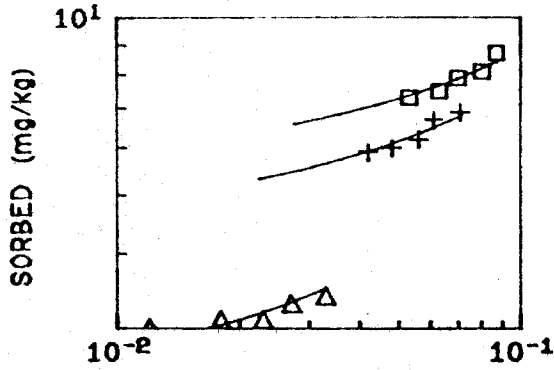
Fig. 12. Comparison of data to the prediction that $\pi_x < v_x/m$ for sorption of inorganic chemicals (top) and organic acids, and bases (middle and bottom).

PARATHION - ACID SULPHATE

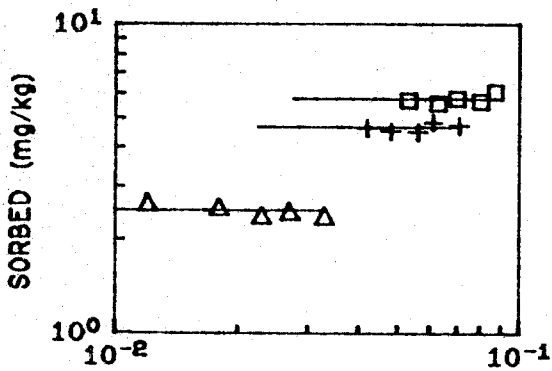
$m = 0.1 \text{ kg/L}$

CONSECUTIVE DESORPTION

$\pi_x = 30.7 \text{ L/kg}$

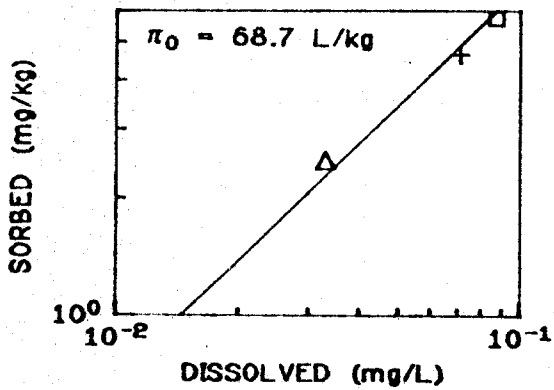


RESISTANT COMPONENT DESORPTION



RESISTANT COMPONENT ADSORPTION

$\pi_0 = 68.7 \text{ L/kg}$

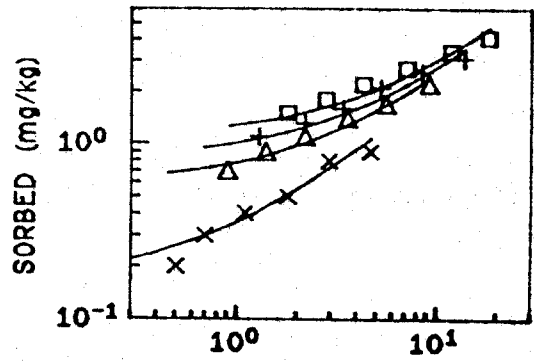


ATRAZINE-SANDY LOAM

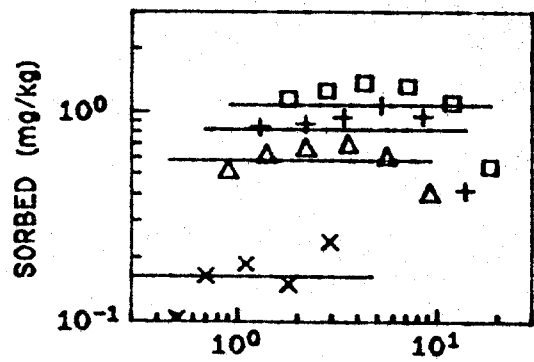
$m = 0.4 \text{ kg/L}$

CONSECUTIVE DESORPTION

$\pi_x = 0.194 \text{ L/kg}$



RESISTANT COMPONENT DESORPTION



RESISTANT COMPONENT ADSORPTION

$\pi_0 = 0.0525 \text{ L/kg}$

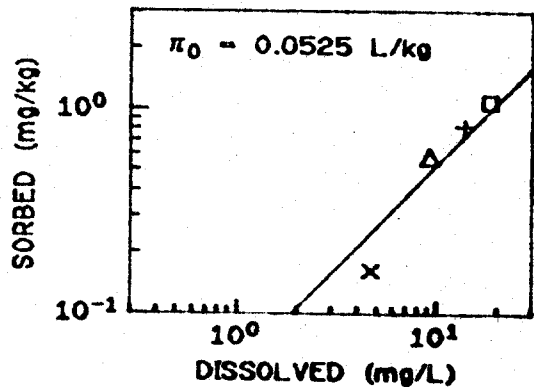


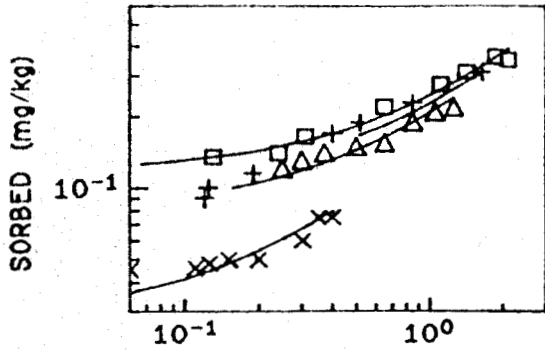
FIGURE 1

PICLORAM - NORGE LOAM

m = 0.1 kg/L

CONSECUTIVE DESORPTION

$\pi_x = 0.129$ L/kg

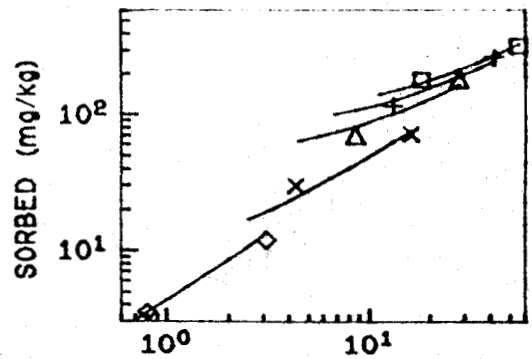


DIURON-CaMONTMORILLONITE

m = 0.1 kg/L

CONSECUTIVE DESORPTION

$\pi_x = 4.3$ L/kg

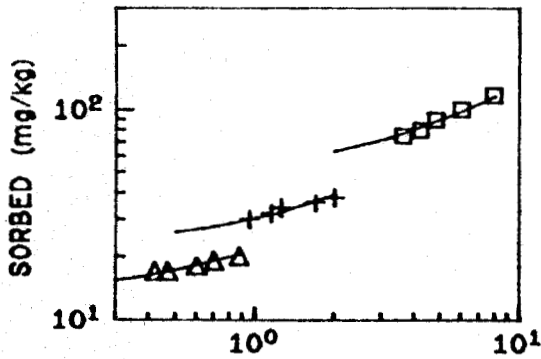


DIURON-LAKE SEDIMENT

m = 0.2 kg/L

CONSECUTIVE DESORPTION

$\pi_x = 8.86$ L/kg

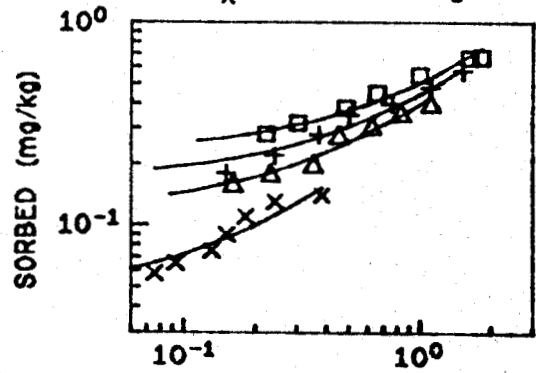


FLUOMETURON-NORGE LOAM

m = 1 kg/L

CONSECUTIVE DESORPTION

$\pi_x = 0.284$ L/kg

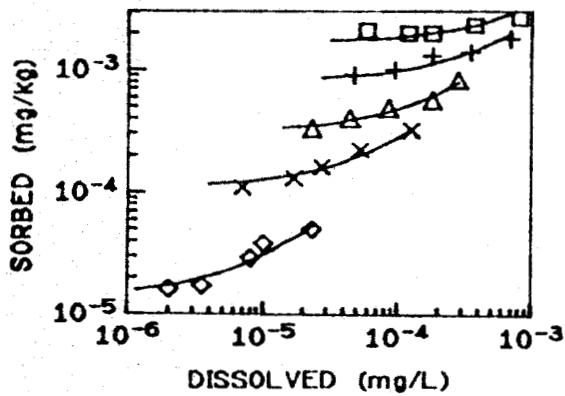


STRONTIUM-90
CALCAREOUS SAND

m = 0.1 kg/L

CONSECUTIVE DESORPTION

$\pi_x = 1.7$ L/kg



1,10-PHENANTHROLINE

-SIALUMINA

m = 0.004 kg/L

CONSECUTIVE DESORPTION

$\pi_x = 232$ L/kg

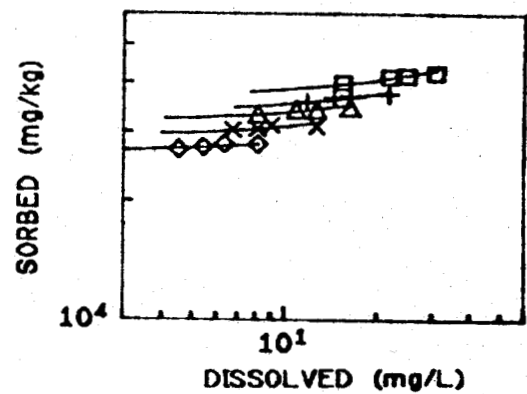


FIGURE 2

REVERSIBLE PARTITION COEFFICIENTS NEUTRAL ORGANIC CHEMICALS - $f_{oc} > 0$

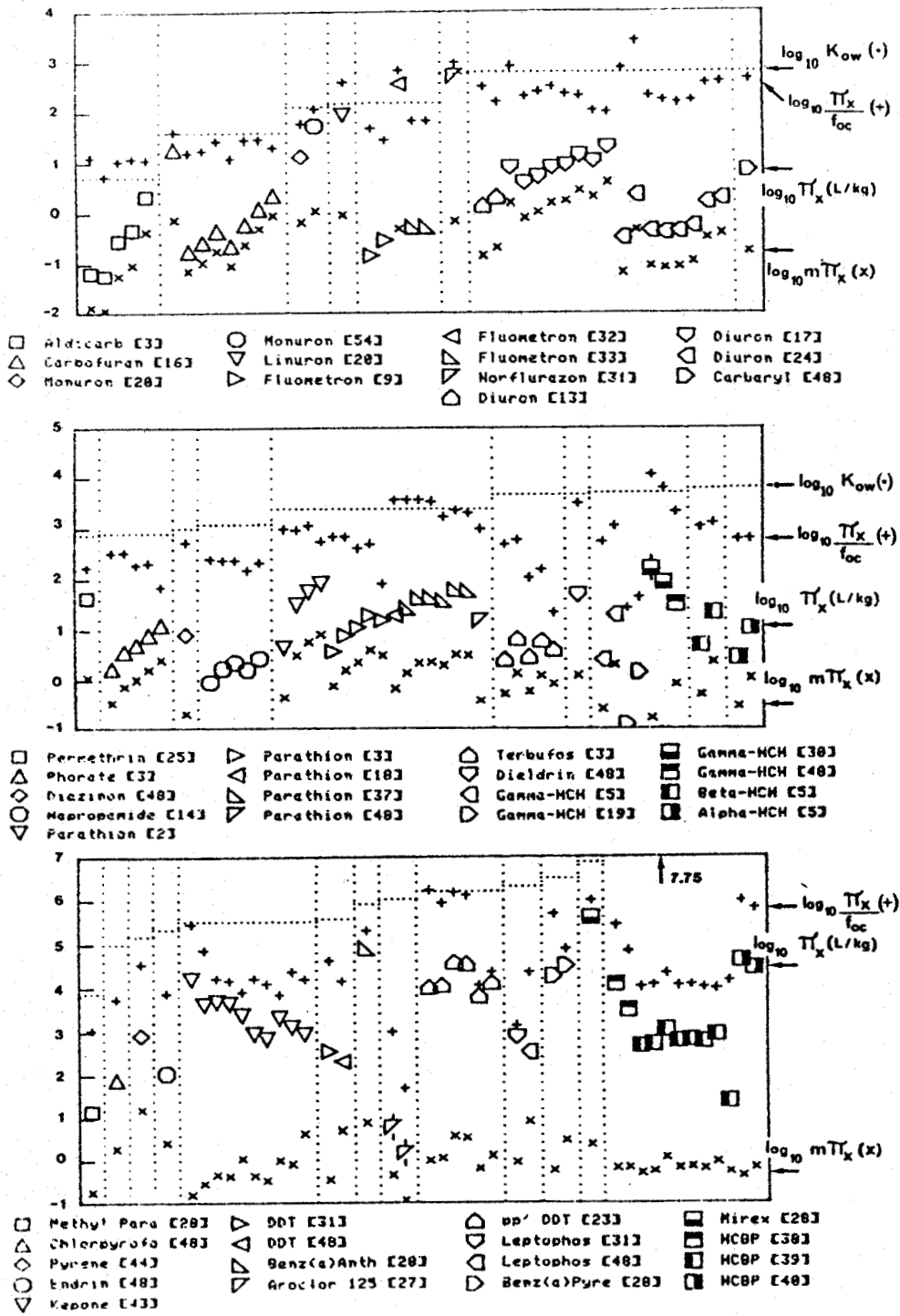


FIGURE 3

REVERSIBLE COMPONENT PARTITION COEFFICIENTS

COMPARISON TO PARTICLE INTERACTION MODEL

NEUTRAL ORGANIC CHEMICALS

$\nu_x = 1.4$

$\log_{10} K_{oc}^x = 0.178 + 0.924 \log_{10} K_{ow}$

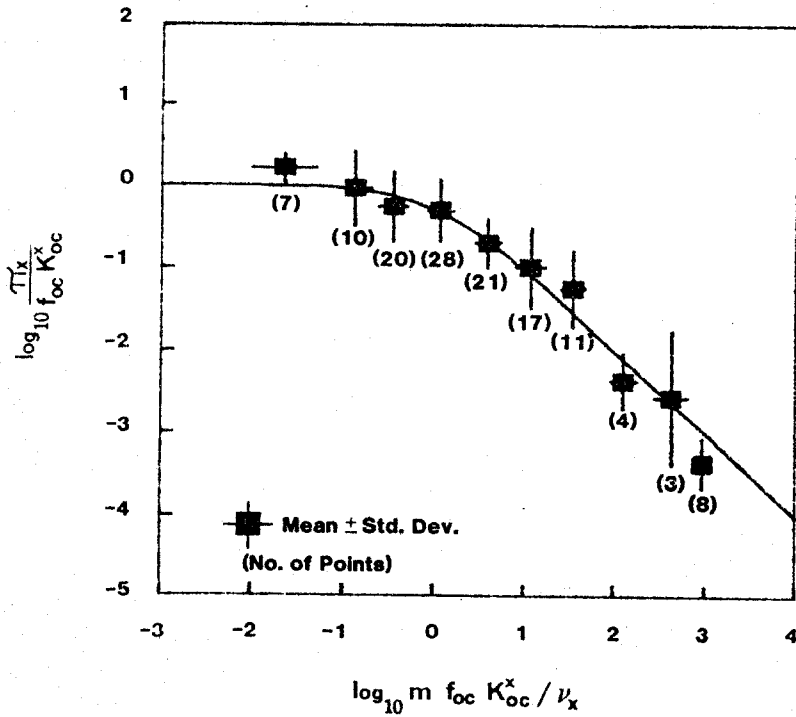
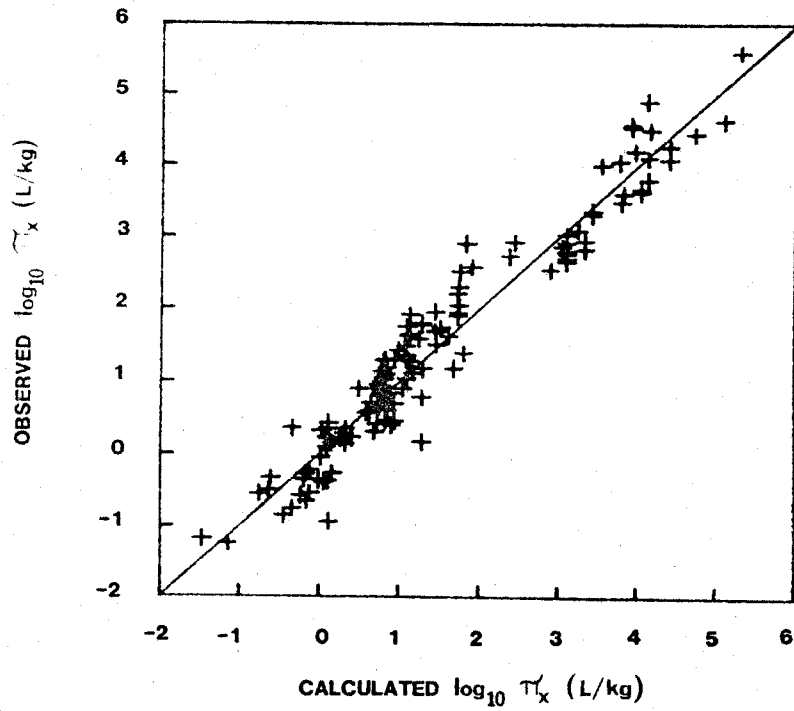
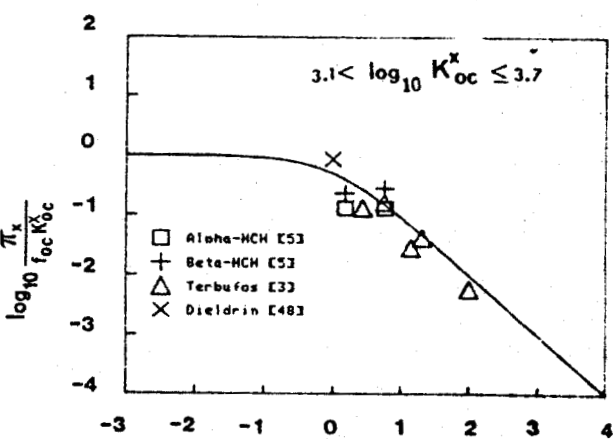
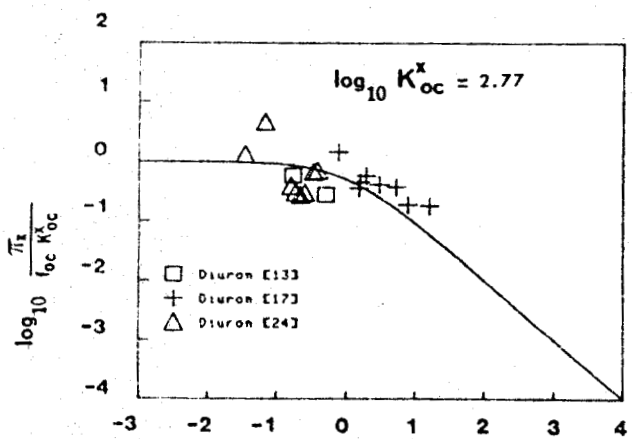
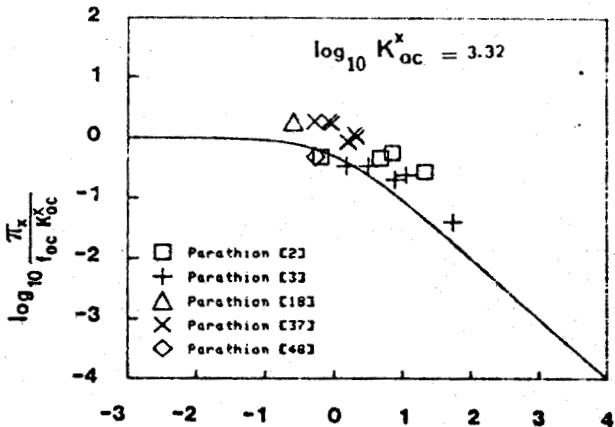
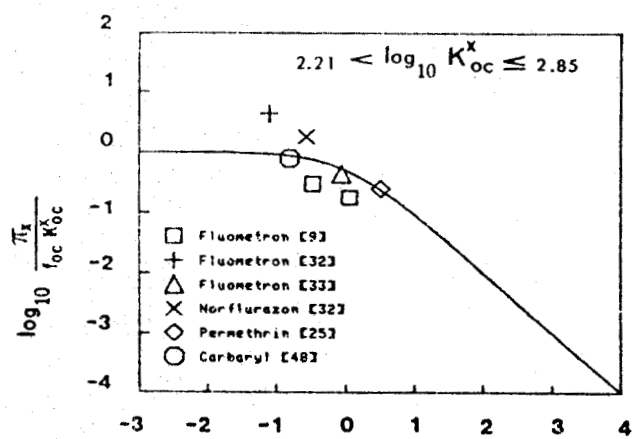
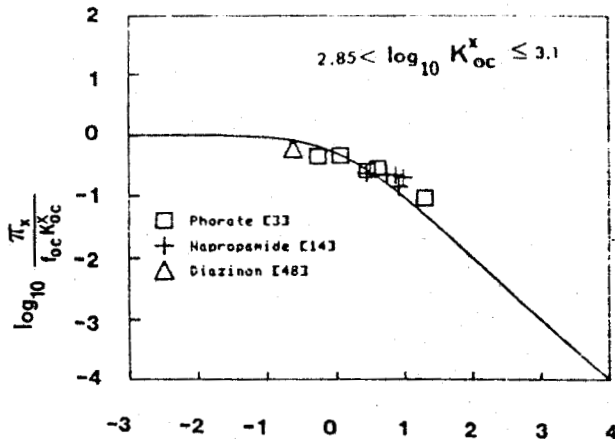
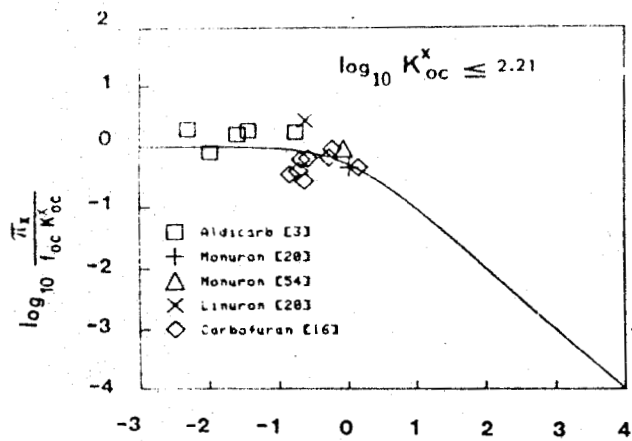


FIGURE 4



$$\log_{10} \frac{m f_{oc} K_{oc}^x}{\nu_x}$$

$$\log_{10} \frac{m f_{oc} K_{oc}^x}{\nu_x}$$

FIGURE 5

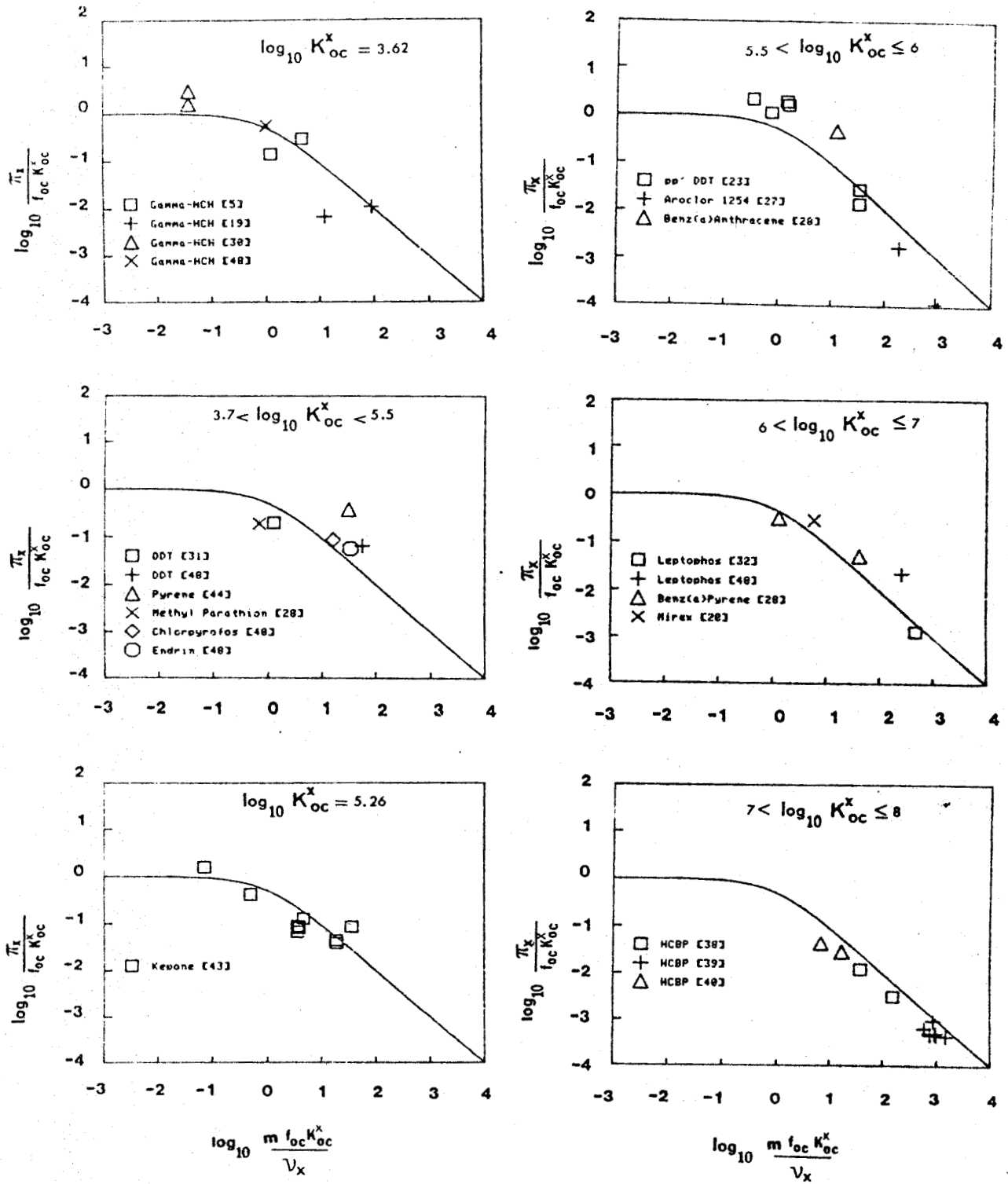


FIGURE 6

Least Mean Square Fitted Parameters

K_{oc}^X and ν_x versus K_{ow}

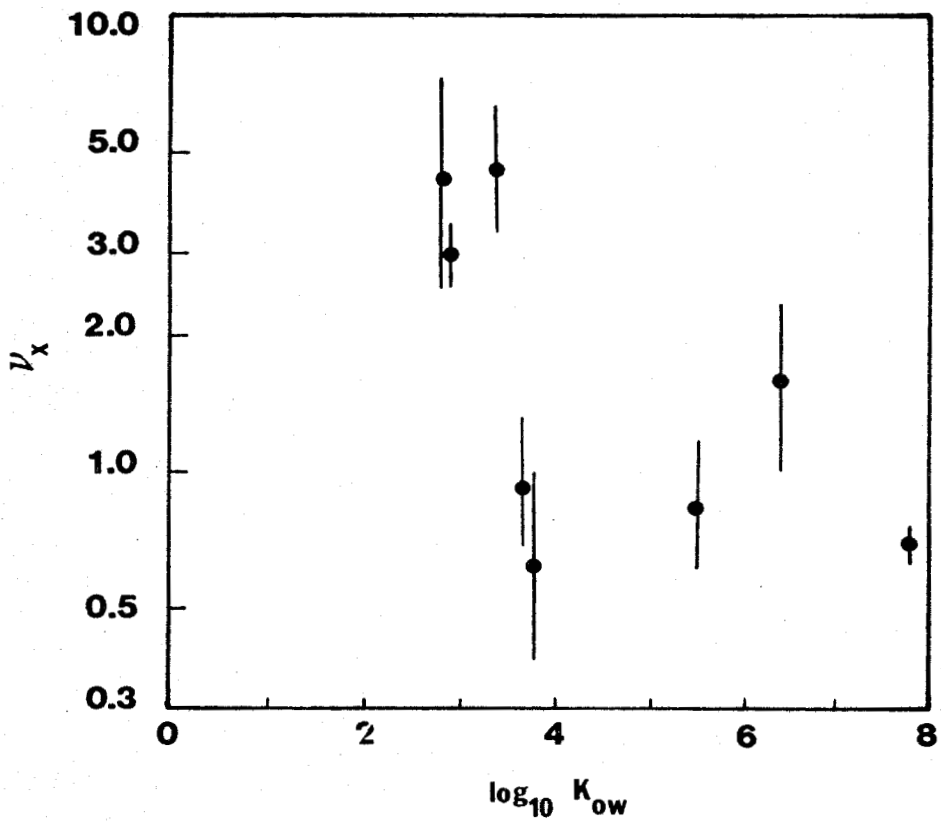
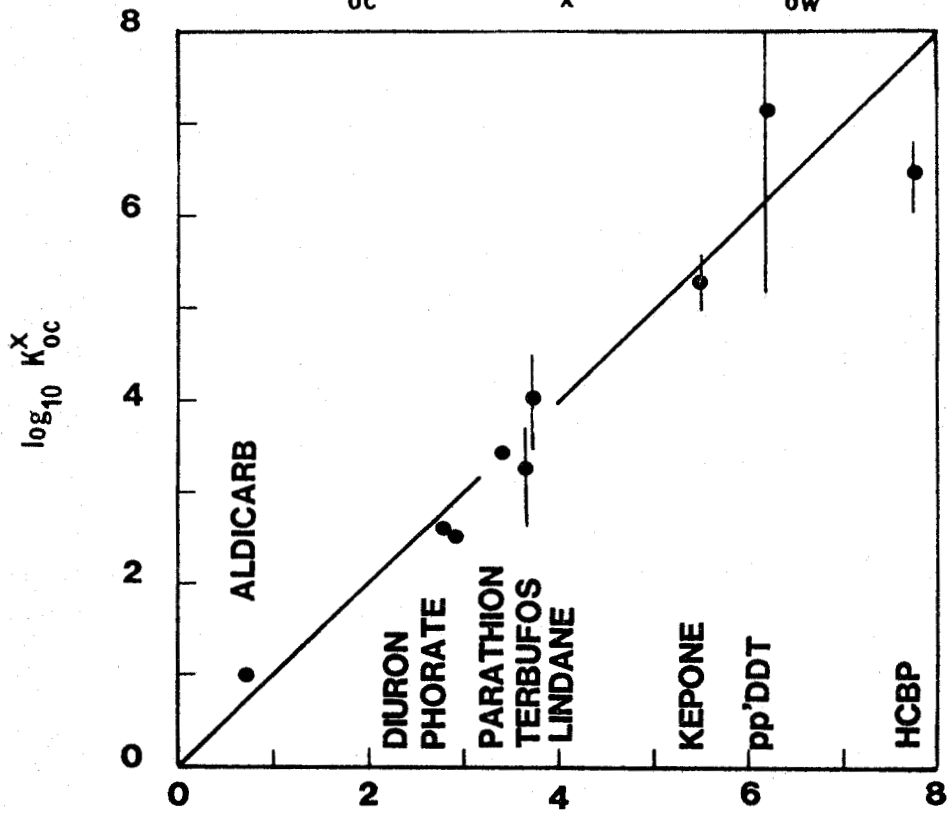


FIGURE 7

REVERSIBLE PARTITION COEFFICIENT
 NEUTRAL ORGANIC CHEMICALS $m f_{oc} K_{oc}^x < 1$
 K_{ow} AND f_{oc} RELATIONSHIPS

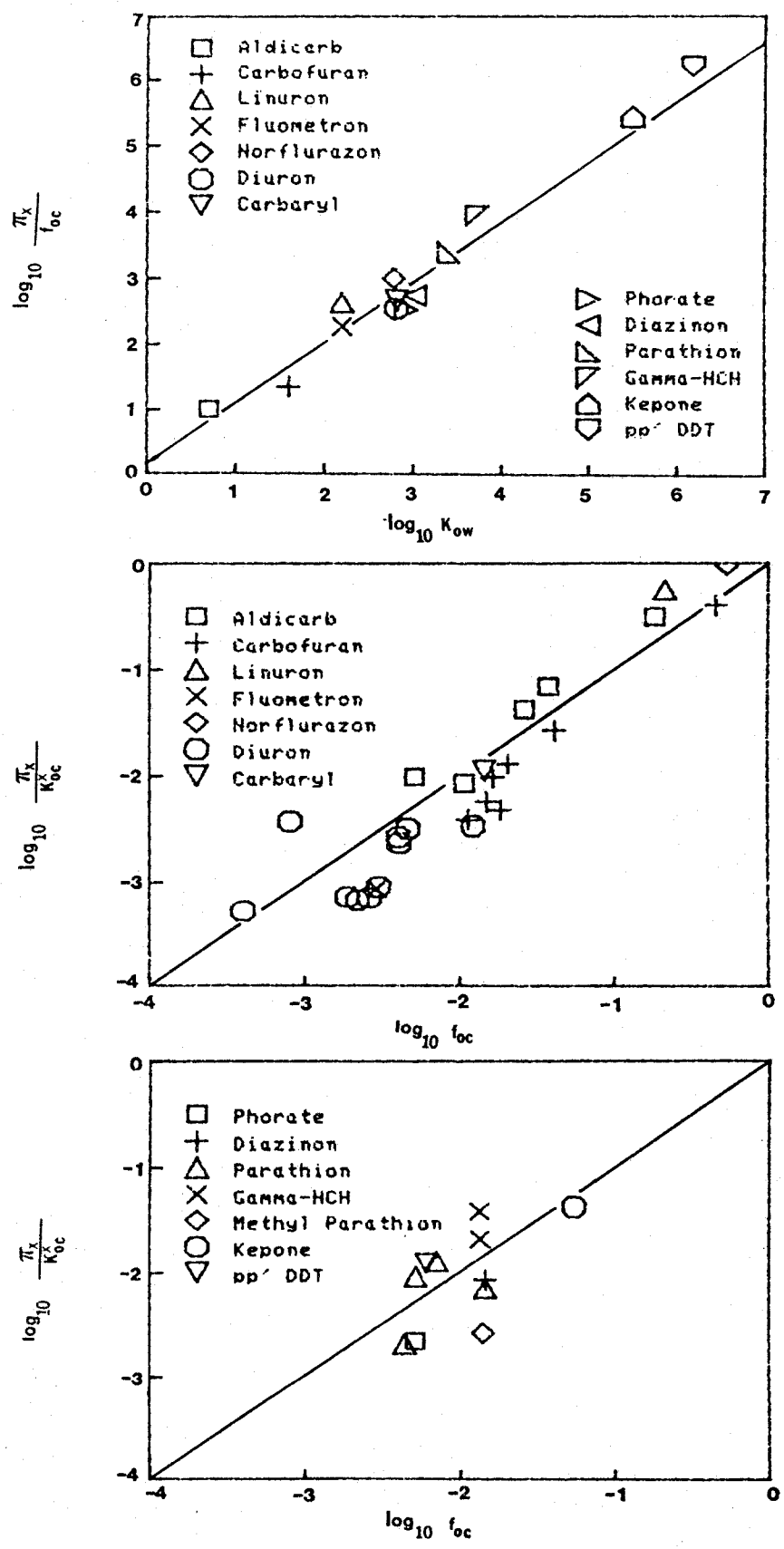


FIGURE 8

REVERSIBLE PARTITION COEFFICIENT
NEUTRAL ORGANIC CHEMICALS

$$m_{foc} K_{oc}^x > 3$$

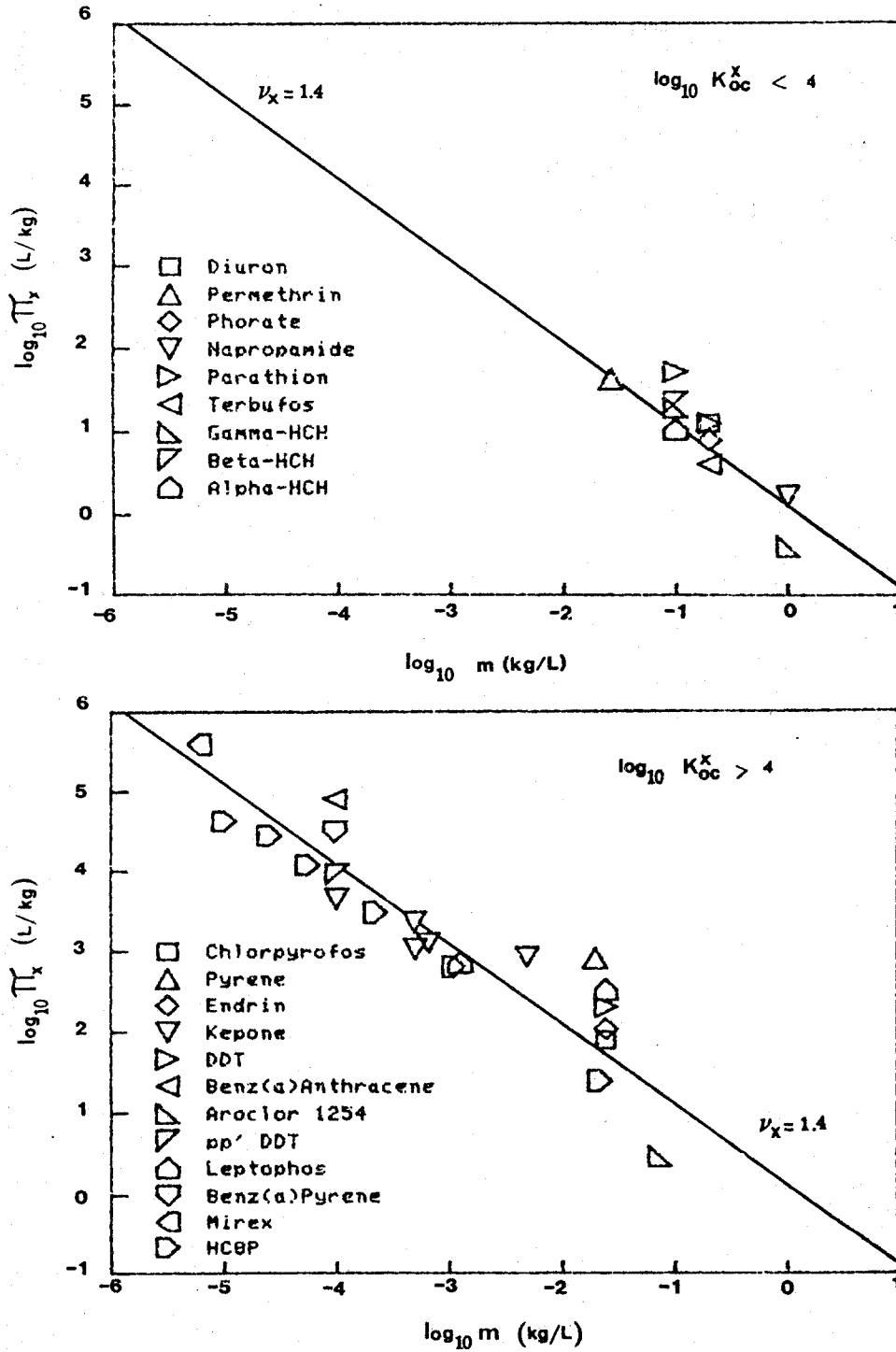
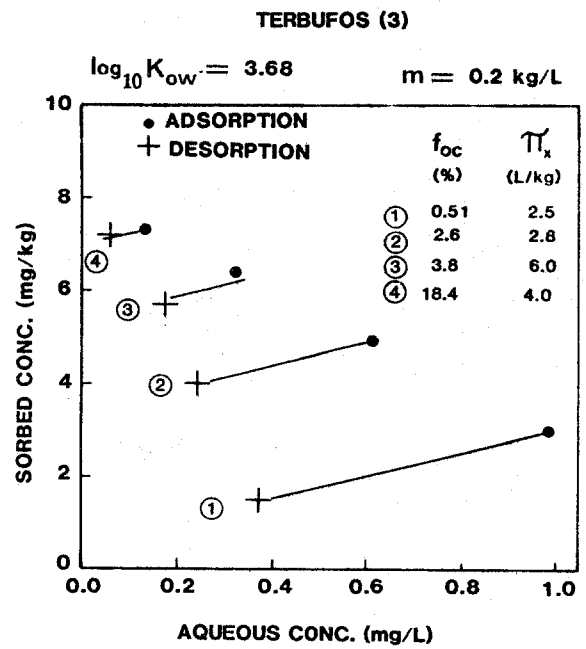
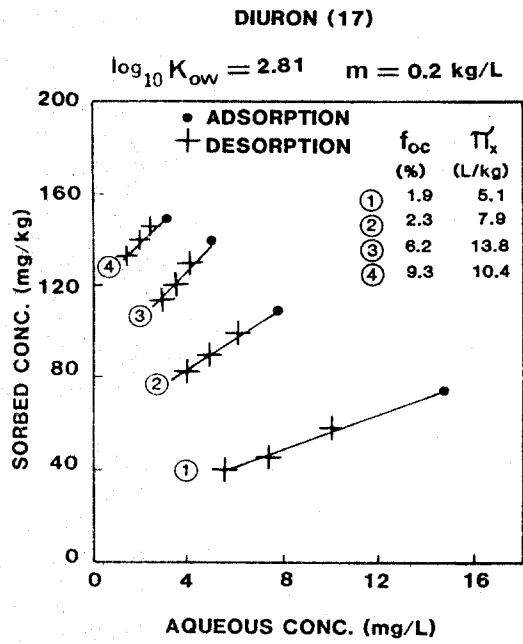


FIGURE 9

EFFECT OF PARTICLE ORGANIC CARBON



EFFECT OF PARTICLE CONCENTRATION

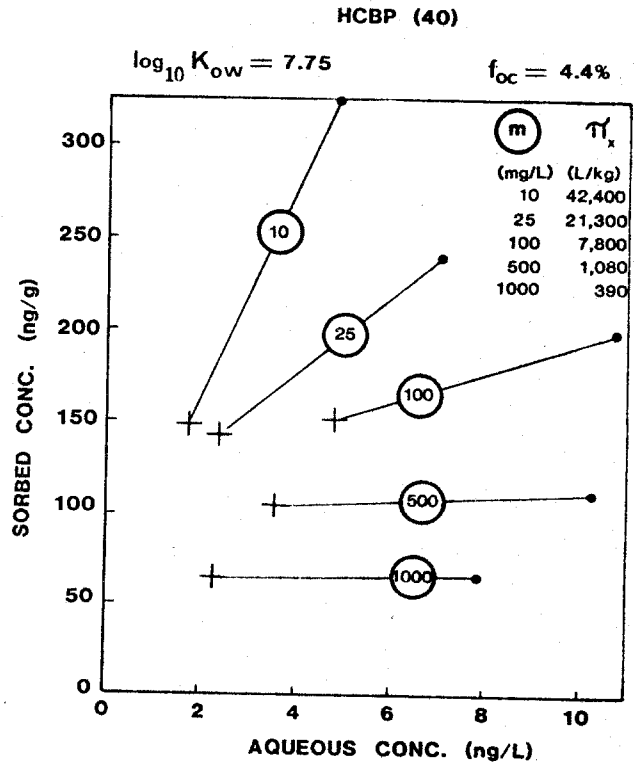
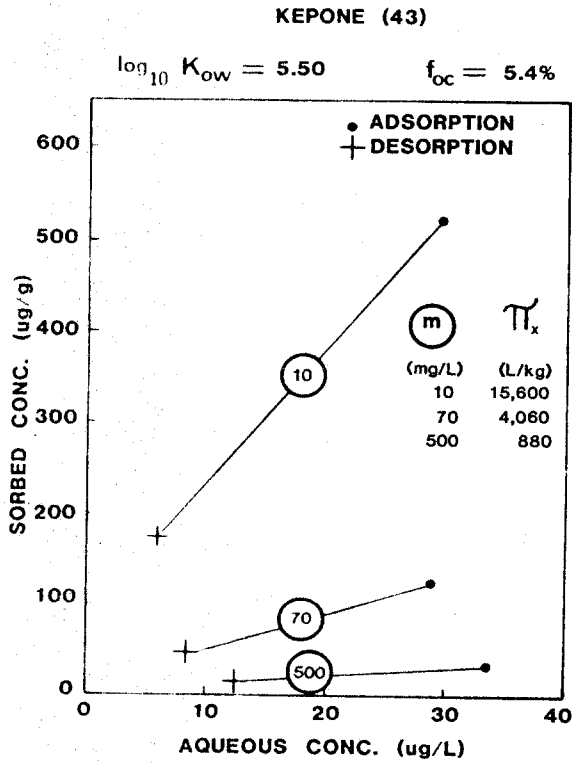


FIGURE 10

REVERSIBLE PARTITION COEFFICIENT
NEUTRAL ORGANIC CHEMICALS-INORGANIC SORBENTS

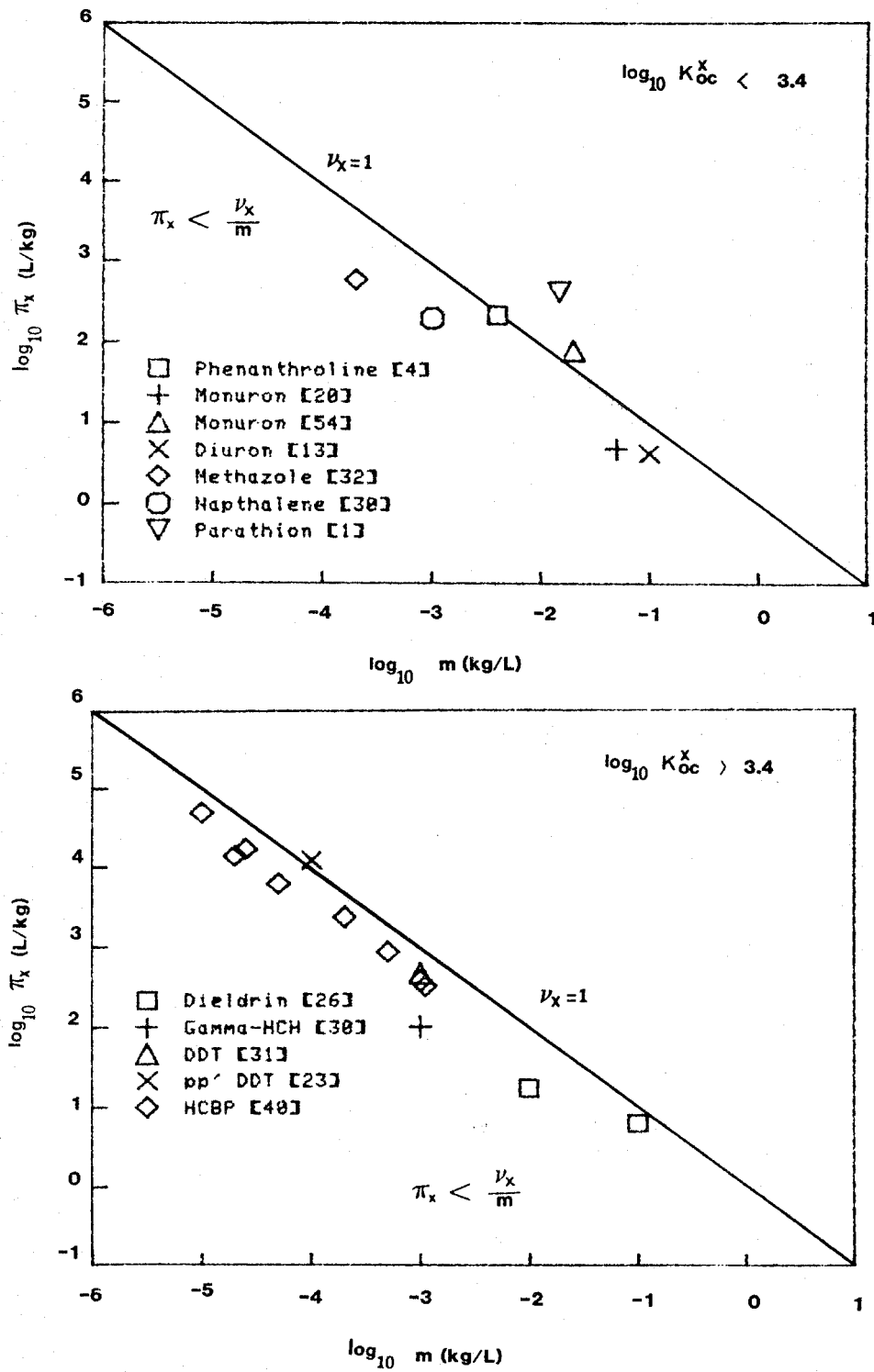
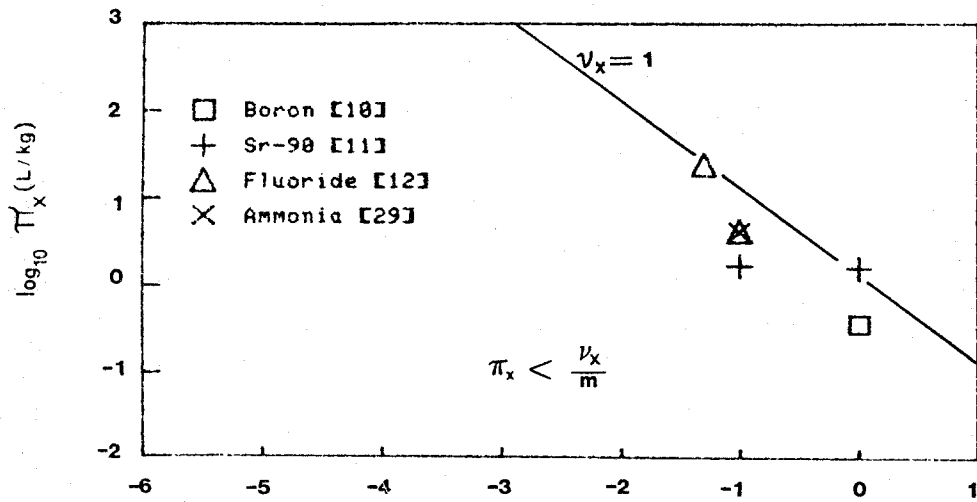
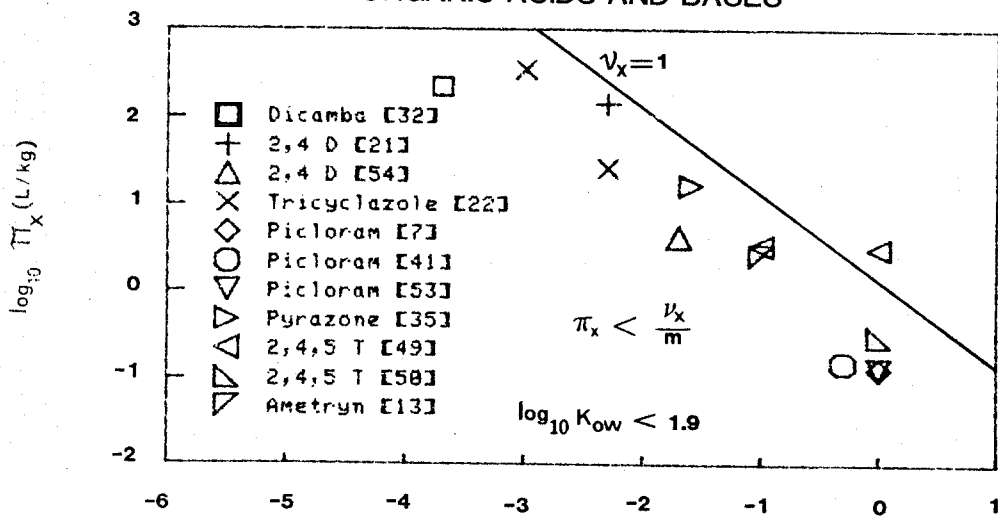


FIGURE 11

REVERSIBLE PARTITION COEFFICIENT
INORGANIC CHEMICALS



ORGANIC ACIDS AND BASES



ORGANIC ACIDS AND BASES

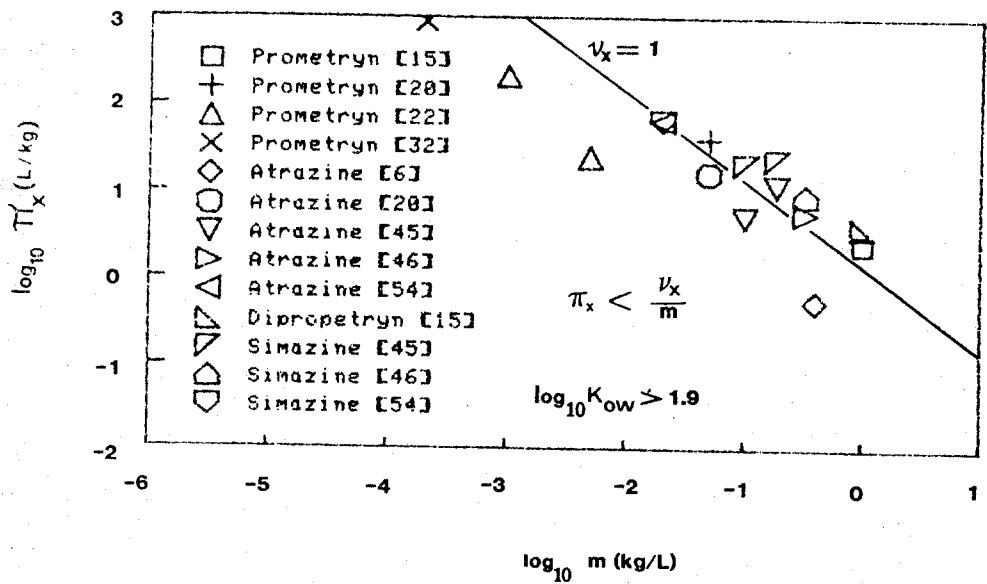


FIGURE 12

APPENDIX III

DIFFUSION AND PARTITIONING OF HEXACHLOROBIPHENYL IN SEDIMENTS

by

Dominic M. Di Toro
John S. Jeris
Daniel Ciarcia

Environmental Engineering and Science Program
Manhattan College
Bronx, New York 10471

April, 1984

I. Introduction

The fate of persistent hydrophobic chemicals in natural bodies of water is greatly influenced by the transport mechanisms between sediments and the overlying water: particle transport (settling and resuspension) and aqueous diffusion. An analysis of each of these mechanisms is required if rational mass balance calculations of chemical fate are to be made. The purpose of this paper is to present an experimental investigation that is designed to evaluate the diffusive mass transport and partitioning of a highly sorbed chemical, hexachlorobiphenyl (HCBP), in sediments.

Conventional reversible sorption theory predicts that the apparent diffusion coefficient of total chemical, D_s^* , is (Berner, 1980):

$$D_s^* = \frac{D_s}{1 + m\pi/\phi} \quad (1)$$

where D_s is the aqueous diffusion coefficient in the interstitial water for nonadsorbing chemicals, m is the sediment solids concentration $m = \rho_s(1 - \phi)$, π is the adsorption-desorption partition coefficient and ϕ is the porosity. For the classical theory to apply, adsorption and desorption are assumed to be described by a linear reversible isotherm.

The initial concern was: what would be the effect of non-reversible HCBP adsorption-desorption, which has been observed in agitated suspended sediment experiments (Di Toro and Horzempa, 1982), on the rate of diffusion in sediments. The importance of the question is related to the burial of chemical by sedimentation. If contaminated sediment is buried by uncontaminated sediment faster than interstitial water diffusion can contaminate the newly deposited layer, then sedimentation in the absence of bioturbation provides an ultimate sink for sorbed chemical. For soil column leaching experiments, it has been found that significantly greater mass transport occurs than is implied by eq. (1) (Gersty, et al., 1979). The concern is that this effect may also be exhibited by highly sorbed chemicals such as HCBP. On the other hand, non-reversible behavior may inhibit migration as has been observed for soil column leaching experiments (van Genuchten, 1977).

The experiment is not without its practical difficulties. If l is the distance from the initially contaminated sediment layer, then the time, t , to reach this distance is on the order of:

$$\ell \sim \sqrt{\frac{\pi}{2D_s t}} \quad (2)$$

For example, if $m/\phi = 1 \text{ kg/L}$, $\pi = 10^5 \text{ L/kg}$, and $D_s = 1 \text{ cm}^2/\text{day}$, then after one day, the concentration is predicted to migrate a distance of $\ell = 0.045$ millimeters and after 100 days, the distance is increased only ten-fold. Thus, it is necessary to be able to measure changes of concentrations in distances on the order of 0.1 mm and to be able to wait for time periods on the order of 10^2 days (Duursma, 1966; Walker and Crawford, 1970).

The experimental design is illustrated in fig. 1. The vessel is a hypodermic syringe from which top assembly is removed. A layer of uncontaminated sediment is deposited, allowed to settle, and the supernatant is removed. A layer of HCBP contaminated sediment is added, allowed to settle, and the supernatant is removed. A final layer of uncontaminated sediment is added, settled, the supernatant removed, and the syringe is capped.

After a specified period of time has elapsed for migration to take place, the syringe is mounted on a device which is equipped with a screw-driven mechanism that advances the syringe plunger in small (0.005-0.01 inch) increments. The exuded sediment slices are carefully removed and analyzed for radioactivity. Thus, it is possible to examine the profile of HCBP in 0.005-0.01 inch increments throughout the sediment column.

The initial design involved only HCBP tagged sediment. However, it was soon discovered that ambiguous results could be obtained since it is not possible to exclude the possibility that, initially, the interface regions between tagged and untagged sediment were not exactly perpendicular (to within ~ 0.01 inch) to the syringe axis. As a consequence, the horizontal slices, through a tilted interface, would give the false impression of migration.

The solution to the problem was a double tag experiment. A small quantity of an absolute particle tracer, C^{14} -graphite particles, was added to the tritiated HCBP tagged sediment. The liquid scintillation counter can distinguish the tritium and carbon-14. The migration of the HCBP is then unambiguously monitored since if it appears in a sediment slice in excess of the C^{14} -graphite concentration, the only possibility is that aqueous phase diffusive transport has occurred.

SEDIMENT MIGRATION EXPERIMENTAL DESIGN

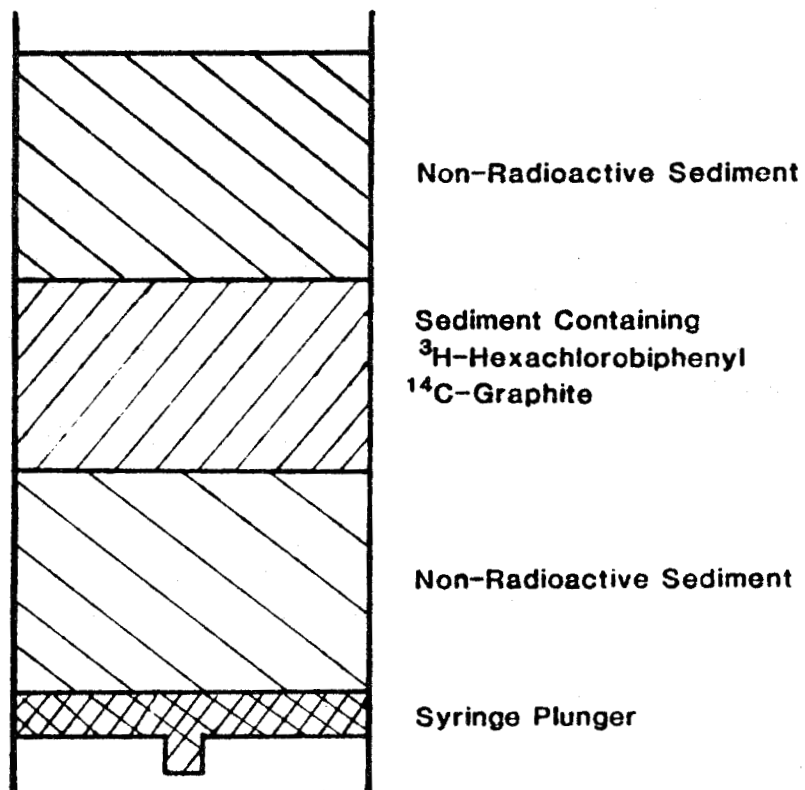


Figure 1. Schematic Diagram of Experimental Vessel.

Materials and Methods

The sediment employed in these experiments was obtained from Saginaw Bay (Station #50) (see Di Toro et al., 1982 for station location and sediment properties). The sediment was wet sieved through a #200 sieve (75 μm) to remove the coarse material which would interfere with the slicing. Table 1 lists the sieved sediment characteristics. The preparation of the dual tag sediment began with the transfer of the contents of an ampule containing 40 μCi of ^3H -HCBP into a 250 ml erlenmeyer flask. This ^3H -HCBP was a concentrated stock solution of custom synthesized 2,4,5,2',4',5' hexachlorobiphenyl in acetone with a high specific concentration (38.2 Ci/m mole New England Nuclear Corp.). The ampule was rinsed twice with acetone, and the rinse placed into the flask. The acetone was evaporated by purging the flask with a moderate flow of nitrogen which first passes through a distilled water trap. To prevent atmospheric contamination, the exit gas was passed through octanol and amyl alcohol traps.

After the acetone was evaporated, 25 grams of wet sediment (approx. 20 ml) and 10 ml distilled water were added to the flask to make the thick sediment less viscous. The flask was placed on a wrist action shaker and allowed to shake for four days. At this point, samples were removed from the flask, and analyzed for H^3 radioactivity. The final step was the addition of 2 μCi C^{14} -graphite particles (10 mCi/m mole) to the flask which was then shaken overnight. The weight fraction of added graphite was insignificant. The flask contents were allowed to settle for 24 hours, and 9 ml of supernatant were withdrawn with a syringe. The remaining sediment mixture containing both C^{14} -graphite and sorbed H^3 -HCBP was used as the stock sediment for the dual isotope experiments. The concentration of sorbed HCBP was 23 ng HCBP/g dry sediment.

Disposable plastic syringes (3 ml, 0.8 cm I.D. Benton Dickenson) with their tips removed using a lathe to assure a parallel cut, were the experimental vessels. Approximately 0.4 ml of untagged sediment was added to the syringe and the sediment was allowed to settle for approximately 1 month. Any overlying water was carefully removed. Approximately 0.3 ml of tagged sediment was added in the same manner, and allowed to settle for four days. Overlying water was removed and 0.3 ml of untagged sediment added. Stoppers were placed in the top of the reaction vessel syringes, and the vessels placed in the humidifier.

Reaction vessels were removed from the humidifier at the appropriate time, and placed in the extraction device. The plunger of the reaction vessel syringe was moved slowly and accurately by using an unconfined compression machine (Soiltest). The proving ring normally used in this device was removed and replaced with a stationary mounting block. Displacement was measured by a strain gage connected to the mounting block. A single edged safety razor was used to slice the sediment. Glass tracks, mounted on the top of the block, were used to guide the cutting razor across the top of the reaction vessel. The upper end of the syringe is positioned flush with the glass tracks and clamped securely. A slice is taken by raising the platform the desired slice thickness and slowly moving the razor along the glass tracks on the mounting block. The sediment slice, which adheres to the razor, is carefully jetted with water into a 20 ml counting vial using a 1 ml syringe with 1 ml of distilled water, 10 ml of Aquasol is added, and mixed using a vortex mixer for 15 sec. The vial is counted for 2 minutes on a liquid scintillation counter using the carbon 14 window. The vial is then centrifuged at 6000 g for 15 min. in order to remove both the C^{14} -graphite and sediment particles. The toluene base Aquasol extracts the HCBP into the liquid phase, which is decanted into another vial, and then counted for 2 minutes using the tritium window to measure the concentration of 3H -HCBP in the slice.

Identically prepared syringes were used to measure the diffusion coefficient of tritiated water. To a 3 ml syringe containing 1.4 ml of consolidated sediment, 300 $\mu\ell$ of distilled water was added and after 1 hr, 30 $\mu\ell$ of 3H - H_2O is added. Samples of this overlying water (5 $\mu\ell$) are taken at intervals and counted.

Analysis of Tritiated Water Diffusion

An independent measurement of the interstitial water diffusion coefficient can be made using a non-adsorbing substance. Tritiated water is an ideal choice since its presence does not significantly alter the ionic composition of the interstitial water as would be the case if, for example, high concentrations of a major cation or anion were introduced.

The conventional method (e.g. Hesslein, 1980) is to introduce a quantity of tracer into the water overlying the sediment, and after the passage of a suitable length of time, to measure the depth distribution of the tracer.

The problem with this approach when applied to the syringe experimental design is that a considerable time is required to slice the sediment and, during this time, the tracer continues to diffuse within the progressively shortening sediment column. Although it is possible to numerically compute the spatial distribution of tracer to be expected for this situation, the method lacks a directness which can be achieved by simple modification.

Instead of relying on the depth distribution of the tracer at a fixed time, it is possible to measure the decline of tracer concentration in the overlying water with time as the tracer diffuses into the sediment (e.g. Officer, 1982). If the volume ratio of overlying water to interstitial water is suitably small so that the decline is appreciable, and the tracer measurement is sufficiently sensitive so that only small volumes need to be removed from the overlying water, then the analysis of this experiment is direct.

Let ℓ_1 be the depth of the overlying water, and ℓ_2 be the depth of sediment. Let $C_{T1}(t)$ and $C_{T2}(z,t)$ be the tracer concentrations in the overlying and interstitial water, respectively. The mass balance equation for the overlying water is:

$$\ell_1 A \frac{dC_{T1}}{dt} = D_s A \left. \frac{\partial(\phi C_{T2})}{\partial z} \right|_{z=0} \quad (3)$$

where A is the interfacial area. This equation states that the time rate of change of tracer in the overlying water is due to the diffusive flux of tracer into the sediment. The mass balance equation in the sediment is:

$$\frac{\partial(\phi C_{T2})}{\partial t} - D_s \frac{\partial^2(\phi C_{T2})}{\partial z^2} = 0 \quad (4)$$

The boundary conditions correspond to continuity of fluid tracer concentration at $z=0$:

$$C_{T1}(t) = C_{T2}(0,t) \quad (5)$$

and a zero flux condition at the sediment bottom:

$$\left. \frac{\partial C_{T2}(z,t)}{\partial z} \right|_{z=\ell_2} = 0 \quad (6)$$

The solutions of these equations is known to be (Carslaw and Jaeger, 1959):

$$C_{T1}(t) = \frac{C_{T1}(0)}{1+k} [1 + 2k(k+1) \sum_{i=0}^{\infty} \frac{\exp(-\alpha_i^2 T)}{P_i}] \quad (7)$$

$$C_{T2}(z,t) = \frac{C_{T1}(0)}{1+k} [1 + 2k(k+1) \sum_{i=0}^{\infty} \frac{\exp(-\alpha_i^2 T) \cos(\alpha_i^2(1-z/\ell_2))}{P_i \cos(\alpha_i)}] \quad (8)$$

where:

$$k = \ell_2 \phi / \ell_1 \quad (9)$$

$$P_i = \alpha_i^2 + k(k+1) \quad (10)$$

$$T = D_s t / \ell_2^2 \quad (11)$$

and α_i are the positive roots of:

$$k \tan \alpha_i + \alpha_i = 0 \quad (12)$$

For small times a fairly large number of roots are required for accurate solutions but no computational problems arise. The solution is easily checked at $t=0$ to determine the maximum number of terms required in the sums. Note that at $t \rightarrow \infty$, the solutions conserve mass:

$$\ell_1 C_{T1}(0) = \ell_1 C_{T2}(\infty) + \ell_2 \phi C_{T2}(z, \infty) \quad (13)$$

as they should.

One refinement is required is to account for the effect of sample withdrawal on the volume, and therefore the depth, ℓ_1 , of the overlying fluid. Initially $v_1 = \ell_1 A = 330 \mu\ell$ whereas at the end of the experiment, $v_1 = 255 \mu\ell$. This is enough of a change to influence the computations. However, instead of solving this problem directly, the following approximation is employed. At each time, t , the average depth:

$$\bar{\ell}_1(t) = \frac{1}{t} \int_0^t \ell_1(t) dt \quad (14)$$

is computed and this is used in equation (7) for C_{T1} . While this is not a rigorously correct solution it appears to be a reasonable approximation. One check is to compare the actual tracer mass lost via sampling to that removed from the computation by using $\bar{l}_1(t)$: $(l_1 - \bar{l}_1(t))C_{T1}(0)$ at each sampling time. The average absolute error for the volume ratio employed in this experiment is 17%. Errors are positive during the early periods (more mass lost than computed) and negative in the latter stages. However the approximation appears reasonable and simple to apply.

The results of the analysis are shown in fig. 2a, for two separate experiments. The coefficients and relevant parameters are listed in Table 2. The apparent sediment diffusion coefficient is found to be $D_{s, H_2O} = 1.5 \text{ cm}^2/\text{day}$.

As a confirmation of this result, a spatial profile that resulted after an exposure time of 2.5 hrs is shown in fig. 2b. Beyond the first few slices, the flattening of the data profile due to the increased dispersion during the slicing is evident. Nevertheless the data are in reasonable agreement with the dispersion coefficient estimated from the penetration experiment.

The apparent sediment diffusion coefficient found from these experiments can be compared to empirical correlations that apply to natural sediments. The relationship between the molecular diffusion coefficient, D , and the apparent sediment diffusion coefficient, D_s , is (Berner, 1980):

$$D_s = D/\theta^2 \quad (15)$$

where θ is the tortuosity: the ratio of the length of the actual diffusion path to the linear length of the sediment. It has been shown that:

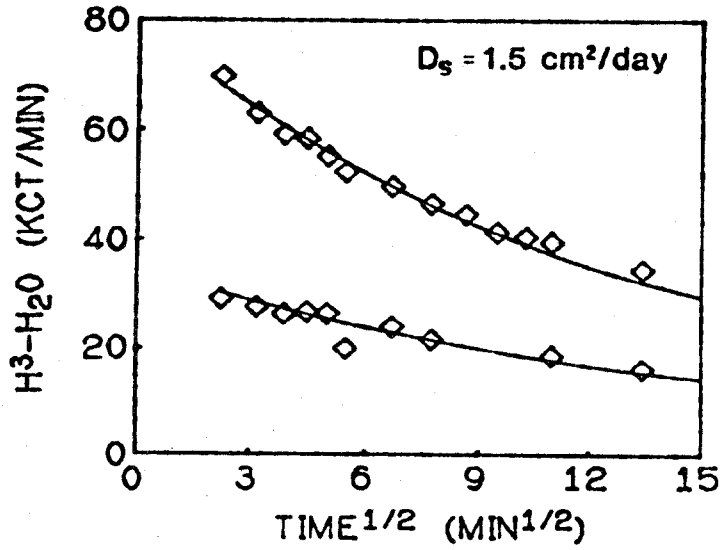
$$\theta^2 = \phi F \quad (16)$$

where F is the formation factor: $F = R/R_0$, the ratio of the electrical resistivity of the bulk sediment to the pore fluid. Manheim (1970) has shown that:

$$F = \phi^{-n} \quad (17)$$

where $n = 2.8$. If $n = 2$, this relationship is known as Archie's law. Thus:

TRITIATED WATER DIFFUSION
OVERLYING WATER vs TIME



INTERSTITIAL WATER vs DEPTH

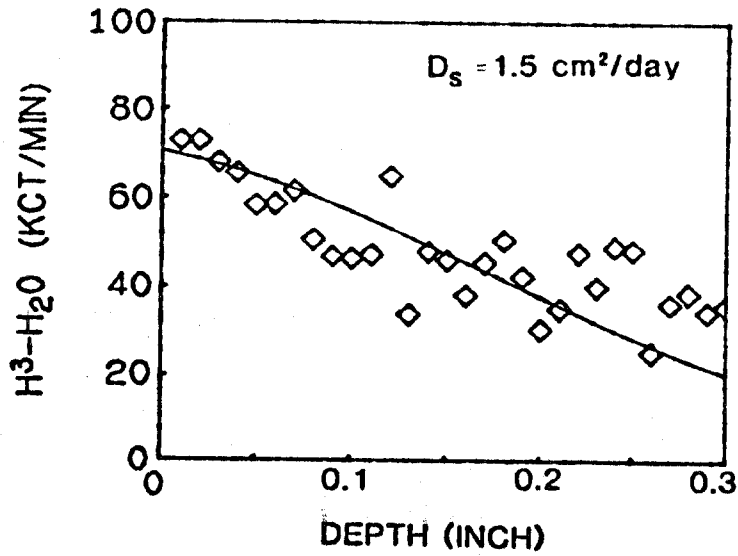


Figure 2. Tritiated Water Diffusion. Overlying water concentration versus time (top). Total H³-H₂O concentration versus depth after t = 2.5 hr. (bottom).

$$D_s = D \phi^{1.8} \quad (18)$$

For the syringe experiments: $\phi = 0.75$ and $D_{H^3-H_2O} = 1.81 \text{ cm}^2/\text{day}$ (Wang et al., 1953) so that the expected value is $D_{s,H_2O} = 1.08 \text{ cm}^2/\text{day}$ which can be compared to $D_{s,H_2O} = 1.5 \text{ cm}^2/\text{day}$ found experimentally.

Analysis of HCBP Diffusion

The distribution of an adsorbing chemical in a sediment is determined by the diffusive migration in the interstitial water and its adsorption-desorption behavior. If reversible adsorption-desorption is assumed, with a linear isotherm applicable to both adsorption and desorption, and if adsorption-desorption equilibrium is attained on a time scale which is short relative to the diffusive time constant, then it has been shown (e.g. Berner 1980) that the governing equation is:

$$\frac{\partial(\phi C_T)}{\partial t} - \frac{\partial}{\partial z}(\phi D_s^* \frac{\partial C_T}{\partial z}) = 0 \quad (19)$$

For the syringe experiments, the initial condition is:

$$C_T(z,0) = C_{T0} \quad z > 0 \quad (20)$$

$$C_T(z,0) = 0 \quad z < 0 \quad (21)$$

where $z=0$ is the interface boundary and the syringe boundaries are far enough from the interface so that an infinite spatial domain is a reasonable approximation. For these conditions the solution is known to be (Crank, 1975):

$$C_{T1}(z,t) = \frac{C_{T0}}{2} \operatorname{erfc}\left(\frac{-z}{2\sqrt{D_s^* t}}\right) \quad z < 0 \quad (22)$$

$$C_{T2}(z,t) = \frac{C_{T0}}{2} \left[1 + \operatorname{erf}\left(\frac{z}{2\sqrt{D_s^* t}}\right)\right] \quad z > 0 \quad (23)$$

where:

$$f_d = \frac{1}{1 + m\pi/\phi} \quad (24)$$

$$D_s^* = f_d D_{s,HCBP} \quad (25)$$

$m = \rho_s(1-\phi)$, the solids concentration and π is the partition coefficient.

The experimental measurements do not produce the continuous profiles that actually exist but rather the slice average concentrations. The theoretical slice average concentrations can be computed from eqs. (22-23) by spatially averaging the solutions:

$$\bar{C}_T(z,t) = \frac{1}{d} \int_z^{z+d} C_T(z,t) dt \quad (26)$$

to yield:

$$\bar{C}_{T1}(z,t) = \frac{C_{To}}{2} \frac{\sqrt{4D_s^*t}}{d} \left[\text{ierfc}\left(\frac{-z-d}{2\sqrt{D_s^*t}}\right) - \text{ierfc}\left(\frac{-z}{2\sqrt{D_s^*t}}\right) \right] \quad (27)$$

$$\bar{C}_{T2}(z,t) = \frac{C_{To}}{2} \left\{ 2 - \frac{\sqrt{4D_s^*t}}{d} \left[\text{ierfc}\left(\frac{z}{2\sqrt{D_s^*t}}\right) - \text{ierfc}\left(\frac{z+d}{2\sqrt{D_s^*t}}\right) \right] \right\} \quad (28)$$

where:

$$\text{ierfc}(z) = \frac{1}{\sqrt{\pi}} e^{-z^2} - z \text{erfc}(z) \quad (29)$$

is the integral of the complimentary error function and d is the slice thickness.

In order to estimate the partition coefficient via eqs. (24-25) the molecular diffusion coefficient of HCBP, D_{HCBP} is required. This is estimated using the Wilke-Chang correlation to molal volume (Reid, et al., 1977). The latter is computed from the LeBas additive volume increments of the molecular constituents (C,H,Cl, corrected for the two 6-member rings). The result is $D_{HCBP} = 0.461 \text{ cm}^2/\text{d}$ (20°C). Using the known molecular diffusivity of water, $D_{H_2O} = 1.81 \text{ cm}^2/\text{d}$ (20°C) (Wang et al., 1953) and the measured tri-

tiated water diffusion coefficient in the syringe: $D_{s,H_2O}^* = 1.5 \text{ cm}^2/\text{d}$ it follows that the molecular diffusivity of HCBP in the syringe in the absence of adsorption is: $D_{s,HCBP} = (D_{s,H_2O}/D_{H_2O})D_{HCBP} = 0.382 \text{ cm}^2/\text{d}$. The apparent diffusivity of HCBP follows from:

$$D_{s,HCBP}^* = \frac{D_{s,HCBP}}{1 + m\pi/\phi} \quad (30)$$

for partition coefficient, π .

A correction is required for the tilted interface, since slicing through it produces a profile which indicates an apparent diffusive motion. The method adopted is to simultaneously fit the C^{14} -graphite and ^3H -HCBP data profiles to the solutions (eqs. 27-28 with $C_{T0} = 1$) normalized as:

$$N_C(z) = N_{CO} + (N_{C1} - N_{CO})\bar{C}_T(z, t_g, D_{s,HCBP}^*) \quad (34)$$

$$N_H(z, t) = N_{HO} + (N_{H1} - N_{HO})\bar{C}_T(z, t_g + t, D_{s,HCBP}^*) \quad (35)$$

where N_{CO} , N_{HO} ; N_{C1} , N_{H1} are the background (untagged region) and the tagged region counting rates for C^{14} and H^3 respectively far from the interface. The location of the interface, $z=0$, is chosen by examining the C^{14} profiles. The idea is that at $t = 0$ both the graphite and HCBP profiles are identical (this is the initial condition) and as t increases, HCBP diffuses relative to the graphite. This strategem eliminates the need to solve eq. (19) for an arbitrary initial condition. Rather a convenient initial condition: $\bar{C}_T(z, t_g, D_{s,HCBP}^*)$ is used which is itself a solution of eqs. (27-28) with t_g chosen to fit the graphite profile. As time, t , increases the HCBP profile evolves from that initial condition.

The experimental data: the logs of the ^3H , ^{14}C , and $^3\text{H}/^{14}\text{C}$ ratio are fit to eqs. (34-35) using a nonlinear least squares method (Marquardt, 1963) to estimate the six unknown parameters: π , t_g , N_{CO} , N_{C1} , N_{HO} , N_{H1} .

Figure 3 illustrates the fits obtained for various elapsed times. Slice average concentrations are connected with a smooth curve for ease of presentation. The diffusive motion of HCBP relative to the graphite particle profile is evident. The observed HCBP profiles are remarkably regular and agree

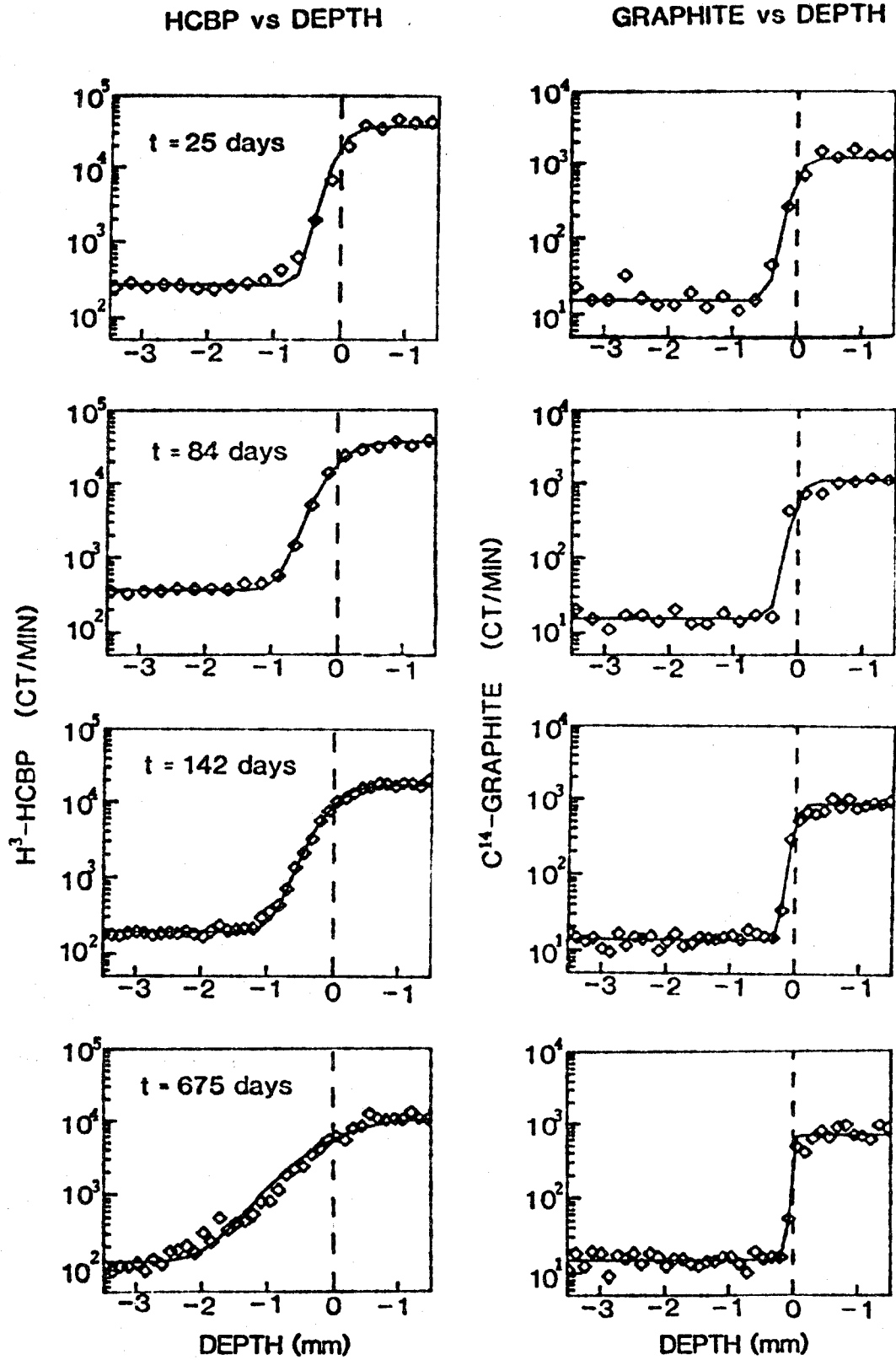


Figure 3. HCBP and graphite concentration versus depth at various elapsed times. Curves are computed using parameters in Table 3.

with the theoretical calculations over two orders of magnitude of HCBP concentration. Initially the slice thickness used was 0.01 inch. However it was found that a more refined profile could be obtained using a slice thickness of 0.005 inches. This was the procedure used for the syringes with $t > 140$ days.

The initial apparent diffusive motion of HCBP at $t = 25$ day is actually due to a tilted interface. This can more clearly be seen in fig. 4 which presents the $^3\text{H-HCBP}/^{14}\text{C-graphite}$ count ratio. This is the most sensitive measure of the extent of HCBP diffusion. Excess $^3\text{H}/^{14}\text{C}$ counting rate over the background ratio to the left of the interface can only be the result of diffusive migration of the $^3\text{H-HCBP}$ in the interstitial water since the graphite particles are immobile. Depletion of HCBP to the right of the interface is also detectable at longer elapsed times. The computed slice average $^3\text{H}/^{14}\text{C}$ concentration ratios, $N_{\text{H}}(z,t)/N_{\text{C}}(z)$ are displayed as a staircase function over the slice thickness so that a more detailed comparison can be made to the data.

The lack of significant excess HCBP for $t = 25$ days indicates that no substantial interfacial mixing occurred during the preparation of the syringe or during the slicing procedure. The extent of migration increases regularly as elapsed time increases. However even at the termination of the experiment (almost two years) the extent of migration is no more than 2-3 mm. It is this fact that necessitates the dual tag experimental design. Table 3 tabulates the parameter estimates.

Discussion and Conclusions

As illustrated in figs. 3-4 the diffusion-linear reversible equilibrium model of chemical transport in sediments satisfactorily reproduces the individual syringe observations. The estimates of apparent sediment diffusion and partition coefficients versus elapsed time are shown in fig. 5. No temporal trends are evident so that the assumption of constant linear partition coefficient, $\bar{n} = 10^{5.06 \pm 0.13}$, and therefore apparent sediment diffusivity, $D_s^* = 3.95 \pm 1.12 \times 10^{-6} \text{ cm}^2/\text{d}$, is reasonable.

The partition coefficient for HCBP obtained from these experiments is compared in fig. 6 and Table 4 to predictions from empirical hydrophobic

EXCESS HCBP vs DEPTH

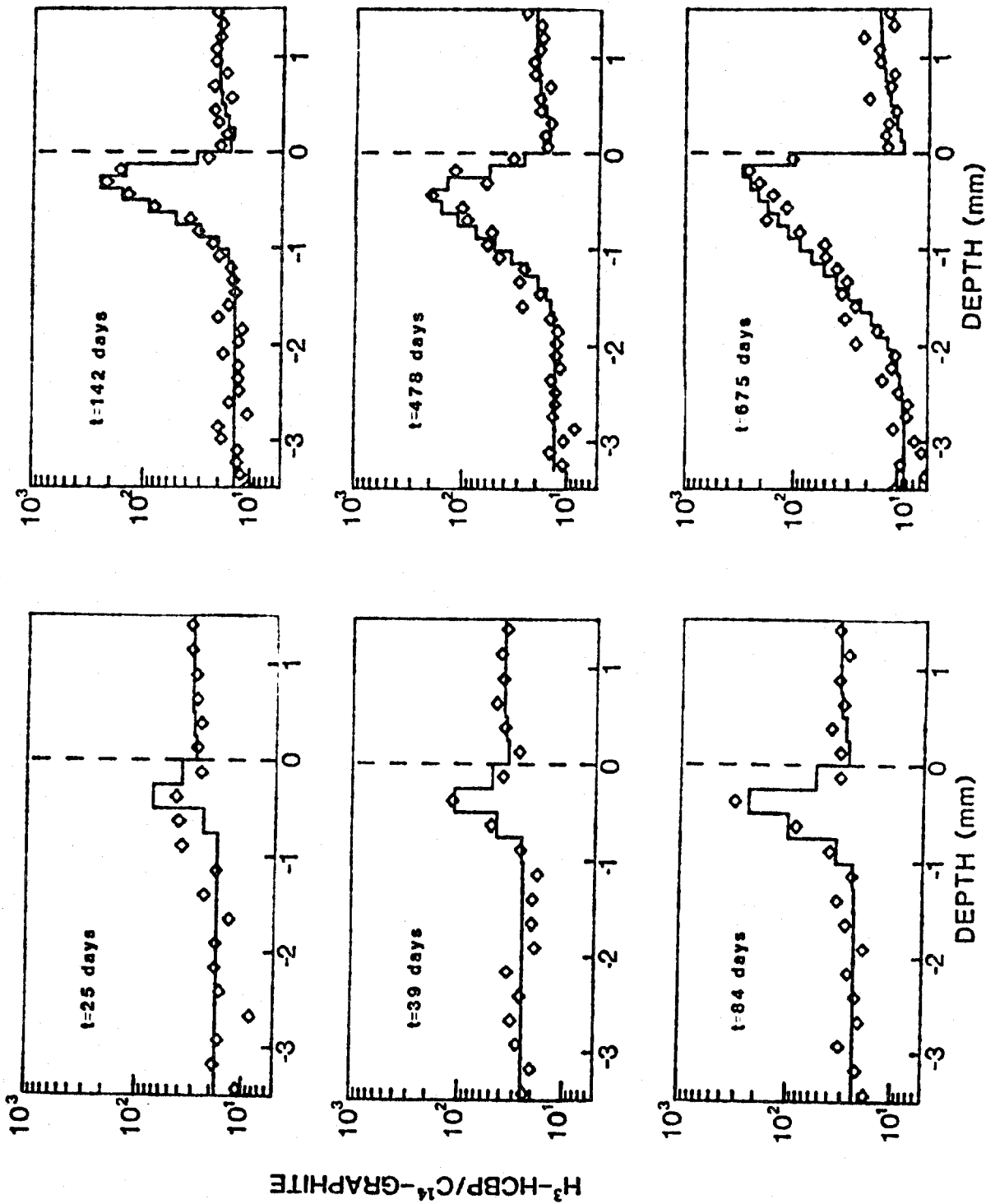


Figure 4. Excess HCBP (ratio of HCBP to graphite concentration) versus depth at various elapsed times. Staircase curves are slice average ratios, computed using parameters in Table 3.

Partition (π) and Apparent Sediment Diffusion (D_S^*) Coefficients of HCBP

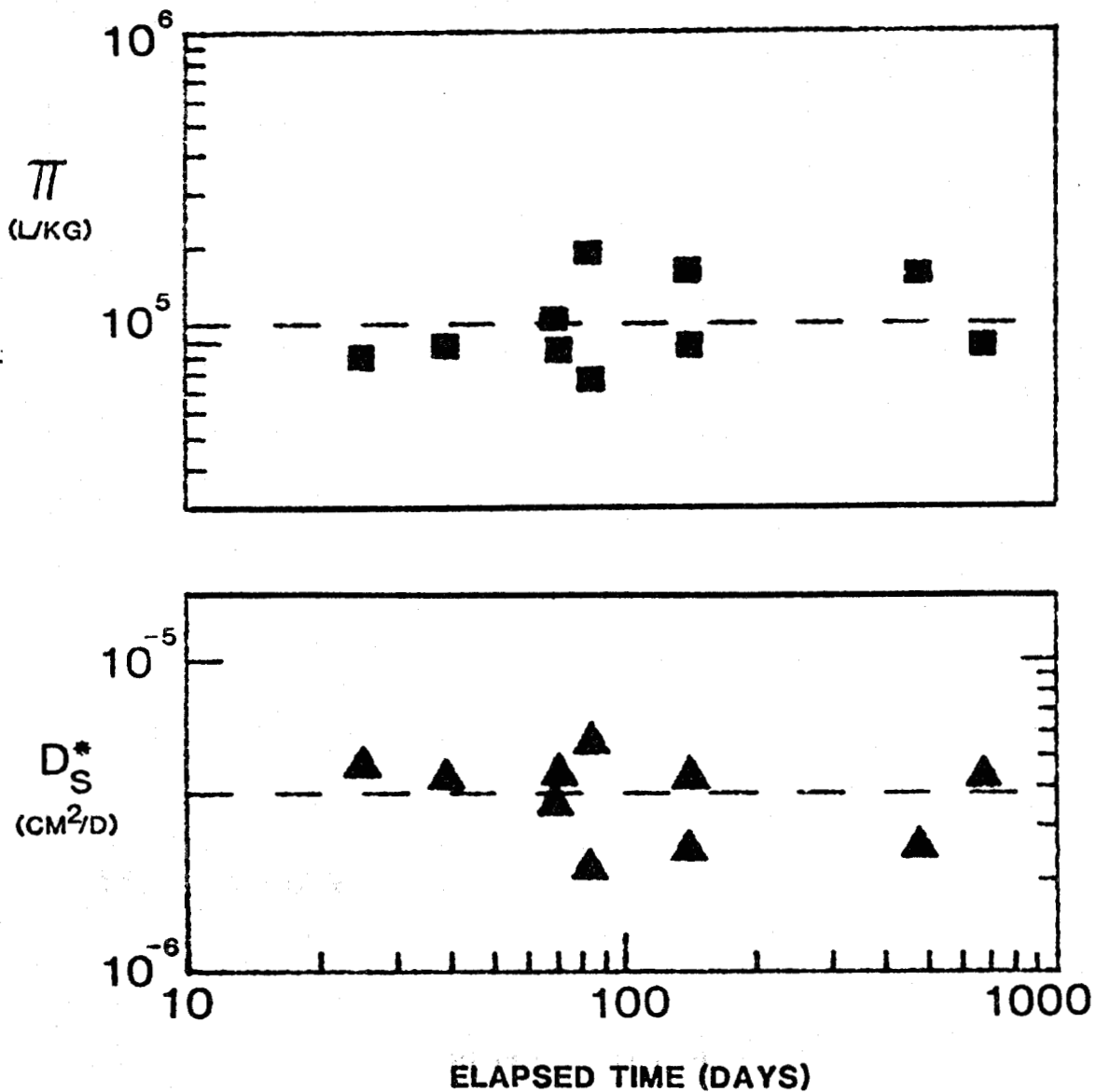


Figure 5. Partition coefficient (upper and left axis) and apparent sediment diffusion coefficient (lower and right axis) versus elapsed time for all syringes analyzed.

SEDIMENT ORGANIC CARBON VS OCTANOL-WATER PARTITION COEFFICIENTS

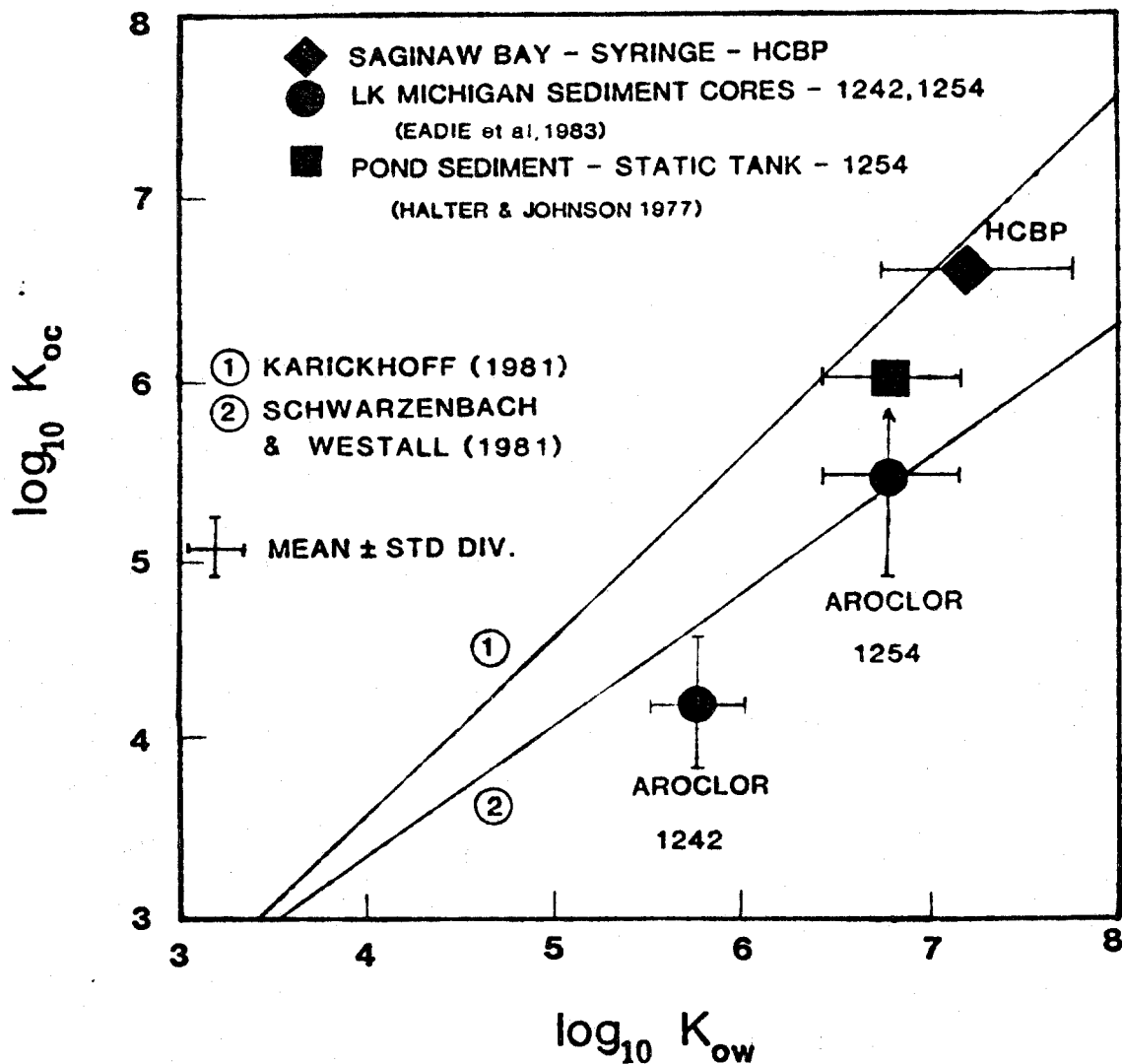


Figure 6. Sediment Organic Carbon Partition Coefficient (K_{oc}) versus Octanol-Water Partition Coefficient (K_{ow}) for HCBP and PCB Aroclors.

partitioning equations based on octanol-water partition coefficient and with the few available direct (Eadie et al., 1983) and indirect (Halter and Johnson, 1977) observations of PCB partitioning in sediments. The octanol-water partition coefficients, K_{ow} , are somewhat uncertain for PCBs. Table 5 summarizes the available values. The value for HCBP is reasonable accord with the predictions of the Karickhoff (1981) correlations whereas the Lake Michigan results are somewhat lower although they are in reasonable accord with the Schwarzenback & Westall (1981) correlation.

The situation with respect to inferred apparent diffusivities is less satisfactory. Static leaching experiments using contaminated sediments have been reported in two cases. An analysis based upon observed fluxes measured by recirculating the overlying water through a foam plug (Fisher et al., 1983) indicated sediment diffusivities of $D_s^* = 0.0012 - 0.85 \times 10^{-6}$ cm/d for four PCB isomers. An analysis of the reported overlying water PCB concentration versus time in a static quiescent leaching experiment (Halter & Johnson, 1977) which parallels the analysis used for the tritium penetration experiment yields $D_s^* = 0.05 \times 10^{-6}$ cm²/day. These values are one to three orders of magnitude lower than the syringe results.

For both these experiments the organic carbon fractions were similar to the syringe sediment so that these apparent diffusivities would suggest PCB partition coefficient of $\log_{10} K_{oc} \sim 7.5 - 10.5$ by comparison to $\log_{10} K_{oc} = 6.6$ found for the syringe experiments (fig. 6). Such large partition coefficients appear unrealistic. It may be that a large fraction, 90-99.9%, of the total PCB in the sediments used in the leaching experiments are non-reversibly bound. Since the framework used to estimate D_s^* assumes completely reversible behavior the inferred partition coefficient would be artificially large in order to account for the large non-reversible fraction bound to the particles.

It should be pointed out that although the syringe experiments exhibited fully reversible behavior, this may not apply to native PCBs in sediment. For the Saginaw Bay sediment employed, 23 ng ³H-HCBP/g were added to sieved Saginaw Bay Sta. #50 sediment. Non-sieved Saginaw Bay sediments from similar locations have native Arochlor 1254 concentrations of ~ 400 ng/g (Richardson, 1983; Thomann and Mueller, 1983). Since 2,4,5,2',4',5' HCBP is 3.67% of Arochlor 1254 (Rapaport & Eisenreich, 1984) it is likely that > 15 ng HCBP/g of native chemical already was present in the sieved experimental sediment.

In terms of the reversible-resistant model of PCB sorption (Di Toro & Horzempa, 1982) the additional radiolabeled chemical may not have sorbed to any available resistant sites (which would happen only if the tagged concentration were in excess of the native concentration) but, instead, only isotopically exchanged with the native reversible component already present. Since only the reversible component was radiolabeled, and since only very small concentrations migrated into the untagged (but HCBP containing) sediment, it is likely that the syringe experiment actually measured the reversible component partition coefficient, K_x . Whether native PCBs are fully reversible remains to be determined.

It is also possible that unlike quiescent diffusion within a sediment the transport of PCBs between the sediment and overlying water in a leaching experiment is not well modeled using diffusion equation formulations. Very thin layers (1 mm) are involved in short term leaching experiments and the mass transport mechanisms may not be entirely diffusive in character. A one to three order of magnitude discrepancy invites a more careful experimental investigation of the mechanisms controlling static leaching fluxes.

The dual tag syringe experiments clearly indicate that molecular diffusion and linear reversible partitioning are the mechanisms that determine the rate of mobility of the (reversible) component of HCBP. The resulting partition coefficient is in conformity with empirical correlations. This methodology may be the most direct route for measuring partition coefficients of highly sorbed chemicals.

Acknowledgement

The authors are pleased to acknowledge the assistance and continuing support of our colleagues: the members of the EPA Large Lakes Research Station: William Richardson, Nelson Thomas (ERL-Duluth); and our group at Manhattan College: Donald O'Connor, Robert Thomann, and Lewis Horzempa (Envirosphere Corp.). The research described in this paper was supported by EPA Grant R805229 and Cooperative Agreement CR807853.

TABLE 1
Sediment Properties
Saginaw Bay Sta. #50 (< 75 μm fraction)

Organic Matter	= 7.6%
Organic Carbon Fraction	= 2.8%
Surface Area	= 12.8 m^2/g

<u>Size Fractions</u> (μm)	<u>% Total Weight</u>
1-2	4
2-10	15
10-30	20
30-75	61

TABLE 2
Tritiated Water Diffusion Experiment

Porosity in Syringe:	$\phi = 0.75$
Solids density:	$\rho_s = 2.65 \text{ g/cm}^3$
Solid-liquid phase ratio:	$m/\phi = \rho_s (1-\phi)/\phi = 0.883 \text{ kg/l}$
Sediment Volume:	$v_2 = 1400 \text{ }\mu\text{L}$
Diffusion Coefficient:	$D_{s, \text{H}_2\text{O}} = 1.5 \text{ cm}^2/\text{day}$

Overlying Water Volume	
<u>t (min)</u>	<u>v_1 (μL)[*]</u>
0	330
30	290
120	255
180	255

* Volume is linearly interpolated between the tabulated values

TABLE 3
Estimates of Diffusion and Partition Coefficients

Elapsed time t(days)	Initial Condition t_g (days)	$D_{s,HCBP}^*$ ($\text{cm}^2/\text{d} \times 10^{-6}$)	$\log_{10} \pi$ (ℓ/kg)	\log_{10} S.E. of π (ℓ/kg)
25	23.3	4.82	4.95	0.12
39	28.3	4.43	4.99	0.058
69	37.3	3.66	5.07	0.16
71	12.4	4.56	4.98	0.042
83	0.21	2.26	5.28	0.042
84	16.1	5.70	4.88	0.036
140	28.4	2.60	5.22	0.046
142	9.7	4.44	4.99	0.019
478	45.1	2.66	5.21	0.027
675	0.35	4.43	4.99	0.022
		3.95 ± 1.12	5.06 ± 0.13	

TABLE 4
PCB Sediment Partition Coefficients

Chemical	Sediment	Organic Carbon fraction (%)	$\log_{10} K_{oc} = \pi/f_{oc} \pm \log_{10} \text{Std. Dev.}$	Reference
Aroclor 1242	Lake Michigan	0.7-3.8	4.17 ± 0.38	Eadie et al. (1983)
Aroclor 1254	Lake Michigan	0.7-3.8	5.44 ± 0.55	Eadie et al. (1983)
Aroclor 1254	Pond	2.0	6.0	Halter & Johnson (1977)
2,4,5,2',4',5'	Saginaw Bay	2.8	6.61 ± 0.13	This study

TABLE 5
PCB Octanol-Water Partition Coefficient

Aroclor	Aroclor 1254	HCBP (2,2',4,4',5,5')	Reference
5.58	6.72	-	Veith & Morris (1978)
-	6.47	-	Veith et al. (1979)
-	-	6.72	Chiou et al. (1977)
5.90 (a)	7.17 (a)	7.75	Rapaport & Eisenreich (1984)
-	-	7.44	Rapaport & Eisenreich (1984)
5.74 ± 0.23	6.79 ± 0.35	7.30 ± 0.53	Mean \pm Std. Deviation.

(a) Computed as $\sum f_i K_{ow} / \sum f_i$ each fraction, f_i , of isomer with octanol-water partition coefficient K_{ow} , in the mixture.

References

- Carslaw, H.S., Jaeger, J.C. (1959). Conduction of Heat in Solids. Oxford Univ. Press, London, 2nd Edition, p. 129.
- Chiou, C.T., Freed, V.H., Schmedding, D.W., Kohnert, R.L. (1977). Partition Coefficient and Bioaccumulation of Selected Organic Chemicals Environ. Sci. Technol. 11(5), p. 475-478.
- Crank, J. (1975) The Mathematics of Diffusion, Oxford Univ. Press, London, 2nd Edition, p. 39.
- Di Toro, D.M., Horzempa, L.M., Casey, M.M., Richardson, W. (1982). Reversible and Resistant Components of PCB Adsorption-Desorption: Adsorbent Concentration Effects. J. Great Lakes Res. 8(2), p. 336-349.
- Di Toro, D.M., Horzempa, L.M. (1982). Reversible and Resistant Components of PCB Adsorption-Desorption: Isotherms. Environ. Sci. Technol. (16)9, p. 594-602.
- Duursma, E.K. (1966). Molecular Diffusion of Radioisotopes in Interstitial Water of Sediments. Proc. Sym. Disposal of Radioactive Wastes into Seas, Oceans, and Surface Waters. International Atomic Energy Agency, Vienna, p. 355-371.
- Eadie, B.J., Rice, C.P., Frez, W.A. (1983). The Role of the Benthic Boundary in the Cycling of PCBs in the Great Lakes. In Physical Behavior of PCBs in the Great Lakes, ed. D. Mackay, S. Paterson, S.J. Eisenreich, M.S. Simmons, Ann Arbor Science, p. 213-228.
- Fisher, J.B., Petty, R.L., Lick, W. (1983). Release of Polychlorinated Biphenyls from Contaminated Lake Sediments: Flux and Apparent Diffusivity of Four Individual PCBs. Environ. Pollut. (Series B) 5, p. 121-132.
- Gerstl, Z., Yaron, B., Nye, P.H. (1979). Diffusion of a Biodegradable Pesticide: I. In a Biologically Inactive Soil, Soil Sci. Soc. Am. J. 43, p. 839-842.
- Halter, M.T., Johnson, H.E. (1977). A Model System to Study the Desorption and Biological Availability of PCB in Hydrosoils. Aquatic Toxicology and Hazard Evaluation. ASTM STP 634, F.L. Mayer & J.L. Hamelink, Eds. Am. Soc. for Testing and Materials, p. 178-195.
- Hesslein, R.H. (1980). In Situ Measurements of Pore Water Diffusion Coefficients Using Tritiated Water, Can. J. Fish. Aquat. Sci., Vol. 37, p. 545-551.
- Karickhoff, S.W. (1981). Semi-empirical Estimation of Sorption of Hydrophobic Pollutants on Natural Sediments and Soils. Chemosphere 10, p. 833.

Manheim, F.T. (1970). The Diffusion of Ions in Unconsolidated Sediments. *Earth Planet Sci. Letters*, Vol. 9, p. 307-309.

Marquardt, D.W. (1963). An Algorithm for Least-Squares Estimation of Non-Linear Parameters. *J. Soc. Indust. Appl. Math* 11(2), p. 431-441.

Officer, C.B. (1982). Fluid and Material Diffusion Coefficient Determinations from Sediment Cores. *Estuarine, Coast, Shelf Sci.* 14, p. 459-464.

Rapaport, R.A., Eisenreich, S.J. (1984). Chromatographic Determination of Octanol-Water Partition Coefficients for 58 Polychlorinated Biphenyl Congeners. *Environ. Sci. Technol.* (18)3, p. 163-170.

Reid, R.C., Prausnitz, J.M., Sherwood, T.K. (1977). The Properties of Gases and Liquids, McGraw-Hill Book Co., N.Y., p. 567.

Richardson, W.L., Smith, V.E., Wethington, R. (1983). Dynamic Mass Balance of PCB and Suspended Solids in Saginaw Bay - A Case Study. In Physical Behavior of PCBs in the Great Lakes, Ed. D. Mackay, S. Paterson, S.J. Eisenreich, M.S. Simmons, Ann Arbor Science, p.329-366.

Schwarzenbach, R.P., Westall, J. (1981). Transport of Non-polar Organic Compounds from Surface Water to Groundwater. *Environ. Sci. Technol.* 15(11), p. 1360.

Thomann, R.V., Mueller, J.A. (1983). Steady State Modeling of Toxic Chemicals - Theory and Application to PCBs in the Great Lakes and Saginaw Bay. In Physical Behavior of PCBs in the Great Lakes, Ed. D. Mackay, S. Paterson, S.J. Eisenreich, M.S. Simmons, Ann Arbor Science, p. 283-310.

van Genuchten, M. Th., Wierenga, P.J., O'Connor, G.A. (1977). Mass Transfer Studies in Sorbing Porous Media: III. Experimental Evaluation with 2,4,5-T, *Soil Sci. Soc. Am. J.* 47, p. 278-284.

Veith, G.D., De Foe, D.L., Bergstedt, B.V. (1979). Measuring and Estimating the Bioconcentration Factor of Chemicals in Fish. *J. Fish. Res. Bd. Can.* 36, p. 1040-1048.

Veith, G.D., Morris, R.T. (1978). A Rapid Method for Estimating Log P for Organic Chemicals. ERL-Duluth, EPA-600/3-78-049.

Walker, A., Crawford, D.V. (1970). Diffusion Coefficients for Two Triazine Herbicides in Six Soils. *Weed Res.* Vol. 10, p. 126-132.

Wang, J.H., Robinson, C.V., Edelman, J.S. (1953). Self Diffusion and the Structure of Liquid Water III. Measurement of the Self Diffusion of Liquid Water with H^2 , H^3 and O^{18} as Tracers. *J. Am. Chem. Soc.* Vol. 75, p. 466-470.